

**Pitch control for wind turbine load mitigation and enhanced wake mixing
A simulation and experimental validation study**

Frederik, J.A.

DOI

[10.4233/uuid:09e98a0c-65f8-46d3-b356-459987c0228a](https://doi.org/10.4233/uuid:09e98a0c-65f8-46d3-b356-459987c0228a)

Publication date

2021

Document Version

Final published version

Citation (APA)

Frederik, J. A. (2021). *Pitch control for wind turbine load mitigation and enhanced wake mixing: A simulation and experimental validation study*. [Dissertation (TU Delft), Delft University of Technology]. <https://doi.org/10.4233/uuid:09e98a0c-65f8-46d3-b356-459987c0228a>

Important note

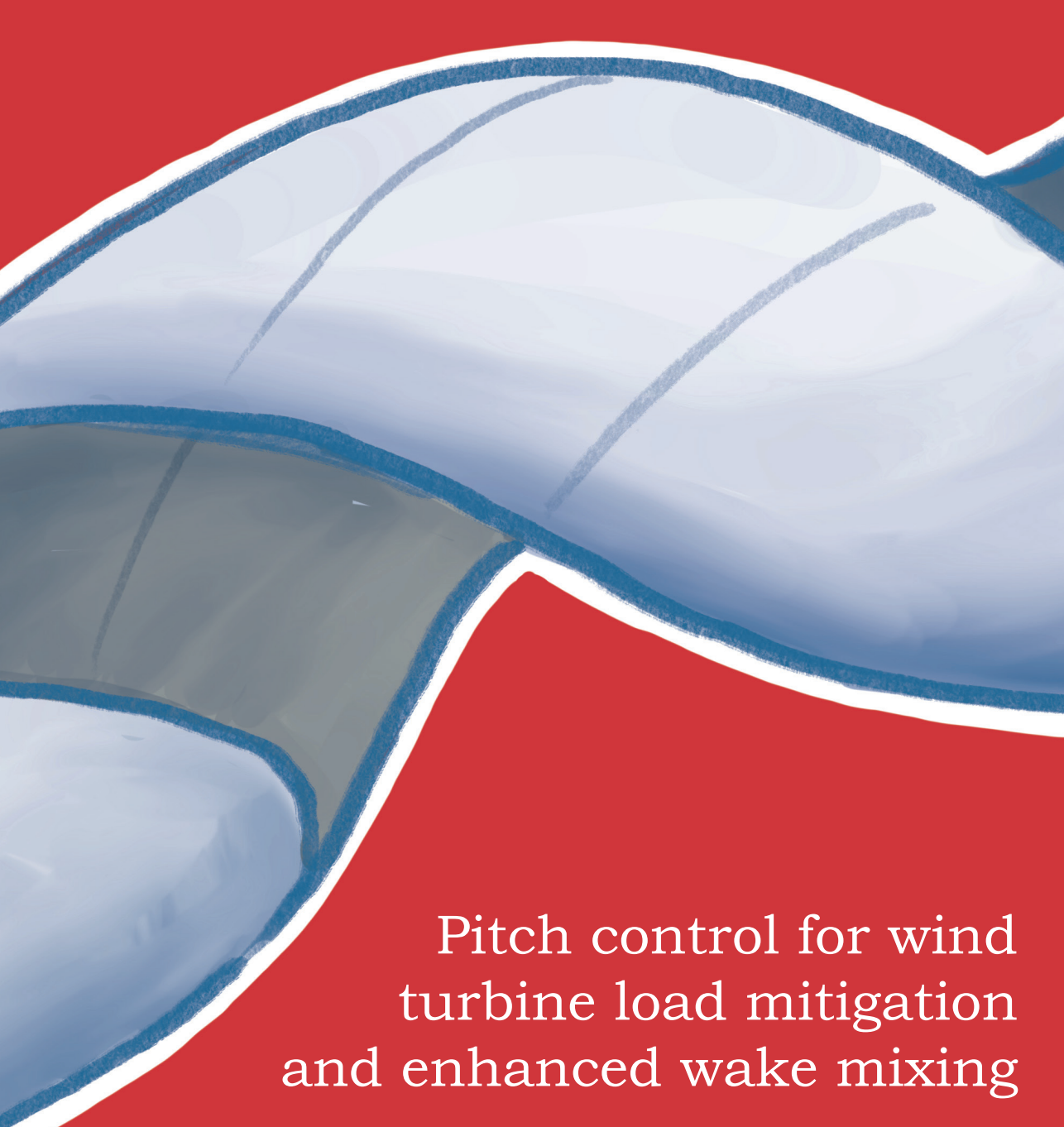
To cite this publication, please use the final published version (if applicable).
Please check the document version above.

Copyright

Other than for strictly personal use, it is not permitted to download, forward or distribute the text or part of it, without the consent of the author(s) and/or copyright holder(s), unless the work is under an open content license such as Creative Commons.

Takedown policy

Please contact us and provide details if you believe this document breaches copyrights.
We will remove access to the work immediately and investigate your claim.



Pitch control for wind
turbine load mitigation
and enhanced wake mixing

A simulation and experimental validation study

Joeri A. Frederik

Pitch control for wind turbine load mitigation and enhanced wake mixing

A simulation and experimental validation study

Proefschrift

ter verkrijging van de graad van doctor
aan de Technische Universiteit Delft,
op gezag van de Rector Magnificus Prof. dr. ir. T.H.J.J. van der Hagen,
voorzitter van het College voor Promoties,
in het openbaar te verdedigen op 4 maart 2021 om 15:00 uur

door

Joeri Alexis FREDERIK

Ingenieur in de systeem- en regeltechniek,
Technische Universiteit Delft, Nederland,
geboren te Utrecht, Nederland.

Dit proefschrift is goedgekeurd door de

promotor: Prof. dr. ir. J.W. van Wingerden
promotor: Prof. dr. ir. M. Verhaegen
copromotor: Dr. R. Ferrari

Samenstelling promotiecommissie bestaat uit:

Rector Magnificus	voorzitter
Prof. dr. ir. J.W. van Wingerden	Technische Universiteit Delft
Prof. dr. ir. M. Verhaegen	Technische Universiteit Delft
Dr. R. Ferrari	Technische Universiteit Delft

Onafhankelijke leden:

Prof. dr. R. Babuska	Technische Universiteit Delft
Prof. dr. S.J. Watson	Technische Universiteit Delft
Prof. dr. C.L. Bottasso	Technische Universität München, Duitsland
Prof. dr. A. Croce	Politecnico di Milano, Italië



Keywords: wind turbine control, wind farm control, data-driven control, individual pitch control, wind tunnel experiments, enhanced wake mixing, helix approach

Printed by: Gildeprint

Front & Back: Saimi Triemstra

Copyright © 2021 by J.A. Frederik

ISBN 978-94-6366-373-1

An electronic version of this dissertation is available at
<http://repository.tudelft.nl/>.

*I was expecting applause
but I guess stunned silence is equally appropriate.*

– Dr. Sheldon Lee Cooper

Contents

List of abbreviations	ix
Summary	xiii
Samenvatting	xvii
1 Introduction	1
1.1 Wind energy in the Netherlands	3
1.2 Wind turbines and wind farms	7
1.3 Control objectives and inputs	9
1.4 Load mitigating control	11
1.5 Power maximization control	12
1.5.1 Greedy control	12
1.5.2 Axial induction control	13
1.5.3 Wake redirection control	15
1.5.4 Dynamic control	15
1.6 Dissertation objective	17
1.6.1 Motivation	17
1.6.2 Research questions	18
1.6.3 Outline of the dissertation	19
2 Data-driven IPC for load mitigation	21
2.1 Introduction	23
2.2 Test Setup	24
2.2.1 Active Grid	24
2.2.2 Wind Turbine	28
2.2.3 Real-time environment	29
2.3 Subspace Predictive Repetitive Control	29
2.3.1 Motivation	30
2.3.2 Subspace Identification	30
2.3.3 Repetitive Control	32
2.3.4 Benchmark controller	36
2.4 Results	37
2.4.1 Constant operating conditions	37
2.4.2 Changing operating conditions	40
2.5 Conclusions	42

3	Dynamic induction control	43
3.1	Introduction	45
3.2	Control Strategy	46
3.3	Simulation environment.	49
3.4	Experimental Setup	50
3.4.1	Wind turbine models.	50
3.4.2	Control system	52
3.5	Simulation Results.	52
3.6	Experimental Results	56
3.6.1	Power production.	56
3.6.2	Controller comparison.	60
3.7	Conclusions	61
4	The helix approach	63
4.1	Introduction	65
4.2	Simulation Environment	67
4.3	Control Strategy	68
4.3.1	Static Induction Control.	68
4.3.2	Periodic Dynamic Induction Control	68
4.3.3	Dynamic Individual Pitch Control	69
4.4	Results	73
4.4.1	Single turbine.	74
4.4.2	Two-turbine wind farm	78
4.5	Conclusions	79
5	Conclusion and recommendations	81
	Bibliography	89
	Acknowledgements	99
	Curriculum Vitæ	105
	List of Publications	107

List of abbreviations

1D, 2D, ...	One, two, ... rotor diameters
1P, 2P, ..., NP	Once, twice, ..., N times per rotation
A/D	Analog-to-Digital
ABL	Atmospheric Boundary Layer
AEP	Annual Energy Production
AIC	Axial Induction Control
AIF	Axial Induction Factor
BEM	Blade Element Momentum
CCW	Counterclockwise
CIPC	Conventional Individual Pitch Control
Cp-Lambda	Code for Performance, Loads, Aeroelasticity by Multi-Body Dynamic Analysis
CW	Clockwise
D/A	Digital-to-Analog
DAQ	Data Acquisition board
DARE	Discrete Algebraic Riccati Equation

DEL	Damage Equivalent Load
DIC	Dynamic Induction Control
DIPC	Dynamic Individual Pitch Control
DLC	Design Load Case
DMD	Dynamic Mode Decomposition
DTU	Technical University of Denmark
FLORIS	FLOw Redirection and Induction in Steady-state
IPC	Individual Pitch Control
LCoE	Levelized Cost of Energy
LES	Large Eddy Simulations
LiDAR	Light Detection And Ranging
LQG	Linear Quadratic Gaussian
LTI	Linear Time-Invariant
MBC	Multi-Blade Coordinate
MFC	Macro Fiber Composite
MIMO	Multiple-Input Multiple-Output
MPC	Model Predictive Control
NTM	Normal Turbulence Model
NREL	National Renewable Energy Laboratory
PI	Proportional-Integral
PID	Proportional-Integral-Derivative
PIV	Particle Image Velocimetry
Polimi	Politecnico di Milano

PSD	Power Spectral Density
RC	Repetitive Control
rpm	revolutions per minute
SIC	Static Induction Control
SISO	Single-Input Single-Output
SOWFA	Simulator for On/Offshore Wind Farm Applications
SPRC	Subspace Predictive Repetitive Control
<i>St</i>	Strouhal number
TI	Turbulence Intensity
TU Delft	Delft University of Technology
TUM	Technical University of Munich
Var	Variance
WF	Wind Farm

Summary

In the transition from fossil fuels to renewable energy sources, wind energy is expected to play a vital role. To make wind energy competitive with fossil fuel-based energy sources, it is essential to reduce the so-called Levelized Cost of Energy (LCoE). This performance indicator takes into account both the costs of construction and maintenance of a power plant, and the energy generated by this plant over its entire lifetime. A straightforward way to reduce the LCoE of wind turbines is by grouping them together to create wind farms, as this reduces construction and maintenance costs. This practice does have a downside: in wind farms, turbines interact with each other through their wakes, which has a negative effect on performance. As a result, optimizing wind farm performance in terms of optimizing LCoE is not as easy as finding the optimum for each individual turbine. Wind farm control is the field of research that investigates the optimization of wind farms as a whole. Wind farm control can improve the LCoE in two different ways: by 1) increasing power generation, and 2) decreasing Damage Equivalent Loads (DELs). These two objectives conflict, as maximizing one usually results in a decreased performance of the other.

The research objective of this dissertation is to *develop and validate novel pitch control technologies that further decrease the levelized cost of wind energy*. A wind turbine has a number of settings that can be controlled. The angle that the blades of a turbine make with respect to the wind is one of these settings. This angle is referred to as the blade pitch angle. In this dissertation, existing pitch control strategies are validated by executing scaled wind tunnel experiments. These experiments bring the technologies one step closer to the application in commercial wind farms. Furthermore, a novel pitch technology is introduced that creates an additional control degree of freedom to the optimization of wind farms. The results that are obtained with respect to these technologies are described here by answering the dissertation sub-questions.

First, Individual Pitch Control (IPC) technologies that aim to mitigate turbine loads are compared in wind tunnel experiments with realistic, reproducible wind conditions. This is accomplished by fitting an active grid to the open jet wind tunnel at the University of Oldenburg. The active grid is fitted with 80 servomotors that can rotate flaps to disturb the wind as desired. With this approach, wind profiles as measured in the field can be mimicked and reproduced to test control algorithms. Two different control strategies have been evaluated: Conventional Individual Pitch Control (CIPC) and data-driven Subspace Predictive Repetitive Control (SPRC). CIPC is a well-established load mitigation technology that has been validated in field experiments. SPRC on the other hand has only been evaluated in simulations and wind tunnel experiments with a uniform wind profile. In these experiments, different wind speeds and turbulent flow conditions are evaluated, and, as a result,

this technology is brought one step closer to implementation on commercial wind farms. The performance of SPRC is shown to be better than achieved with CIPC. On average, a slightly higher blade load reduction is achieved with less the pitch action. This indicates that the increased strain on the pitch bearings, which is considered a major drawback of IPC, is also lower with SPRC. These experiments therefore display the potential of SPRC compared to current state-of-the-art technologies.

The second pitch control strategy that is investigated in this dissertation is Dynamic Induction Control (DIC) with periodic excitation. Unlike SPRC, this strategy aims to increase wind farm power generation. This technology shows great promise in simulation studies, but has not been assessed in an experimental environment yet. Scaled wind tunnel experiments have been performed in the wind tunnel at the Politecnico di Milano. In these experiments, three G1 turbine models are placed in the tunnel, aligned with the wind direction. Periodic DIC is applied to the first turbine to induce wake mixing such that the downstream turbines can increase their power generation. The periodic excitation is varied in amplitude and frequency to find the optimal settings. Compared to the baseline case where all turbines are operated at their individual optimum, a wind farm power increase of up to 4% is recorded. The state-of-the-art alternatives to DIC, static induction and yaw control, are also tested in order to enable a comparison. Static induction is found to be less effective, losing power with respect to the baseline case, while yaw control yields a similar power gain as DIC. These scaled wind tunnel experiments therefore show that DIC is a viable alternative to existing wind farm power maximization control technologies.

One major drawback of DIC is that the periodic variations in the pitch angles lead to increased dynamic loads on the turbine blades and tower. These loads can lead to more frequent damage to the turbine, which could negate the benefit of increased power generation. The effect that DIC has on the loads of a turbine are therefore investigated by means of aeroelastic simulations with and without DIC. The Damage Equivalent Load (DEL) of different turbine components is evaluated in both cases, to assess the effect of DIC on the lifetime. Due to the low frequency of excitation, it is found that the blade and hub DELs increase only slightly. The most significant load increment is observed at the tower. Overall, the increase in terms of percentage is similar to the gain in power, with only the tower experiencing a significantly higher DEL. This dissertation therefore confirms the potential of DIC as a possible wind farm power maximization technology.

With the potential of DIC validated in wind tunnel experiments, the question is raised whether there exist other dynamic control strategies that are perhaps even more effective. In the search for such a technology, this dissertation proposes a novel pitch control strategy which intends to increase wind farm power generation. This strategy uses the Individual Pitch Control (IPC) capabilities of modern wind turbines to dynamically manipulate the location of the wake. This dynamic manipulation leads to increased wake mixing similar to DIC, but without the large variations on the turbine thrust force. As the proposed technology results in a helical wake, it is called the *helix approach*. A proof of concept of this approach is given by means of high-fidelity flow simulations. The helix approach is applied to the upstream unit

of a two-turbine wind farm, and the power generation and thrust force of both turbines are analyzed. These simulations indicate that the helix approach is a more effective power maximization technology than DIC. The power production of the two-turbine wind farm is increased by up to 7.5 %, whereas DIC achieves a 4.6 % increase in these simulations. Furthermore, the variations of the thrust force on both turbines is reduced significantly with respect to DIC, indicating that the helix approach results in lower tower loads.

The contribution of this dissertation comprises the advancement of two existing pitch control strategies for wind turbines in wind farms, and the introduction of a third, novel technology. The next crucial step in verifying the effectiveness of these approaches is taken by validating results from the literature in scaled wind tunnel experiments. The results from these experiments solidify the conclusion that these technologies can reduce the levelized cost of wind energy when applied to commercial wind farms. Furthermore, the proposed helix approach introduces a new degree of freedom to be used in wind farm control. This result is therefore not only a relevant addition to existing literature, but also opens up countless possibilities for additional research.

Samenvatting

Windenergie speelt een cruciale rol in de transitie van fossiele brandstoffen naar duurzame alternatieven. Om windenergie competitief te maken met bestaande energiebronnen, is het essentieel om de zogenaamde *Levelized Cost of Energy* (LCoE), ofwel genivelleerde energiekosten, terug te brengen. Deze graadmeter staat voor de verhouding van de investeringen voor de aanleg en het onderhoud van turbines over de gehele levensduur ten opzichte van de opgewekte energie. Een voor de hand liggende manier om de LCoE terug te dringen is door turbines bij elkaar te plaatsen in windparken. Derhalve wordt het overgrote deel van de windenergie opgewekt in zulke parken. Hier zijn echter ook nadelen aan verbonden: in windparken ontstaat interactie tussen verschillende turbines, wat de prestaties van turbines negatief beïnvloedt. Het optimaal laten functioneren van een windpark is daarom niet zo simpel als het vinden van de optima van de individuele turbines. Windparkregeling is het onderzoeksgebied dat zich richt op de optimalisatie van een windpark als geheel. Dit kan de LCoE op twee verschillende manieren verlagen: door 1) het opgewekte vermogen te doen toenemen, en 2) de schade als gevolg van de belastingen te verminderen. Deze twee doelstellingen zijn tegenstrijdig, aangezien het maximaliseren van de één vaak leidt tot verminderde prestaties bij de ander.

Het onderzoeksdoel van dit proefschrift is om nieuwe bladhoeksturingstechnieken te ontwikkelen en valideren die de genivelleerde kosten van windenergie verlagen. Een windturbine heeft een aantal instellingen die dit kunnen beïnvloeden, waar de hoek van elke wiek ten opzichte van de wind, ook wel de bladhoek genoemd, er één van is. In dit proefschrift worden bestaande bladhoekaanstuurtechnieken gevalideerd door windtunnelexperimenten uit te voeren. Deze experimenten brengen de technieken een stap dichterbij de toepassing in commerciële windparken. Daarnaast wordt een nieuwe bladhoekaanstuurtechniek geïntroduceerd die een extra vrijheidsgraad toevoegt aan het optimalisatieprobleem van windparken. De resultaten met betrekking tot deze technieken wordt hier beschreven door de deelvragen van dit proefschrift te beantwoorden.

Ten eerste zijn verschillende technieken die Individuele Bladhoekaansturing (IBA) gebruiken om bladbelastingen te verminderen vergeleken in windtunnelexperimenten met realistische, reproduceerbare condities. Dit laatste is bewerkstelligd door middel van een actief raster aangebracht op de open windtunnel van de Universiteit van Oldenburg. Het actieve raster gebruikt 80 servomotoren om kleppen te roteren, die zo de wind naar gelang kunnen verstoren. Op deze manier kunnen gemeten windprofielen worden nagebootst en gereproduceerd om regeltechnische algoritmes te testen. Twee verschillende technieken zijn onderzocht: conventionele individuele bladhoekaansturing (CIBA) en een datagestuurde techniek genaamd Subspace Predictive Repetitive Control (SPRC). CIBA is een gevestigde regeltech-

niek voor het verlichten van bladbelastingen die reeds gevalideerd is in veldexperimenten. SPRC daarentegen is nog enkel onderzocht in simulaties en windtunnel-experimenten met een uniform windprofiel. Verschillende windsnelheden en turbulentieprofielen zijn onderzocht, en op deze manier wordt deze technologie een stap dichterbij implementatie op commerciële windturbines gebracht. SPRC overtreft de prestaties van CIBA in deze experimenten. Gemiddeld genomen worden de bladbelastingen iets meer gereduceerd met minder bladhoekbediening. Dit laatste is een indicatie dat de toename van de belasting op de lagers van de wieken, wat als het belangrijkste nadeel van IBA wordt gezien, lager zijn met SPRC. Deze experimenten tonen zodoende het potentieel van SPRC vergeleken met de huidige stand van de techniek op het gebied van IBA.

De tweede bladhoekregeltechniek die onderzocht wordt in dit proefschrift is dynamische inductie-aansturing (DIA) met een periodieke excitatie. In tegenstelling tot SPRC wordt deze strategie gebruikt om het gegenereerde vermogen van windparken te doen toenemen. Deze techniek heeft veelbelovende resultaten behaald in simulatiestudies, maar is nog nooit getest in een experimentele omgeving. Geschaalde experimenten zijn uitgevoerd in de windtunnel op de Politecnico di Milano waarbij drie G1 turbinemodellen in de tunnel zijn geplaatst, uitgelijnd met de windrichting. Periodieke DIA is toegepast op de voorste turbine om de menging van het zog te bevorderen opdat de achterste turbines meer vermogen kunnen genereren. De amplitude en frequentie van de periodieke excitatie is gevarieerd om de optimale instellingen te vinden. In vergelijking met de standaardcasus waar alle turbines op hun individuele optimum opereren is een winst in vermogen van 4 % geregistreerd. De gebruikelijke alternatieven van DIA, statische inductie en gieraansturing, zijn tevens getest om als vergelijking te dienen. Statische inductie is aanmerkelijk minder effectief, en verliest zelfs vermogen ten opzichte van de standaardcasus. Gieraansturing levert een vergelijkbare toename in vermogen op als DIA. Deze windtunnel-experimenten tonen daarom aan dat DIA een rendabel alternatief is voor bestaande technieken die het gegenereerde vermogen van windparken maximaliseren.

Een belangrijk nadeel van DIA is het feit dat de periodieke variaties in de bladhoeken verhoogde dynamische belastingen op de wieken en de toren tot gevolg hebben. Deze belastingen kunnen leiden tot het vaker voorkomen van schade aan de turbine, wat het profijt van het verhoogde vermogen teniet zou kunnen doen. Daarom zijn aero-elastische simulaties met en zonder DIA uitgevoerd om te bepalen welke invloed DIA heeft op de levensduur van windturbines. De schade-equivalente belastingen (SEB's) van verschillende turbinecomponenten is bestudeerd in beide cases om te beoordelen wat het effect van DIA is op de levensduur van een turbine. Vanwege de lage excitatiefrequentie blijken de SEB's van de wieken en de naaf slechts licht toe te nemen. Enkel de toren blijkt een significante belastingtoename te ervaren. De toename is over het geheel genomen van dezelfde orde grootte als de toename in vermogen, met uitzondering van de toren. Dit proefschrift bevestigt zodoende het potentieel van DIA als een mogelijke technologie voor het doen toenemen van het vermogen van windparken.

Nu het potentieel van DIA gevalideerd is in windtunnelexperimenten, rijst de vraag of er ook andere dynamische regelstrategieën bestaan die wellicht zelfs nog

effectiever zijn. In de zoektocht naar een dergelijke techniek draagt dit proefschrift een nieuwe bladhoekaanstuurtechniek aan die als doel heeft het vermogen van windparken te doen toenemen. Deze strategie gebruikt de IBA-capaciteiten van moderne windturbines om de locatie van het zog dynamisch te sturen. Dit leidt tot verhoogde menging in het zog net zoals met DIA, maar dan zonder de grote variaties in de stuwkracht op de turbine. Aangezien deze techniek leidt tot een schroefvormig zog, is het de *helixaanpak* genoemd. De werking van dit concept is aangetoond door simulaties met hoge betrouwbaarheid uit te voeren. De helixaanpak is toegepast op de voorste turbine twee met de wind uitgelijnde turbines en het vermogen en de stuwkracht van beide turbines is geanalyseerd. Deze simulaties duiden aan dat de helixaanpak effectiever is in het maximaliseren van vermogen dan DIA. Het vermogen van dit park bestaande uit twee windturbines neemt toe met 7.5%, terwijl DIA een toename van 4.6% behaalt in deze simulaties. Bovendien zijn de variaties van de stuwkracht op beide turbines significant lager dan met DIA, wat aanduidt dat de helixaanpak leidt tot lagere torenbelastingen.

De bijdrage van dit proefschrift is zodoende dat twee bestaande bladhoekregeltechnieken vooruitgebracht zijn, terwijl een derde, nieuwe techniek geïntroduceerd wordt. De volgende cruciale stap in de verificatie van deze technieken is bewerkstellend door de resultaten vanuit de literatuur te valideren met geschaalde windtunnelexperimenten. De resultaten van deze experimenten versterken de conclusie dat deze technieken de genivelleerde kosten van windenergie kunnen verbeteren wanneer ze worden toegepast op commerciële windparken. Bovendien introduceert de voorgestelde helixaanpak een nieuwe vrijheidsgraad die gebruikt kan worden in windparkregelingen. Dit resultaat is daarom niet alleen een relevante toevoeging tot de bestaande literatuur, maar opent tevens de deur voor talloze aanvullende onderzoeken.

1

Introduction

*A mind needs books like a sword needs a whetstone,
if it is to keep its edge.*

Tyrion Lannister,
on the importance of reading.

This opening chapter presents an introduction into the world of wind energy research through the eyes of a control engineer. The relevance of this scientific field is illustrated, and a brief overview of the state of the art is given. Taking this as a starting point, ongoing challenges can be extracted that this dissertation strives to tackle. The contributions of this dissertation can be summarized by its objective: to develop and validate novel pitch control technologies that further decrease the levelized cost of wind energy.

1.1. Wind energy in the Netherlands

Daily news in the year 2020 was dominated by the outbreak of COVID-19. However catastrophic, the worldwide pandemic also had a silver lining from an environmental point of view. As countries went into lockdown to prevent the spread of the coronavirus, factories were shut down and international traffic came to a standstill. Subsequently, CO₂-emissions were temporarily reduced by an estimated 17 % worldwide (Le Quéré *et al.*, 2020) and air pollution was significantly decreased (Berman and Ebisu, 2020). In some regions, the improvement in air quality might even result in a health benefit that outweighs the deaths attributed directly to a COVID-19 infection (Chen *et al.*, 2020). These benefits are a side-effect of the lockdown measures taken for entirely different reasons and cannot be considered a long-term solution. However, they do show that drastic measures can be effective.

Climate change is still, by the words of Sir David Attenborough, "our greatest threat in thousands of years" (Attenborough, 2018). Solving this threat is a challenge in which renewable energy sources in general, and wind energy in particular, play a key role (Panwar *et al.*, 2011). According to the latest DNV-GL Energy Transition Outlook, renewable energy delivers over 60 % of global power by 2050, with half of that coming from wind (DNV-GL, 2020). This report also predicts that wind will be the largest contributor to the world electricity generation by that time, see Figure 1.1. One would expect that the Netherlands are, for both historical and geographical reasons, at the center of the global transition to wind as a major energy source.

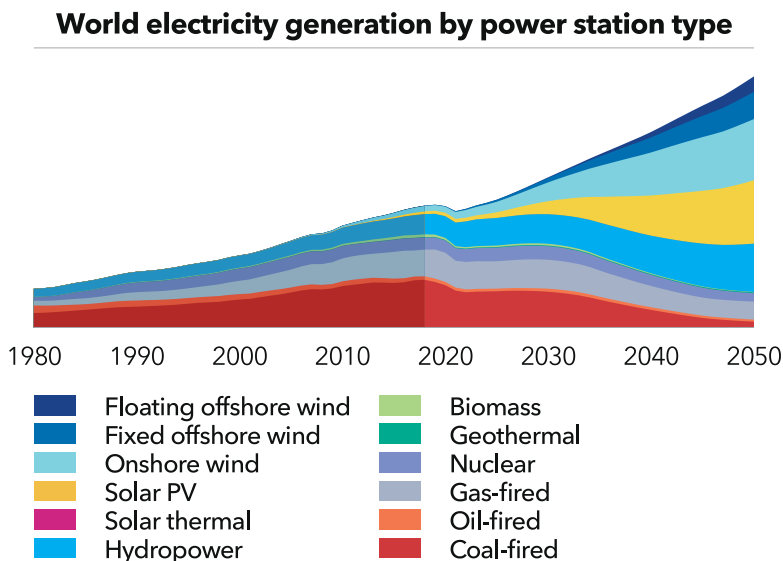


Figure 1.1: The historical and projected electricity generation by power station type. Taken and adapted from DNV-GL (2020).

1

Historically, windmills are as Dutch as *stroopwafels* (a Dutch cookie) and *Oranjegekte* (the nation-wide euphoria that occurs when the national football team performs well). Engineer Jan Adriaanszoon Leeghwater famously used windmills to drain the Beemster area around 1609, thus creating the first so-called *polder*, a piece of land reclaimed from a lake. Dutch windmills would be used to reclaim land for almost two centuries, until steam-driven pumping stations took over at the beginning of the 19th century. The windmills at Kinderdijk are one of the most popular Dutch tourist attractions, and were added to the list of UNESCO world heritage sites in 1997. Ask a person who has never been in the Netherlands to draw a (stereotypical) Dutch person, and the result will most likely be someone wearing *klompen* (wooden shoes), eating *kaas* (cheese) in front of a *molen* (windmill) with *tulpen* (tulips) in his hand.

A transition to wind energy would make even more sense out of geographical motives. Partly due to the many polders in the Netherlands, over one fourth of the land area lies below sea level – as shown in Figure 1.2. This includes most of the densely populated area known as the *Randstad*, a conurbation that covers the cities of Amsterdam, Rotterdam, The Hague and Utrecht, and almost everything in



Figure 1.2: A map of the Netherlands showing land height with respect to the sea. All blue area's are below sea level. Taken from Actueel Hoogtebestand Nederland (AHN).

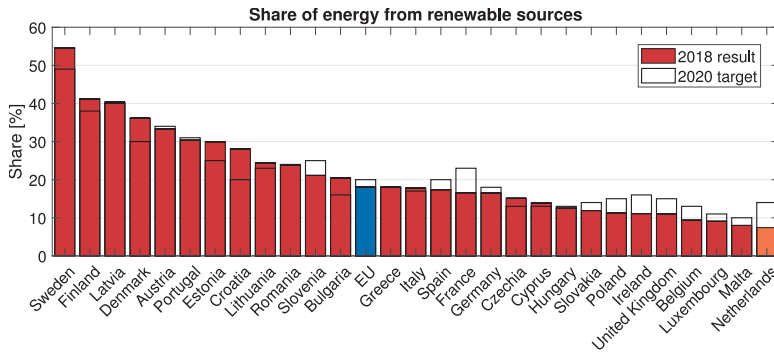


Figure 1.3: The share of energy coming from renewable sources for all EU member states, with the Netherlands in last place at 7.4%. This is 6.6% below the 2020 target of 14%. Data obtained from Eurostat (2020).

between (including Delft). Over 8 million people live in the Randstad (Centraal Bureau van de Statistiek, 2019), approximately half of the entire Dutch population. A relatively small increase in sea level associated with global warming could therefore have catastrophic consequences for the Netherlands. All the more reason for the Netherlands to prioritize a timely energy transition.

Despite the two reasons elaborated above, the opposite is true. As shown in Figure 1.3, the Netherlands is currently last in the European Union when it comes to implementing renewable energy sources (Eurostat, 2020). The share of wind energy in the total Dutch electricity usage is currently below 10% (Centraal Bureau van de Statistiek, 2019), whereas for example Denmark has a wind energy share of 47% (Wind Denmark, 2020).

These are troubling statistics, but the Netherlands are planning to make up for lost ground. In 2019, the Dutch government pledged in the *Klimaatakkoord (Rijksoverheid)* that by 2030, offshore wind energy should account for 40% of the national electricity demand. This is an increase by a factor 10 with respect to the current situation. The government aims to achieve this by building six large wind farms in the North Sea, as shown in Figure 1.4. The year 2020 saw the connection of the first turbines of the 731 MW Borselle III wind farm to the electricity network.

Clearly, further investments into offshore wind farms are expected to be made in the upcoming decade. To give a perspective: the Prinses Amalia wind farm shown in Figure 1.4, small in comparison to the newly planned wind farms, cost an estimated 390 million euros. Although future projects are expected to be more cost efficient, the scale of these plans leads to investments into billions of euros.

Clearly, the transition towards sustainable energy sources is a worldwide challenge, not just a Dutch one. However, the situation in the Netherlands illustrates how urgent the problem is, and the role that wind energy plays in solving it. As illustrated in Figure 1.1, wind energy is expected to supply roughly one third of the global electricity demand by the year 2050. The following section explains why wind farms are crucial in achieving this.



Figure 1.4: Dutch plans for wind farms in the North Sea, as described by [Rijksoverheid \(2020\)](#). The dark green wind farms are already in operation, while lighter green area's are planned.

1.2. Wind turbines and wind farms

The expectations given in [DNV-GL \(2020\)](#) evidently show that wind farms play a major role in the global energy transition in general and, as stated in [Rijksoverheid \(2019\)](#), for the Dutch energy transition in particular. This is where wind farm control comes into play. Before going into detail, the basic concepts of a wind turbine, as well as the complications associated with grouping turbines together, are briefly explained.

A wind turbine can be defined as a machine that converts the kinetic energy of wind into electricity. The vast majority of wind energy worldwide is generated by so-called horizontal-axis wind turbines. These turbines have a number of blades (usually 2 or 3) that rotate around a horizontal axis. Although also vertical axis wind turbines are still an active field of research, this thesis only considers this type of wind turbine.

To give an idea of how such a turbine works, Figure 1.5 shows a simplified representation of the streamtube around a turbine. The turbine is represented here as a rotor disk that exerts a force on the flow, resulting in a streamtube that expands. As the turbine extracts energy from the wind, the velocity of the flow behind the rotor disk is lower than in front of the rotor disk.

In 1919, [Betz](#) showed that the absolute limit of the steady state energy extraction ratio from a wind stream is $16/27$, approximately 59%. Modern wind turbines come close to reaching this Betz limit. Such optimal energy extraction results in a velocity behind the turbine that is $1/3$ of the velocity in front of the turbine. This area of lower wind speed is generally called the *wake* of a turbine. Not only is the kinetic energy lower in a wake, but the turbulence in the wind is also higher.

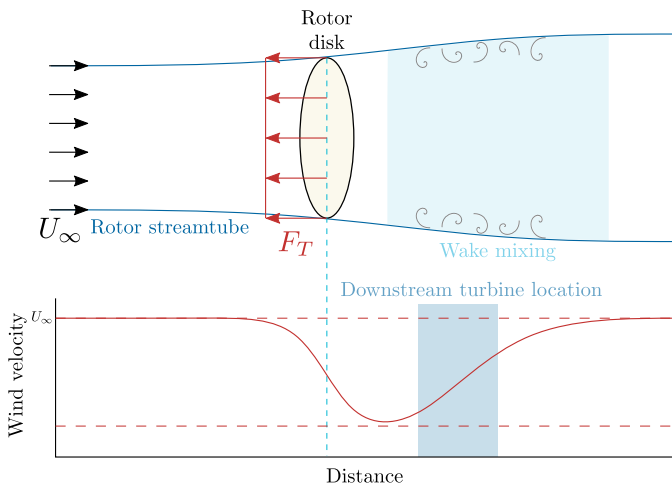


Figure 1.5: A schematic representation of the flow of the wind around a turbine, represented here as a rotor disk. The graph below shows the approximate velocity in the streamtube as a function of distance. Close behind the turbine, the velocity is at its lowest, after which it slowly converges back to the inflow wind speed due to interaction with the free-stream flow around the streamtube.

As shown in Figure 1.5, the speed in the wake slowly increases again as the distance to the turbine increases. This process is called *wake recovery* and is caused by the interaction between the flow in the rotor streamtube and the surrounding air flow. Around the streamtube, the wind has not been slowed down by the turbine, resulting in mixing between the low-velocity flow in the streamtube and the high-velocity flow around it. Therefore, at a large enough distance behind the turbine, the velocity is recovered to the free-stream velocity U_∞ . Usually, this distance is (much) larger than the distance between turbines in a wind farm, depending on the wind direction.

In wind farms, turbines are placed together. This methodology has a number of (mostly economically motivated) advantages, see, e.g., [Boersma et al. \(2017\)](#):

- The amount of land or sea required for generating a certain amount of energy is reduced;
- Deployment and maintenance costs are reduced;
- Connection to the power grid is easier and cheaper.

There are however also disadvantages and challenges associated with placing turbines together in wind farms. Most of these challenges are caused by wakes: when turbines are located close to each other, downstream machines can be affected by the wake of upstream turbines. These downstream machines not only have lower power generation due to the reduced wind speed, but also experience higher loads because of the increased turbulence. It is this interaction that motivates wind farm control: without wake interaction, individual turbine control usually



Figure 1.6: A famous photograph by Christian Steiness of the Horns Rev wind farm in Denmark, which clearly shows the wakes behind turbines. The downstream rows of turbines experience lower wind speeds and higher turbulence intensities as a result of the operation of the upstream turbines.

suffices. It is for this reason exactly that Figure 1.6 is part of almost every presentation involving wind farm control. It shows a wind farm in Denmark where, due to unique weather conditions, the interaction between turbines is plainly visible.

When all turbines in a wind farm experience the free-stream flow, the control problem is relatively simple. In that case, operating all turbines at their individual optimum also leads to the best wind farm performance. However, if there are turbines located in the wake of other turbines, solving the individual turbine control problems might no longer lead to the overall optimal performance (Johnson and Thomas, 2009). This is where **wind farm control** comes into play. In wind farm control, some turbines (usually the ones located upstream) are operated at suboptimal individual conditions such that downstream turbines can increase their performance. The goal of this approach is always to increase the performance of the wind farm as a whole. How this performance is defined, is further elaborated in the upcoming section.

1.3. Control objectives and inputs

Control engineers like to see the world as a collection of systems that they aim to control in such a way that the system behaves as desired. To achieve this, they use sensors to measure the state that the system is in, and actuators to manipulate this state. The challenge of control engineers is to develop a control algorithm that prescribes control signals to the actuators such that the output of the system, usually called the *plant*, exhibits the desired behaviour. A typical way control engineers visualize this is by means of a block scheme, as shown in Figure 1.7.

In wind farm control, the desired behaviour can generally be described as minimizing the Levelized Cost of Energy (LCoE). The LCoE takes into account all costs associated with building and operating wind turbines in a wind farm (e.g., Ashuri et al., 2014). As a control engineer, the LCoE can be improved in two, often conflicting, ways:

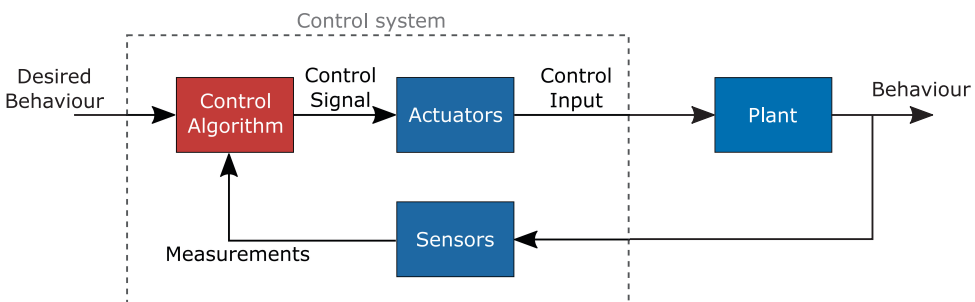


Figure 1.7: A general representation of a control system as typically used by control engineers. In wind farm control, the plant is the wind farm consisting of the turbines and the wind flow field. The turbines often fulfill both the role of actuator and sensor. The desired behaviour is generally related to minimizing the Levelized Cost of Energy (LCoE).

1. By increasing the overall power capture of the wind farm. If a higher amount of energy can be extracted from the wind with the same amount of costs, the LCoE is also decreased.
2. By reducing the occurrence of damage or failures to the turbines. As damage need to be repaired and lead to a temporarily nonoperational turbine, decreasing the occurrence of failures decreases the LCoE. An obvious approach to accomplish this is by minimizing the loads experienced by the turbines, as these usually cause the failures.

Although there is research that aims at optimizing both these objectives simultaneously, most research focuses on either load mitigating control or power maximization control. Both individual objectives are therefore discussed in more detail in Sections 1.4 and 1.5, respectively.

The flow of the wind through the farm can be considered the state of the plant. The turbines therefore play an important dual role in wind farm control: they function both as sensor and as actuator. Turbines are usually equipped with all kinds of sensors, such as a wind vane, an anemometer and load sensors. Furthermore, the power generation of a turbine can also be considered a measurement that not only gives information about the output of the plant, but also about the state. The turbine behaves as an actuator, since the control settings of the turbine affect the wind behind the turbine (see Section 1.2). Considering that the free-stream wind flow can not be controlled, the turbines are the only way the control engineer can influence the state of this plant.

Modern wind turbines can impact the flow of the wind in a number of different ways. First of all, the flow field can be manipulated by controlling the angle of the rotor disk with respect to the wind. This is called the *yaw angle* of a turbine. By giving the yaw angle an offset, the wake can be steered in a desired direction, for example away from a downstream turbine. Although this is a very interesting and popular research field (see, e.g., Doekemeijer (2020)), it is not the focus of this thesis.

Secondly, the energy extraction of a turbine from the flow can be manipulated: a lower energy extraction means higher wind speeds in the wake. This can be achieved by controlling either the angle of attack of the blades with respect to the wind, called *pitching*, or the torque of the turbine generator. In this thesis, blade pitch control is the main method used to change the turbine energy extraction.

The yaw angle, pitch angles and generator torque do not only influence the flow field, but also the performance of the turbine itself. A yaw offset or a pitch angle resulting in lower energy extraction naturally also means that the power generation of the wind turbine in question goes down. Furthermore, pitch angles play a large role in the loads experienced by a turbine, specifically by the blades. How these control inputs can be used to optimize the wind farm control objectives mentioned above, is elaborated in the following sections.

1.4. Load mitigating control

The most effective way to reduce turbine damage is by minimizing the fatigue loads, as these normally cause turbine breakdown (Sutherland, 1999; Spudis *et al.*, 2010). For individual turbines, these fatigue loads are caused by the rotation of the blades, leading to:

- *Gravitational loads*, caused by gravity: when it is moving upwards, a blade experiences a different gravitational load than when it is moving downwards. This results in a blade load with a frequency of once per rotation of the blade ($1P$).
- *Aerodynamic loads*, loads caused by the wind. As the wind is never uniform over the entire rotor-swept area, variations in wind speed and direction lead to $1P$ loads on the blades.
- *Tower shadow*, loads caused by blades passing the tower. This leads to a $1P$ load on the blades and an nP load on the tower, where n is the number of blades of the turbine.

By controlling the angle of attack of a blade with respect to the wind, such periodic loads can be mitigated. Controlling the angle of attack of a blade is called *pitching*, and when each blade has a different pitch angle, this is usually named Individual Pitch Control (IPC). IPC is a widely investigated method for mitigating periodic loads on turbine blades, but as this leads to a pitch angle that deviates from the steady-state optimum, the power capture of the turbine goes down slightly (Bossanyi, 2003, 2005). This shows that the objectives of load minimization and power maximization often conflict.

The initial research presented in Bossanyi (2003) used a relatively simple approach with PI-controllers to minimize the horizontal and vertical moments acting on the rotor disk. This simple approach is already able to reduce loads by 20–40%. More recently, field tests have validated this conventional IPC approach (e.g. Bossanyi *et al.*, 2013; van Solingen *et al.*, 2016) and Mulders *et al.* (2019) has suggested a simple adjustment to further improve load mitigation.

A different approach is proposed in Navalkar *et al.* (2014). The authors use measurements of the bending moments acting on the blades to identify a linear model, which is employed to find the optimal control input, exploiting the fact that the blade loads exhibit repetitive behavior. As subspace identification methods are used, the approach is called Subspace Predictive Repetitive Control (SPRC). The approach has produced promising results in simulations (Navalkar *et al.*, 2014) and wind tunnel experiments with uniform flow conditions (Navalkar *et al.*, 2015). Moreover, recent analysis has shown that SPRC, unlike the conventional IPC approach, is still effective in the case of blade faults (Liu *et al.*, 2020). However, to further validate this approach, experiments in realistic wind conditions would be necessary.

1.5. Power maximization control

As briefly mentioned in Section 1.3, the most straightforward approach to decrease the cost of wind energy from a control engineers perspective is to increase the power generation of existing wind farms. This is therefore a popular research topic in wind farm control. In this section, the most promising wind farm power maximization strategies are briefly discussed.

An easily implementable approach to wind farm control is to simply apply turbine control to the individual turbines. This results in all turbines operating in such a way that they maximize their own power generation. Assume now that there is no interaction between a wake and the free-stream flow around it. In other words: the energy extracted from the wind is never recovered. This case is discussed in detail in Rotea (2014). The following sections demonstrate that, in this case, the turbine control strategy does not result in the optimal wind farm power generation.

1.5.1. Greedy control

Using the blade pitch angles and generator torque of a turbine (see Section 1.3), the Axial Induction Factor (AIF) a of a turbine can be controlled. The AIF is a measure for the velocity reduction caused by a turbine, defined as:

$$a = \frac{U_{\text{inf}} - U_r}{U_{\text{inf}}}, \quad (1.1)$$

where U_{inf} is the free-stream velocity and U_r the rotor velocity. According to the Betz limit, the optimal AIF is $a = 1/3$. Operating turbines using the optimal AIF is often referred to as *greedy control*, since this implies that each turbine greedily extracts as much energy from the wake as possible.

In the case of no wake recovery, the wind speed in the wake can be calculated using the AIF:

$$U_w = (1 - 2a)U_\infty, \quad (1.2)$$

where U_w is the wind speed in the wake, and U_∞ is the wind speed in front of the turbine.

Next, a wind farm consisting of three turbines that are perfectly aligned with the wind, as shown in Figure 1.8, is given. Since the downstream turbines are positioned in the wake of the upstream turbine, they experience a lower wind speed. It is straightforward to deduce from Equation (1.2) that the wind speed in the wake of a turbine operating at the Betz limit is $U_w = U_\infty/3$. In other words, the downstream turbine experiences a wind speed that is a factor 3 lower with respect to the upstream turbine.

The power generation of a wind turbine is given by the equation

$$P = \frac{1}{2}\rho AU^3 4a(1 - a)^2, \quad (1.3)$$

where U is the incoming wind speed, and ρ (air density) and A (rotor disk area) are considered to be constant. Clearly, the power scales with the wind speed cubed.

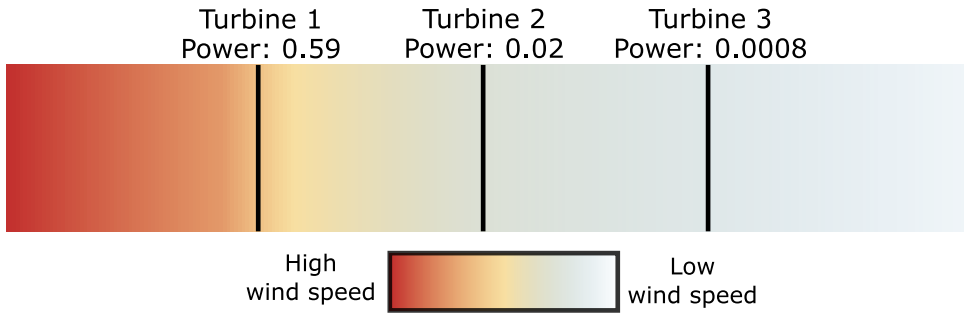


Figure 1.8: Schematic representation of a simple wind farm consisting of three turbines, as seen from above. The wind flows from left to right, and slows down as each turbine extracts energy from the wind. This results in a significantly lower power generation for the downstream turbines.

Therefore, a turbine that experiences a wind speed that is a factor 3 lower has a power generation that is a factor $3^3 = 27$ lower. If a third turbine is located behind this second one, its power generation is another factor 27 lower, i.e., a factor $27^2 = 729$ with respect to the first turbine. It can be shown that in this case, the energy extraction of a row of N turbines quickly converges towards a maximum as N increases. As $N \rightarrow \infty$, the energy extraction approaches

$$P_{\max} = \lim_{N \rightarrow \infty} \left(\sum_{n=1}^N \frac{1}{(3^{n-1})^3} \right) \eta_B = \frac{27}{26} \cdot \frac{16}{27} = \frac{16}{26}, \quad (1.4)$$

with $\eta_B = 16/27 \approx 0.593$ the Betz limit. Clearly, the maximum energy extraction obtained from an infinitely long row of turbines, $P_{\max} = 16/26 \approx 0.615$, is only slightly higher than the energy extraction of a single turbine operating at the Betz limit. With three turbines, the energy extraction is already at 99.99% of this limit. Adding more turbines to this row would evidently be futile, as they would contribute less than 0.01% to the overall power.

1.5.2. Axial induction control

In the previous section, the AIF of each turbine was set at the individual optimum of $a = 1/3$. But suppose now that the axial induction factor of upstream turbine can be lowered¹. In that case, the power generation of this *derated* turbine would go down, but the wind speed in the wake would increase. This strategy is called Axial Induction Control (AIC). Can the increased velocity in the wake lead to downstream turbines compensating for the power loss at the derated turbine? Can AIC, in other words, lead to more effective farm-wide energy capture?

To answer this question, the same case of a three-turbine wind farm with no

¹In theory, the AIF can also be increased above the value of $1/3$. However, this approach makes no sense from a power maximization point of view, as both the power generation of the turbine and the wind speed in the wake would in that case decrease with respect to the greedy optimum. The optimal value of the AIF of each turbine therefore lies in the domain $0 \leq a \leq 1/3$.

wake recovery is investigated. The control challenge is to find the set of AIFs

$$(a_1, a_2, a_3)$$

that maximizes the total power

$$P_{\text{tot}} = P_1 + P_2 + P_3, \quad (1.5)$$

with P_n , $n = 1, 2, 3$, the power generation of turbine n .

Analogous with Equation (1.3), the power of each individual turbine is now given as

$$P_n = \frac{1}{2} \rho A U_n^3 4a_n (1 - a_n)^2, \quad (1.6)$$

where U_n is the wind speed in front of turbine n . Obviously,

$$U_1 = U_\infty.$$

Using Equation (1.2), U_2 and U_3 can be expressed as a function of U_∞ and control inputs a_1 and a_2 :

$$\begin{aligned} U_2 &= (1 - 2a_1)U_\infty \\ U_3 &= (1 - 2a_2)U_2 \\ &= (1 - 2a_2)(1 - 2a_1)U_\infty. \end{aligned}$$

By substituting these expressions in Equation (1.6), the power generation of each individual turbine can be written as

$$\begin{aligned} P_1 &= \frac{1}{2} \rho A U_\infty^3 (4a_1(1 - a_1)^2) \\ P_2 &= \frac{1}{2} \rho A U_\infty^3 ((1 - 2a_1)^3 \cdot 4a_2(1 - a_2)^2) \\ P_3 &= \frac{1}{2} \rho A U_\infty^3 ((1 - 2a_2)^3 \cdot (1 - 2a_1)^3 \cdot 4a_3(1 - a_3)^2). \end{aligned}$$

As expected, the power of all turbines is a function of a_1 , while a_3 only influences P_3 . From the above equations, it follows that the objective given in Equation (1.5) can be written as a function of the individual AIFs. The optimal AIF settings can then be found recursively by determining the root of the derivative with respect to the control input²:

$$(a_1, a_2, a_3) = (0.14, 0.2, 0.33).$$

Applying these AIFs to determine the total power shows a power extraction from the wind of 65.3%. Considering again an infinitely long row of turbines, the limit of power extraction goes towards 2/3 of the available energy (Rotea, 2014). This

²For a detailed derivation of the optimal AIFs for a cascade of aligned turbines in the theoretical case of no wake recovery, the interested reader is referred to Rotea (2014).

shows that, in theory, AIC can lead to a wind farm power increase of 5.1% with respect to greedy control. This simple example therefore shows that, in specific scenario's, AIC is a viable option to increase wind farm power generation.

Naturally, some level of wake recovery is always present in wind farms. This result is therefore not an accurate estimate of the potential of AIC, but more likely an indication of the upper limit. Recent studies show that the real benefit of AIC is much smaller, and in some cases even non-existing (Campagnolo *et al.*, 2016a; Fleming *et al.*, 2017). As a result, the focus of wind farm control is shifting towards different power maximization strategies.

1.5.3. Wake redirection control

An alternative to axial induction control is called *wake redirection control*. As the name suggests, this approach aims to manipulate the direction of the wake instead. Consequently, the wake of upstream turbines can be steered away from downstream turbines, such that these can increase their power capture. Although this thesis does not focus on wake redirection control for power maximization, a short introduction into this subject is given in this section.

Wake redirection can be achieved in a number of different ways:

- Yawing the rotor of a turbine with respect to the wind direction, as first investigated in Jiménez *et al.* (2010). This leads to a horizontal deflection of the wake;
- Tilting the rotor of a turbine, as first suggested in Annoni *et al.* (2017);
- By means of individual pitch control, as coined in Fleming *et al.* (2014).

Yaw and tilt control are essentially two sides of the same coin. Both use the principle that by placing the rotor disk under an angle with the wind, the wake can be deflected. The most fundamental difference between these two methods is the fact that modern turbines have yaw capabilities, but lack the tilt degree-of-freedom. As a result, wake redirection by yaw is the more heavily investigated method in literature. This approach has seen promising results in wind tunnel experiments (Bastankhah and Porté-Agel, 2016; Campagnolo *et al.*, 2016b,c) as well as in recent field tests (Fleming *et al.*, 2019, 2020; Doekemeijer *et al.*, 2020). Recently, this technology has also been introduced as a commercial product for implementation in wind farms (Siemens Gamesa Renewable Energy, 2019).

The third approach, using IPC to manipulate the direction of the wake, is very interesting from a scientific perspective, as pitching blades can be achieved more quickly and easily than yawing a turbine. The concept of IPC wake steering is visualized in Figure 1.9. However elegant, the initial results showed that the achievable deflection of the wake was limited (Fleming *et al.*, 2014). Subsequently, wake steering by IPC has seen very limited further investigation in literature.

1.5.4. Dynamic control

Although the methods that have been described in the previous sections are all very different, they do have one important thing in common. Given the flow conditions,

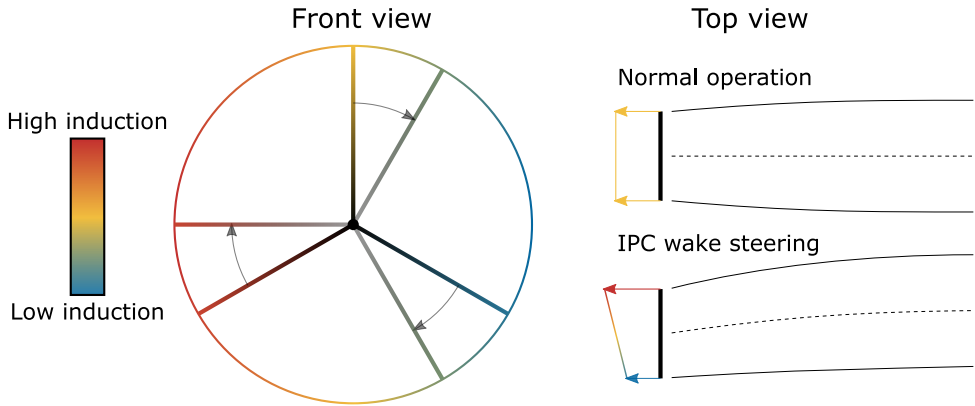


Figure 1.9: An illustration of how the direction of a wake can be manipulated using individual pitch control. The color of a blade represents its induction factor. As the blades rotate, the pitch angle, and subsequently the induction, is adjusted. In the example shown here, the induction in the right half plane is lower than in the left half plane. Subsequently, the resulting force on the rotor plane redirects the wake to the left.

all these strategies search for the optimal *steady-state* control settings that maximize power generation. When this static optimum is reached, the control input, be it the induction factor or the yaw angle of a turbine, is kept constant – assuming of course the flow conditions do not change. But could the power generation be further increased when time-varying signals are considered? In other words: what if the control signals are allowed to be *dynamic*?

It was this exact question that was investigated in [Goit and Meyers \(2015\)](#). In this paper, an advanced control algorithm was used to determine the optimal *dynamic* induction of turbines in a wind farm. The result is an input signal that exhibits large fluctuations over time, and an increase in energy capture of up to 19% is reported. As demonstrated in Section 1.5.2, this energy gain is much higher than the theoretical limit of *static* induction. By varying the turbine input over time, mixing can be enhanced such that downstream turbines experience a much lower wake deficit than achievable with static control. Consequently, dynamic control strategies are also called *wake mixing* strategies. Evidently, the potential of dynamic induction in terms of power maximization is much higher than of its static counterpart.

There are of course some complications to the approach used in [Goit and Meyers \(2015\)](#). First of all, the control algorithm that determines the optimal induction factors is so complicated that the computational effort is significant. As a result, implementation on an actual wind farm is troublesome as it would take too long to determine the next control input. Secondly, the large spikes in the induction signal would lead to a substantial increase of the loads on the turbines. This approach therefore strongly conflicts with the other variable that determines the LCoE of turbines: the occurrence of damage to the turbines.

Nonetheless, the concept of dynamic control settings is an interesting one, and is recently seeing an increasing amount of interest. Perhaps, simpler and less invasive

methods can balance an increased energy capture with practical applicability and acceptable loads.

One such approach is suggested in [Munters and Meyers \(2018a\)](#). The authors noticed that the induction signal of upstream turbines in earlier research ([Munters and Meyers, 2016, 2017](#)) resembled a sine wave. Instead of *any* dynamic input signal, it is suggested to restrain the induction signal to a sinusoid. This approach kills two birds with one stone: the control problem becomes considerably easier (only the optimal amplitude and frequency of the sine wave is to be determined) and the control signals are smooth now (leading to lower turbine loads). Naturally, the potential energy gain is also lower than in the unconstrained approach. Nonetheless, with a wind farm of 4 aligned turbines, an increase of 6% is reported ([Munters and Meyers, 2018a](#)).

As this is a relatively new approach to the wind farm control problem, there is still a lot to be investigated. The studies mentioned above show the effectiveness of dynamic induction in simulations. Can these results be reproduced in wind tunnel experiments or field tests? How do dynamic control strategies affect the turbine loads? Can dynamic control signals other than a sine wave on induction be as effective, or perhaps even more effective, in inducing wake mixing? Future research is necessary to answer these questions.

1.6. Dissertation objective

The previous sections give a short but broad overview of the state of the art of wind turbine and wind farm control. In this section, the contributions of this dissertation are outlined. First, a motivation is given for the research presented in this thesis. Next, the research objective is introduced, along with a number of smaller sub-questions. Finally, the outline of this dissertation is described.

1.6.1. Motivation

In Section 1.3, two wind farm control objectives are posed: maximizing energy capture and minimizing fatigue damage. In both fields of research, new control approaches are being developed, and promising results are being presented. With these new control technologies, the first step is usually to conduct tests in a simulation environment.

To further assess technologies that show promise in simulations, conducting scaled wind tunnel experiments is an attractive way to proceed. With wind tunnel experiments, it is possible to evaluate technologies in the real world. Models of complex systems such as a wind farm are never perfect, and results from physical experiments can validate the reliability of such models. Compared to full-scale field tests, conducting scaled wind tunnel experiments has a number of important advantages:

- *Controllability*: flow conditions can be set as desired.
- *Reproducibility*: flow conditions can be reproduced such that a fair comparison

between control strategies can be made.

- *Low risk*: as new technologies have not yet been tested on actual turbines, there is always the chance of something going wrong or breaking down. In scaled experiments, the consequences of such a failure are much less severe.
- *Time*: as size scales, so does time. Therefore, with scaled experiments, a large amount of data can be gathered in a relatively short time span.
- *Cost*: although using a wind tunnel is not free of charge, it is much cheaper than doing lengthy experiments on real turbines.
- *Availability*: wind turbine manufacturers and wind farm operators are often hesitant to test new, experimental technologies on their expensive turbines.

All these advantages together make that wind tunnel experiments are a logical intermediate step to bridge the gap between simulations and field tests. In this dissertation, this order of testing new technologies is therefore upheld. Novel technologies, both for load mitigation and power maximization, are first tested in a simulation environment. When these simulations produce positive results, these are then validated in wind tunnel experiments. Hence, the next step towards implementation in full-scale wind turbines and wind farms can be taken.

1.6.2. Research questions

The research presented in this dissertation aims to further decrease the levelized cost of wind energy with novel control technologies. This leads to a research objective that is defined as:

Research objective:

Develop and validate novel pitch control technologies that further decrease the levelized cost of wind energy.

As this objective is rather broad, a number of sub-questions have been formulated. These sub-questions give a more specific direction to fulfilling the research objective. The first sub-question is related to reducing turbine blade loads. Different IPC strategies have already been developed in literature (see Section 1.4), and wind tunnel experiments could mean the next step in developing these methods. The first sub-question is therefore formulated as:

I: How do different individual pitch control technologies that aim to mitigate blade loads compare in wind tunnel experiments that generate realistic, reproducible wind conditions?

Apart from increasing the turbine lifetime by mitigating loads, the cost of wind energy can also be improved by increasing wind farm power generation. As elaborated in Section 1.5.4, dynamic control strategies form a new and exciting solution

to this challenge. Such methods show promising results in simulations, but have yet to be proven to work in an actual setup. Therefore, the second sub-question is defined as:

II: How does periodic dynamic induction control perform with respect to wind farm power generation in scaled wind tunnel experiments?

Since dynamic control strategies are expected to increase turbine loads, these should also be evaluated. This leads to the third sub-question:

III: How much do the turbine damage equivalent loads rise when dynamic control technologies are applied, and are these increased loads compensated for by the higher power generation?

As dynamic control is a young field of research, it is likely that dynamic induction is not the only viable control solution. Perhaps, other technologies prove to be more effective in balancing power maximization with minimal turbine loads. Therefore, the final sub-question is formulated as:

IV: Can an alternative dynamic control technology be developed that maximizes power generation while minimizing additional turbine loads?

In this dissertation, research by means of simulations and wind tunnel experiments is conducted to answer the questions posed here. The answers provide valuable knowledge in helping wind become an even more competitive energy source.

1.6.3. Outline of the dissertation

This dissertation combines three articles that have been peer-reviewed and published in scientific journals on either control engineering or wind energy. Each publication has its own chapter, with independent introductions and conclusions. These chapters can therefore be read more or less independently from the rest of the dissertation. Each chapter contains two of the three core elements of the dissertation: wind tunnel experiments, individual pitch control and enhanced wake mixing. The mutual relation between the different chapters is schematically given in Figure 1.10. More specifically, the content of these chapters is described as follows:

Chapter 2 evaluates the effectiveness of IPC-driven load mitigation technologies. To this effect, wind tunnel experiments have been conducted at the University of Oldenburg. The wind tunnel is equipped with an *active grid* such that real turbulent flow profiles can be mimicked and reproduced. Different IPC strategies are compared based on the results of these experiments.

Chapter 3 presents the results of scaled wind tunnel experiments executed at the Politecnico di Milano. In these experiments, periodic dynamic induction

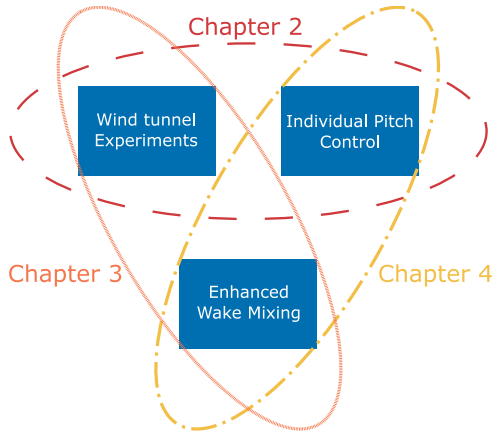


Figure 1.10: The three core components of this dissertation, showing which of these elements is discussed in each chapter.

is applied on the upstream turbine of a three-in-line wind farm setup. The energy capture is evaluated and an analysis of the turbine loads using dynamic induction is performed.

Chapter 4 introduces a novel dynamic control technology called the *Helix approach*. This strategy uses individual pitch control to enhance wake mixing and maximize wind farm power generation. A proof of concept is given by means of high-fidelity flow simulations.

Finally, Chapter 5 combines the conclusions of the individual chapters to form an overarching conclusion of the dissertation. In this chapter, the research objective is evaluated and the corresponding sub-questions are answered, reflecting on the contributions of this dissertation and formulating recommendations for future research.

2

Data-driven individual pitch control for load mitigation

*Research is what I'm doing
when I don't know what I'm doing.*

– Dr. Wernher von Braun,
on the process of conducting scientific research.

A commonly applied method to reduce the cost of wind energy, it is to alleviate the periodic loads on the turbine blades using Individual Pitch Control (IPC) in order to increase the lifetime and decrease the maintenance cost. However, current state-of-the-art IPC methodologies significantly increase the duty cycle of the pitch actuators. In this chapter, a data-driven individual pitch control methodology called Subspace Predictive Repetitive Control (SPRC) is employed. SPRC is investigated as a solution to alleviating periodic loads on a scaled 2-bladed wind turbine in turbulent wind conditions, whilst keeping the actuator duty cycle to a minimum. An open-jet wind tunnel with an innovative active grid is employed to generate reproducible turbulent wind conditions. Significant load reductions are achieved even under these high turbulent conditions, resulting in improved overall performance compared to conventional IPC.

The contents of this chapter have been published as a peer-reviewed research paper in the Control Engineering Practice journal:

J.A. Frederik, L. Kröger, G. Gülker and J.W. van Wingerden, *Data-driven repetitive control: Wind tunnel experiments under turbulent conditions*, Control Engineering Practice **30** 105 (2018).

2.1. Introduction

In the quest to make the cost of wind energy increasingly competitive with conventional energy sources such as fossil fuels, wind turbine structures become increasingly larger and more slender in order to increase their rated power (Van Kuik *et al.*, 2016). Consequently, the loads experienced by the blades of turbines also increase, and it becomes of vital importance to mitigate these loads.

The majority of dynamic loads on wind turbine rotors have a periodic nature, caused by wind shear, tower shadow, gravity and partial wake overlap from upwind turbines (Bossanyi, 2003). To reduce these deterministic loads, Individual Pitch Control (IPC) is a method receiving an increasing amount of attention (Barlas and van Kuik, 2010). In IPC, the pitch angle of each blade is, as the name suggests, controlled individually to decrease the out-of-plane bending moments. This method is relatively easy to implement, since most modern wind turbines already have individual pitch capabilities, as well as measurements of the bending moments. By applying periodic pitch angles to the blades on top of the collective pitch, significant load alleviations can be achieved (Bossanyi, 2003).

Many different IPC approaches are studied in literature. Initially, the focus was mainly on controlling the load occurring once per rotation (1P) using Linear Quadratic Gaussian (LQG) controllers to solve the Multiple-Input Multiple-Output (MIMO) problem (Bossanyi, 2000; Selvam *et al.*, 2009). However, since the 1P loads are symmetric, these loads do not cause the largest loads on the non-rotating parts of the wind turbine structure. These parts experience the largest loads at the blade passing frequency NP , with N the number of blades of the turbine (Bossanyi, 2005). One method of alleviating these NP loads is by applying the Multi-Blade Coordinate (MBC) transformation (Bir, 2008), which transforms the loads into a static reference frame. This allows the use of simple linear Single-input Single-output (SISO) control methods, such as PI-controllers (Bossanyi, 2005; van Solingen and van Wingerden, 2015).

An important downside of IPC is the substantial increase of the pitch actuator duty cycle. Subsequently, the wear on the bearings of the blades is also increased. In the proposed IPC methods, this effect could be enlarged at higher wind turbulence intensities, as these methods might attempt to also control the non-deterministic loads. However, this is a research area that has not yet received a lot of attention. Furthermore, the mentioned IPC algorithms assume constant operating conditions, and are usually not able to adapt to changing rotor velocities.

A novel IPC methodology that deals with both these problems is proposed in Navalkar *et al.* (2014). This methodology is called Subspace Predictive Repetitive Control (SPRC) and combines subspace identification (Van der Veen *et al.*, 2013) with repetitive control. By using measurement data to do online identification, the model can be refined during operation. Furthermore, the repetitive control law targets only the specified deterministic loads, thus lowering the actuator duty cycle. SPRC shows promising results in simulations (Navalkar *et al.*, 2014) and in wind tunnel experiments with laminar flow conditions (Navalkar *et al.*, 2015). These laminar flow conditions are however not a realistic representation of the wind conditions that a turbine in the field would experience.

In this chapter, experiments are presented that form the next vital step in assessing the relevance of SPRC as an IPC algorithm. Using the open jet wind tunnel of ForWind at the University of Oldenburg, which is equipped with a novel active grid, realistic turbulent wind conditions can be created. Furthermore, the active grid makes it possible to reproduce these conditions, thus enabling an evaluation of different control methodologies.

The structure of this chapter is as follows: in Section 2.2, the experimental setup is described. This section contains a description of the flow conditions as created by the active grid (2.2.1), a description of the wind turbine (2.2.2), and an overview of the real-time environment (2.2.3). Section 2.3 covers the SPRC algorithm and its modifications, and Section 2.4 then shows the results of this algorithm subject to turbulent wind conditions. Finally, conclusions are drawn in Section 2.5.

2.2. Test Setup

This section describes the test setup used to conduct the experiments. First, the wind tunnel equipped with the novel active grid is explained, followed by a description of the two-bladed control-oriented wind turbine. Finally, an overview of the real-time environment is given.

2.2.1. Active Grid

The experiments shown in this chapter have been conducted in a low-speed wind tunnel of the University of Oldenburg. This tunnel has a cross section of 3×3 m and can reach wind speeds up to 30 m/s. On the inlet of this tunnel, an active grid is mounted as shown in Figure 2.1. This active grid consists of 20 servomotors at each side that are connected to an axis mounted with rigid square flaps, as introduced by Makita (1991). Consequently, the 80 different axes of the active grid can be actuated individually. The change of the angle γ of the rigid square flaps with respect to the inflowing wind results in either a blockage or a deflection of the inflow.

By dynamically varying γ over time, various turbulent flow fields with specific characteristics such as atmospheric turbulence can be generated at certain positions in the test section (Knebel *et al.*, 2011; Heißelmann *et al.*, 2016). A comprehensive overview of the work in active grid research can be found in the review article of Mydlarski (2017). By repeating a predefined dynamic sequence of input angles γ , defined as an excitation protocol, it is possible to accurately reproduce turbulent flow fields.

To validate the new control concepts of the model wind turbine in turbulent conditions and to validate the reproducibility of the inflow, the flow field acting on the wind turbine is characterized. This was realized using a 2D hotwire system by Dantec Dynamics. This sensor consists of a thin wire suspended between two prongs and measures the wind speed and direction. An x-wire of the type 55P51 was used and operated at a sampling rate of 20 kHz with a low-pass filter at 10 kHz. For the data acquisition an 18-bit National Instruments Analog-to-Digital (A/D) converter was used. These sensors were used to measure the wind speed at the location of

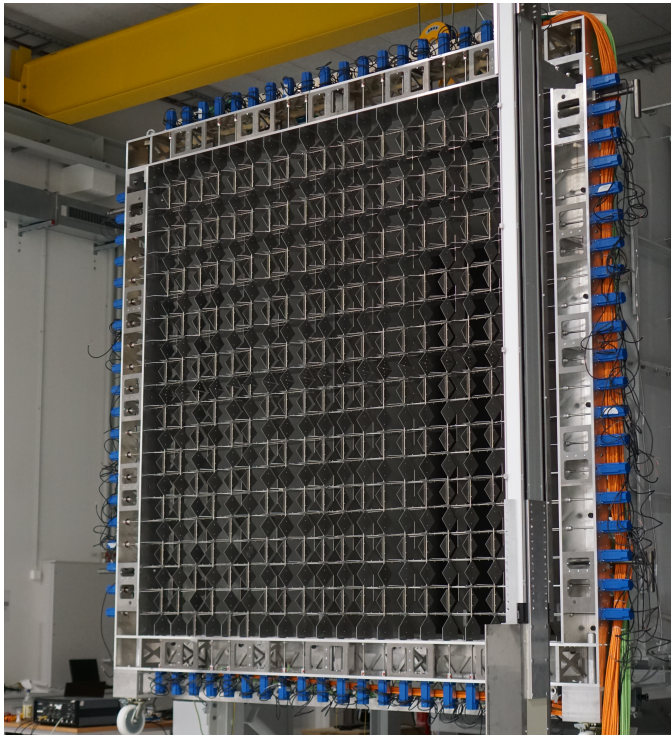


Figure 2.1: The active grid mounted on the 3×3 m wind tunnel inlet in open test section configuration.

the hub of the model turbine at 20 mesh sizes (3 m) distance to the active grid. Additionally, the hotwire was shifted 1 m to either side to determine differences in the flow field in the range of the wind turbine diameter.

Using the active grid described above, different wind conditions can be created. In this chapter, the active grid was used in four different modes: two static and two active cases. For the static cases, the angle of attack of the active grid flaps was set to a constant angle of 0° , corresponding to the orientation of the flaps with minimal blockage, and 45° . In the active cases, two excitation protocols were used. The first one, called the *lidar mode*, is based on atmospheric wind data measured with Light Detection And Ranging (LiDAR), and creates a wind field with intermittent behavior. The second one, called the *gusts mode*, is creating a mexican hat-like wind field with single gusts.

The flow fields of all these modes were investigated for three different mean wind velocities of 4 m/s, 4.5 m/s and 5 m/s. In the following, the different protocols are characterized briefly for the 5 m/s test cases, in terms of reproducibility, flow characteristics, Turbulence Intensity (TI) and the dynamics in the power spectra. The wind speed is measured with a sampling rate of 20 kHz. A full characterization of all modes, including supplementary measurements shifted to the outer radius of the wind turbine and further analysis to determine the reproducibility and intermit-

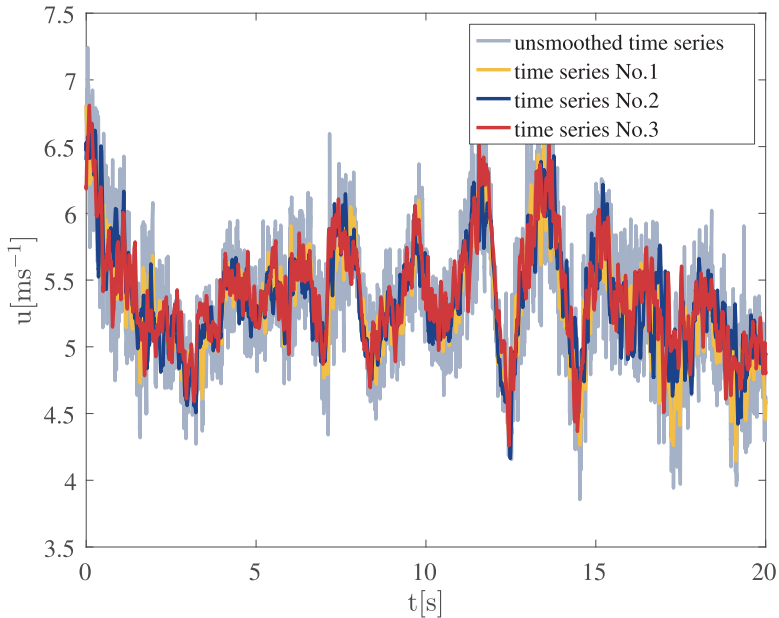


Figure 2.2: Three exemplary wind speed time series generated by the lidar excitation protocol smoothed by a moving average filter for a better comparison. An unfiltered wind speed time series is shown as reference in light gray.

tency of the flow fields, is presented in [Kröger *et al.* \(2018\)](#).

To show the reproducibility, three wind speed time series are shown in [Figure 2.2](#) smoothed by a moving average filter over 1000 samples (i.e., 0.05 s). In light gray, an unsmoothed time series is shown as a reference. These turbulent flow fields were generated by repeating the lidar excitation protocol of the active grid. As shown, the main dynamic features in the flow are highly reproducible, whereas the higher-frequency components show differences in the direct comparison. By inspection of the smoothed power spectra of all four test cases shown in [Figure 2.3](#), further analysis of the dynamics of the flow fields is performed. To show the resemblance between the flow fields generated by repeated excitation, the spectra of five repeated time series are plotted on top of each other, appearing for all test cases nearly as a single line.

As a reference, the $-5/3$ law of the natural decay of turbulence postulated by [Kolmogorov \(1941\)](#) is also shown, to compare the results with the theoretical values. This is valid for the higher frequency ranges of all test cases. The data of the two actively driven test cases both show a significant increase of the energy in the lower frequency ranges of 0.1 – 10 Hz, corresponding to structures in the flow with sizes of 0.5 – 50 m. This results in more realistic turbulent structures acting on the model wind turbine compared to using regular grids, with integral length scales in the range of their mesh width ([Kröger *et al.*, 2018](#)).

To describe the variability of the wind field the TI is used. The TI is defined as

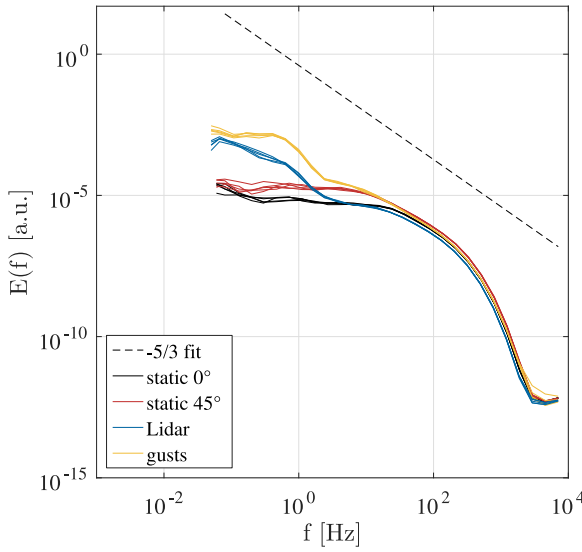


Figure 2.3: Power spectra of all four active grid modes. For every mode the spectra of five repetitions are shown. The $-5/3$ law of the natural decay of turbulence is represented by the dashed line as a reference.

the ratio of the standard deviation and the mean of the wind speed time series:

$$TI = \frac{\sigma_u}{\langle u \rangle}.$$

As every test case was repeated five times, the mean value of the TI over these experiments were determined for the different modes and are shown in Table 2.1. Note that although the gusts mode has relatively low average TIs, this mode creates the largest variations in wind velocity. As a consequence, it might result in higher load variations on the blades than would be expected based on the TI. The TI was determined at the hub of the turbine (*centerline*) as well as at the tip of the blades (*shifted*) to account for the complete rotor-swept area.

Table 2.1: The average turbulence intensities for different modes of the active grid.

Mode	Centerline TI [%]	Shifted TI [%]
Static 0°	2.5	2.7
Static 45°	3.7	5.1
Lidar	8.8	10.1
Gusts	4.2	7.2

2.2.2. Wind Turbine

The wind turbine model that is used for these experiments is presented in [Navalkar et al. \(2015\)](#). It is a two-bladed direct-drive wind turbine that is placed upwind of the wind tunnel. The drive train is shown in Figure 2.4a. The blades are connected with hub through a rigid connection with the shaft of Dynamixel MX-106 servomotors. These servomotors enable rotation of the blades around the longitudinal axis of the blade. The Dynamixel servomotors have a bandwidth of approximately 15 Hz. The azimuth angle of the blades is measured through a position encoder located in the main shaft. For other experiments executed with this turbine, see, e.g., [Van Solingen et al. \(2014\)](#).

The blades used for this experiments are designed and presented in [Navalkar et al. \(2016\)](#) and shown in Figure 2.4b. A Macro Fiber Composite (MFC) piezoelectric sensor is affixed to each blade, located at the root of the blade. These piezo's are used to measure the strain on the blades, which relates directly to the out-of-plane bending moments.

With these blades and the wind conditions described in the previous subsection, rotor speeds of up to approximately 330 rpm (5.5 Hz) can be achieved. Considering the bandwidth of the servomotors, therefore periodic loads up to twice the rotor speed (2P) can be controlled.

Note that the blades also contain free-floating flaps that can be used for control by changing the input voltage of the MFC piezobenders attached to these flaps. These piezobenders have a much higher bandwidth than the servomotors, but the control authority is significantly lower. For results obtained with these flaps, see, e.g., [Navalkar et al. \(2016\)](#). The experiments shown in this chapter are obtained without using the piezobenders on the free-floating flaps as a control input. Furthermore, the wind turbine tower has free yaw capabilities, since it is mounted using two bearings. For the experiments performed for this chapter, the yaw angle of the tower is fixed using a clamp.

To simulate the generator torque of the turbine, the generator is connected in series to a dump load (not shown in the figure). The generator torque is then controlled by setting the current to the dump load.

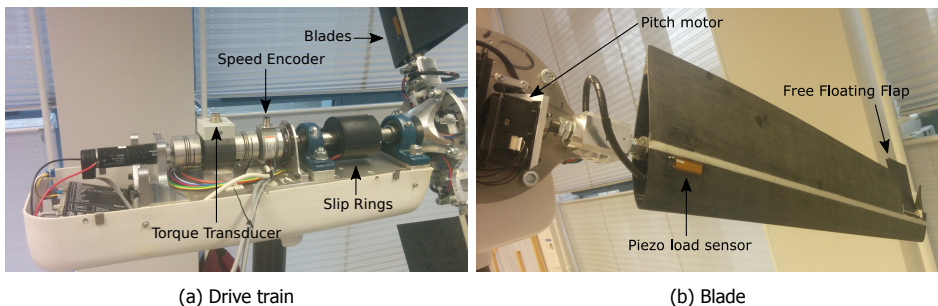


Figure 2.4: Photographs of the drive train (a) and the blade (b) of the two-bladed wind turbine used for the experiments.

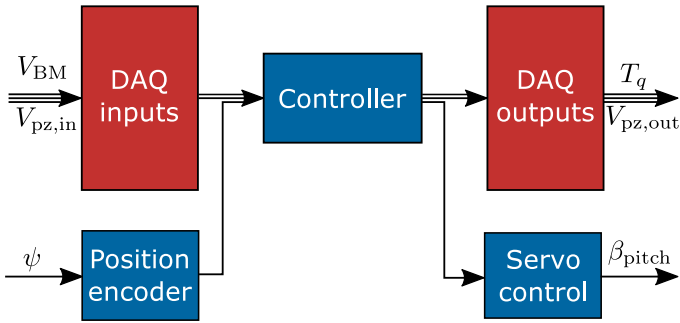


Figure 2.5: A schematic representation of the interconnection between the data acquisition boards (DAQs) and the controller. The blue blocks run at 200Hz, while the red blocks sample at 2kHz. The inputs are the voltages of the bending moments (V_{BM}) and the piezo flaps ($V_{pz,in}$), as well as the rotor word azimuth ψ . Outputs are the generator torque T_q , the desired flap voltage $V_{pz,out}$ and the desired pitch angles β_{pitch} .

2.2.3. Real-time environment

As described above, the system contains 3 actuators (two servomotors controlling the pitch angle and the dump load controlling the generator torque) and sensors (measuring the loads on both blades and the azimuth angle). The communication between the sensors and actuators is realized through Simulink Real-Time (Mathworks, 2015). The desired controller is developed in Matlab-Simulink, and subsequently compiled on a target computer.

The target computer, an HP workstation Z600, communicates with the wind turbine through a National Instruments PCI-6259 data acquisition board (DAQ) as shown schematically in Figure 2.5. The DAQs have a sampling time of 2 kHz, while the shaft position encoder and the Dynamixel servo motors operate at 200 Hz. The controller is configured at the same sampling frequency, since the computation time of the SPRC algorithm on the target computer is slightly below 0.005 s. With a more powerful target computer, it is most likely possible to further decrease this computation time. To enable communication between the signals with different sampling frequencies, the Rate Transition functionality in Simulink is used (Mathworks, 2015).

2.3. Subspace Predictive Repetitive Control

In this section, the Subspace Predictive Repetitive Control (SPRC) methodology is described. In the following subsection, the motivation for using SPRC is given. Subsequently, Section 2.3.2 elaborates on the identification, and Section 2.3.3 covers the Repetitive Control (RC) implementation.

2.3.1. Motivation

As mentioned in the introduction, the dominant frequencies of periodic wind turbine blade loads during operation are dependent on the rotor speed. The once-per-revolution load frequency is called 1P, and its higher harmonics 2P, 3P, etc. As these frequencies form the majority of the loads in wind turbines, the control effort can also be restricted to these frequencies. This can be achieved by using basis functions containing sinusoids of the required frequencies, see Section 2.3.3.

Due to the periodic nature of the loads, RC is an effective methodology to handle these loads. RC determines the optimal control sequence for the next period, and iterates this process over time. Subsequently, the control signal also adapts to changing operating conditions. This makes RC suitable for wind turbine control, as the wind flow is highly variable in real-world operating conditions. Varying rotor speed can be a problem for RC in turbine load control, since this essentially changes the period of the RC problem. However, in this chapter, modifications to the RC algorithm are presented that negate this problem.

To find the optimal RC sequence, a model of the system is necessary. By using data-driven subspace identification methods, the derived model is able to adapt to changing operating conditions. As new data becomes available, it replaces old data based on a forgetting factor λ . This procedure is further explained in the next section.

These combined features of SPRC make the methodology suitable for the task at hand. First, subspace identification is executed online, and the obtained system is used to adapt the RC law. The optimal control sequence is then implemented over the next rotation period to achieve the desired load disturbance rejection.

2.3.2. Subspace Identification

The wind turbine system is identified online using Markov parameters, and this identified system is then used to establish a repetitive control law using basis functions. This method is similar to the one presented in [Navalkar et al. \(2014\)](#), although essential additions have been made to improve performance for varying rotor speed.

The wind turbine system is assumed to be represented by a discrete Linear Time-Invariant (LTI) system with unknown periodic disturbances ([Houtzager et al., 2012](#))¹:

$$x_{k+1} = Ax_k + Bu_k + Ed_k + Ke_k \quad (2.1)$$

$$y_k = Cx_k + Fd_k + e_k, \quad (2.2)$$

where $x_k \in \mathbb{R}^n$ is the state vector, $u_k \in \mathbb{R}^r$ the input vector; in this case the pitch angles of both blades. The output vector $y_k \in \mathbb{R}^l$ contains the blade loads as measured by the MFCs mounted on the blades. Disturbance $d_k \in \mathbb{R}^m$ represents the periodic component on the load of the blades, and $e_k \in \mathbb{R}^l$ the aperiodic component. Rewriting these equations in descriptor form, the following state-space equations

¹The framework is also able to work with periodic time-varying systems. For representation reasons, an LTI system is chosen here.

are obtained:

$$x_{k+1} = \tilde{A}x_k + Bu_k + \tilde{E}d_k + Ky_k \quad (2.3)$$

$$y_k = Cx_k + Fd_k + e_k, \quad (2.4)$$

with $\tilde{A} = A - KC$ and $\tilde{E} = E - KF$. The difference operator δ is then defined as:

$$\delta d_k = d_k - d_{k-p} = 0,$$

where the subscripts indicate the time instance, and P is the time of one full rotation of the blades. Similarly, the (nonzero) signals δu , δy and δe can be defined. Applying the δ -notation on the innovation system yields a representation where the d -term disappears:

$$\delta x_{k+1} = \tilde{A}\delta x_k + B\delta u_k + K\delta y_k \quad (2.5)$$

$$\delta y_k = C\delta x_k + \delta e_k. \quad (2.6)$$

Next, the stacked vector $\delta U_k^{(p)}$ for a given past window p is defined as:

$$\delta U_k^{(p)} = \begin{bmatrix} u_k - u_{k-p} \\ u_{k+1} - u_{k+1-p} \\ \vdots \\ u_{k+p-1} - u_{k+p-1-p} \end{bmatrix}, \quad (2.7)$$

and similarly $\delta Y_k^{(p)}$. Then, by elevating (2.5), the state vector δx_{k+p} can be written as:

$$\delta x_{k+p} = \tilde{A}^p \delta x_k + \begin{bmatrix} \mathcal{K}_u^{(p)} & \mathcal{K}_y^{(p)} \end{bmatrix} \begin{bmatrix} \delta U_k^{(p)} \\ \delta Y_k^{(p)} \end{bmatrix},$$

with:

$$\mathcal{K}_u^{(p)} = [\tilde{A}^{p-1}B \quad \tilde{A}^{p-2}B \quad \dots \quad B] \quad (2.8)$$

$$\mathcal{K}_y^{(p)} = [\tilde{A}^{p-1}K \quad \tilde{A}^{p-2}K \quad \dots \quad K]. \quad (2.9)$$

Here, similar to [Houtzager et al. \(2012\)](#), it is assumed that the system given in Equations (2.5) and (2.6) is asymptotically stable, controllable and observable. It is important to select p sufficiently large, such that $\tilde{A}^j \approx 0 \forall j \geq p$, ([Chiuso, 2007](#)). For such p , the equation above can be simplified to:

$$\delta x_{k+p} \approx \begin{bmatrix} \mathcal{K}_u^{(p)} & \mathcal{K}_y^{(p)} \end{bmatrix} \begin{bmatrix} \delta U_k^{(p)} \\ \delta Y_k^{(p)} \end{bmatrix}. \quad (2.10)$$

Substituting this result into (2.6) yields

$$\delta y_k \approx \begin{bmatrix} C\mathcal{K}_u^{(p)} & C\mathcal{K}_y^{(p)} \end{bmatrix} \begin{bmatrix} \delta U_k^{(p)} \\ \delta Y_k^{(p)} \end{bmatrix} + \delta e_k. \quad (2.11)$$

During online identification, the values of the parameters \mathcal{CK} are estimated based on the measurements y and u . These parameters define the behavior of the wind turbine system, and are called the Markov parameters $\Xi \in \mathbb{R}^{l \times ((r+l) \cdot p)}$:

$$\Xi = \begin{bmatrix} \mathcal{CK}_u^{(p)} & \mathcal{CK}_y^{(p)} \end{bmatrix}. \quad (2.12)$$

A batchwise computation of the Markov estimates $\hat{\Xi}$ at time instant k is then performed by finding the unique solution to the least-squares equation

$$\hat{\Xi}_k = \arg \min_{\hat{\Xi}_k} \sum_{i=-\infty}^k \left\| \delta y_i - \lambda \hat{\Xi}_k \begin{bmatrix} \delta U_{i-p}^{(p)} \\ \delta Y_{i-p}^{(p)} \end{bmatrix} \right\|_2^2. \quad (2.13)$$

In this algorithm, a forgetting factor λ of between 0 and 1 is introduced to adapt to changes in the system dynamics. To improve the robustness of the identification, a large value (e.g., $\lambda = 0.99999$) is chosen, which, as a rule of thumb, represents a window of 10^6 samples (Gustafsson, 2000). Subsequently, the summation given in (2.13) no longer needs an infinite past window. From the definition of Ξ as shown in (2.12), it follows that $\hat{\Xi}$ at time instant k contains estimates of the following matrices:

$$\hat{\Xi}_k = \begin{bmatrix} \widehat{CA^{p-1}B} & \widehat{CA^{p-2}B} & \dots & \widehat{CB} & \widehat{CA^{p-1}K} & \widehat{CA^{p-2}K} & \dots & \widehat{CK} \end{bmatrix}_k. \quad (2.14)$$

It is important that the input of the system is persistently exciting and of a sufficiently high order, in order to guarantee a unique solution of the least-squares problem (2.13) (Verhaegen and Verduyt, 2007). The recursive equivalent of this problem is then solved using a QR recursive least-squares algorithm as presented in van der Veen *et al.* (2012).

Typically, adaptive control methodologies that combine online identification with simultaneous control cannot guarantee certain stability and performance characteristics (Dong and Verhaegen, 2008). Therefore, the method proposed in Navalkar *et al.* (2015) to first run the controller in identification phase at the beginning of each experiment is used.

2.3.3. Repetitive Control

For repetitive control, the output needs to be predicted over period P , with $P \geq p$ but usually $P \gg p$. To achieve this, the output equation needs to be lifted over P to obtain $\delta P_{k+p}^{(P)}$. For this purpose, the Toeplitz matrix $\tilde{H}^{(P)} \in \mathbb{R}^{(l \cdot P) \times (l \cdot P)}$ and the extended observability matrix $\tilde{\Gamma}^{(P)} \in \mathbb{R}^{(l \cdot P) \times n}$ are defined:

$$\tilde{H}^{(P)} = \begin{bmatrix} 0 & 0 & 0 & \dots \\ CB & 0 & 0 & \dots \\ C\tilde{A}B & CB & 0 & \dots \\ \vdots & \vdots & \ddots & \vdots \\ C\tilde{A}^{p-1}B & C\tilde{A}^{p-2}B & C\tilde{A}^{p-3}B & \dots \\ 0 & C\tilde{A}^{p-1}B & C\tilde{A}^{p-2}B & \dots \\ 0 & 0 & C\tilde{A}^{p-1}B & \ddots \\ \vdots & \vdots & \ddots & \ddots \end{bmatrix} \quad (2.15)$$

$$\tilde{\Gamma}^{(P)} = \begin{bmatrix} C \\ C\tilde{A} \\ C\tilde{A}^2 \\ \vdots \\ C\tilde{A}^p \\ 0 \\ \vdots \\ 0 \end{bmatrix}. \quad (2.16)$$

Similarly, $H^{(P)}$ and $\Gamma^{(P)}$ are defined by replacing all \tilde{A} by A . Likewise, $\tilde{G}^{(P)}$ is defined by replacing B by K in $\tilde{H}^{(P)}$. Using these matrices, the lifted output equation can be written as

$$\delta Y_{k+p}^{(P)} = \tilde{\Gamma}^{(P)} \delta x_{k+p} + [\tilde{H}^{(P)} \quad \tilde{G}^{(P)}] \begin{bmatrix} \delta U_{k+p}^{(P)} \\ \delta Y_{k+p}^{(P)} \end{bmatrix}. \quad (2.17)$$

Substituting the approximation of δx_k as given in (2.10) yields

$$\delta Y_{k+p}^{(P)} = \tilde{\Gamma}^{(P)} \begin{bmatrix} \mathcal{K}_u^{(P)} & \mathcal{K}_y^{(P)} \end{bmatrix} \begin{bmatrix} \delta U_k^{(P)} \\ \delta Y_k^{(P)} \end{bmatrix} + [\tilde{H}^{(P)} \quad \tilde{G}^{(P)}] \begin{bmatrix} \delta U_{k+p}^{(P)} \\ \delta Y_{k+p}^{(P)} \end{bmatrix}. \quad (2.18)$$

Notice that the first $(P-p) \cdot r$ columns of $\mathcal{K}_u^{(P)}$ and $\mathcal{K}_y^{(P)}$ are 0. It is also key to note that all the matrices from (2.18) can be constructed by using the elements of the Markov estimates $\hat{\Xi}$. The future output $Y_{k+p}^{(P)}$ are then predicted using the previous outputs $Y_k^{(P)}$ and previous and future inputs $U_k^{(P)}$ and $U_{k+p}^{(P)}$. Subsequently, (2.18) can be rewritten as:

$$Y_{k+p}^{(P)} = \begin{bmatrix} I_{L_P} & \widehat{\Gamma^{(P)} \mathcal{K}_u^{(P)}} & \widehat{\Gamma^{(P)} \mathcal{K}_y^{(P)}} \end{bmatrix} \begin{bmatrix} Y_k^{(P)} \\ \delta U_k^{(P)} \\ \delta Y_k^{(P)} \end{bmatrix} + \hat{H}^{(P)} \delta U_{k+p}^{(P)}. \quad (2.19)$$

This result is obtained by using the following equality's:

$$\begin{aligned} (I - \tilde{G}^{(P)})^{-1} \tilde{\Gamma}^{(P)} &= \Gamma^{(P)} \\ (I - \tilde{G}^{(P)})^{-1} \tilde{H}^{(P)} &= H^{(P)}. \end{aligned}$$

Subsequently, the system is transformed into a state space representation, such that classic state feedback control can be applied (Hallouzi *et al.*, 2006):

$$\underbrace{\begin{bmatrix} Y_{k+P}^{(P)} \\ \delta U_{k+P}^{(P)} \\ \delta Y_{k+P}^{(P)} \end{bmatrix}}_{\hat{\mathcal{X}}_{k+P}} = \underbrace{\begin{bmatrix} I_{l \cdot P} & \Gamma^{(P)} \widehat{\mathcal{K}}_u^{(P)} & \Gamma^{(P)} \widehat{\mathcal{K}}_y^{(P)} \\ 0_{(r \cdot P) \times (l \cdot P)} & 0_{r \cdot P} & 0_{(r \cdot P) \times (l \cdot P)} \\ 0_{l \cdot P} & \Gamma^{(P)} \widehat{\mathcal{K}}_u^{(P)} & \Gamma^{(P)} \widehat{\mathcal{K}}_y^{(P)} \end{bmatrix}}_{\hat{\mathcal{A}}_k} \underbrace{\begin{bmatrix} Y_k^{(P)} \\ \delta U_k^{(P)} \\ \delta Y_k^{(P)} \end{bmatrix}}_{\hat{\mathcal{X}}_k} + \underbrace{\begin{bmatrix} \hat{H}^{(P)} \\ I_{r \cdot P} \\ \hat{H}^{(P)} \end{bmatrix}}_{\hat{\mathcal{B}}_k} \delta U_{k+P}^{(P)}. \quad (2.20)$$

Next, a state feedback controller is synthesized using a Discrete Algebraic Riccati Equation (DARE). As mentioned in Section 2.3.1, the goal of this IPC implementation is to target the 1P and 2P loads. As a result, the control signal should only contain these frequencies. To achieve this, a basis function projection is proposed such that U_k only contains sinusoids of the desired frequencies. This is accomplished by using the following transformation matrix $\phi \in \mathbb{R}^{(r \cdot P) \times (4r)}$:

$$\phi = \begin{bmatrix} \sin \frac{2\pi}{P} & \cos \frac{2\pi}{P} & \sin \frac{4\pi}{P} & \cos \frac{4\pi}{P} \\ \sin \frac{4\pi}{P} & \cos \frac{4\pi}{P} & \sin \frac{8\pi}{P} & \cos \frac{8\pi}{P} \\ \vdots & \vdots & \vdots & \vdots \\ \sin 2\pi & \cos 2\pi & \sin 4\pi & \cos 4\pi \end{bmatrix} \otimes I_r, \quad (2.21)$$

where the symbol \otimes represent the Kronecker product. Considering that the bandwidth of the pitch motors limits the control authority to the 1P and 2P frequencies, only these frequencies are considered. Notice that by taking a linear combination of the sinusoids in this matrix, a control signal containing only the desired 1P and 2P frequencies is obtained. The control input U_k is determined using:

$$U_k^{(P)} = \phi \theta_j, \quad (2.22)$$

where the subscript j represents the rotation count. Subsequently, the vector $\theta \in \mathbb{R}^{4r}$, that determines the amplitude and phase of the sinusoids, is updated every rotation period P .

Note that the system of (2.20) is quite high-dimensional, as $\hat{\mathcal{A}} \in \mathbb{R}^{((2l+r) \cdot P)^2}$. Apart from limiting the frequency content of the control signal, the transformation also reduces the dimensionality of the DARE, as θ only contains $4r$ elements, substantially reducing the computational load of the problem.

As the pitch angles are now limited to sinusoidal signals with frequencies 1P and 2P, and the system is assumed to be linear over one period P , the load signals Y_k is also limited to these frequencies. As a result, we can transform this signal using the same transformation matrix:

$$Y_k = \phi \bar{Y}_j. \quad (2.23)$$

Note that for this transformation to be possible, the number of inputs needs to be equal to the number of outputs, i.e., $r = l$. However, this does not limit the possibilities of the algorithm for load alleviation, since generally the outputs are

chosen as the root bending moments of each blade, and the inputs are the pitch angles of the blades. Consequently, both r and l equal the number of blades.

Similar to (2.23), the lower dimensional signals can be found by using the inverse transformation ϕ^+ , where $+$ represents the Moore-Penrose pseudo-inverse:

$$\theta_j = \phi^+ U_k, \quad \bar{Y}_j = \phi^+ Y_k. \quad (2.24)$$

Using (2.22) and (2.23), we can rewrite (2.20) in the following lower dimensional form:

$$\underbrace{\begin{bmatrix} \bar{Y}_{j+1}^{(P)} \\ \delta\theta_{j+1}^{(P)} \\ \delta\bar{Y}_{j+1}^{(P)} \end{bmatrix}}_{\hat{\bar{X}}_{j+1}} = \underbrace{\begin{bmatrix} I_{l,P} & \phi^+ \Gamma^{(P)} \widehat{\mathcal{K}}_u^{(P)} \phi & \phi^+ \Gamma^{(P)} \widehat{\mathcal{K}}_y^{(P)} \phi \\ 0_{l,P} & 0_{r,P} & 0_{l,P} \\ 0_{l,P} & \phi^+ \Gamma^{(P)} \widehat{\mathcal{K}}_u^{(P)} \phi & \phi^+ \Gamma^{(P)} \widehat{\mathcal{K}}_y^{(P)} \phi \end{bmatrix}}_{\hat{\bar{A}}_j} \underbrace{\begin{bmatrix} \bar{Y}_j^{(P)} \\ \delta\theta_j^{(P)} \\ \delta\bar{Y}_j^{(P)} \end{bmatrix}}_{\hat{\bar{X}}_j} + \underbrace{\begin{bmatrix} \phi^+ \hat{H}^{(P)} \phi \\ I_{r,P} \\ \phi^+ \hat{H}^{(P)} \phi \end{bmatrix}}_{\hat{\bar{B}}_j} \delta\theta_{j+1}^{(P)}. \quad (2.25)$$

The size of this projected matrix $\bar{\mathcal{A}} \in \mathbb{R}^{12l \times 12l}$ is significantly smaller than the original matrix $\mathcal{A} \in \mathbb{R}^{3lP \times 3lP}$. As usually $P \gg 4$, using a basis function transformation significantly reduces the order of the optimization problem. Moreover, the transformation guarantees that the input U_k is a smooth signal with the desired frequency content.

Next, a state feedback control problem is solved to determine the control input θ . The state feedback gain is obtained by minimizing the following quadratic cost function

$$J = \sum_{j=0}^{\infty} \left\| \left(\bar{X}_j \right)^T Q \bar{X}_j + (\delta\theta_j)^T R \delta\theta_j \right\|_2^2, \quad (2.26)$$

where Q and R are weighing matrices for the state and input vector respectively. As in LQR problems, the state feedback control gain can be found by solving the DARE at iteration j using an initial estimate of P_R :

$$P_{R,j+1} = Q + \bar{\mathcal{A}}_j^T (P_{R,j} - P_{R,j} \bar{\mathcal{B}}_j^T (R + \bar{\mathcal{B}}_j^T P_{R,j} \bar{\mathcal{B}}_j)^{-1} \bar{\mathcal{B}}_j^T P_{R,j}) \bar{\mathcal{A}}_j.$$

Subsequently, the optimal state feedback gain K_f is defined as:

$$K_{f,j} = \left(R + \bar{\mathcal{B}}_j^T P_{R,j} \bar{\mathcal{B}}_j \right)^{-1} \bar{\mathcal{B}}_j^T P_{R,j} \bar{\mathcal{A}}_j$$

Now, it is possible to determine the control input vector $\delta\theta_j$, which, after a transformation, can be implemented on the wind turbine. Using the state feedback law:

$$\delta\theta_{j+1} = -K_{f,j} \bar{X}_j. \quad (2.27)$$

Then, using $\delta\theta_{j+1} = \theta_{j+1} - \theta_j$ and introducing variables α and β :

$$\theta_{j+1} = \alpha\theta_j - \beta K_{f,j} \begin{bmatrix} \bar{Y}_j \\ \delta\theta_j \\ \delta\bar{Y}_j \end{bmatrix}. \quad (2.28)$$

In order to add the possibility to manipulate the convergence characteristics of the algorithm, the tuning parameters α and β are included. Both α and β are defined in the interval $[0, 1]$, and give a weight on new and older data respectively. The input signal U_k can now be determined by using the inverse basis function transformation as given in (2.22).

One problem that needs to be dealt with, is the potential variation of rotor speed due to, e.g., wind turbulence or changing inflow wind speed. Therefore, a phase shift between input and output could occur. To prevent this, the rotor azimuth ψ_k measured through the shaft encoder, which is equal to the angle $2\pi k/P$ at time instant k , can be used. As a result, the algorithm is also able to account for variations in rotor velocity. In this chapter, the parameter P , which represents one full rotation, is chosen slightly smaller than the expected rotation period, in order to guarantee a new control sequence at the end of each rotation. This sequence is then implemented when the rotation is completed. The control input at time instant k now becomes

$$u_k = ([\sin \psi_k \quad \cos \psi_k \quad \sin 2\psi_k \quad \cos 2\psi_k] \otimes I_r) \theta_j, \quad (2.29)$$

where input $u_k \in \mathbb{R}^r$ represents the individual pitch angles that are implemented on the wind turbine system at time instant k .

2.3.4. Benchmark controller

As a benchmark load alleviation controller, Conventional Individual Pitch Control (CIPC) is used, first introduced in [Bossanyi \(2003\)](#). In this approach, the MBC transformations ([Bir, 2008](#)) are used to obtain the yaw and tilt moments on the rotor plane. Subsequently, a notch filter and Proportional-Integral (PI) controller are applied, followed by the inverse MBC transformation, to determine the individual pitch actions. Figure 2.6 shows a schematic representation of this control methodology.

In terms of controller implementation, CIPC can be considered less complex than SPRC. The main reason for this is the fact that no system identification is necessary,

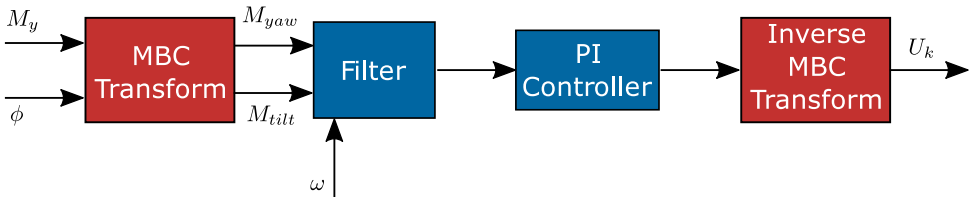


Figure 2.6: A schematic representation of the conventional IPC algorithm, that is used as a benchmark individual pitch controller in this chapter.

instead using the relatively straightforward MBC transformations. However, similar to the SPRC algorithm, some controller parameters do need to be tuned in CIPC to guarantee performance. In this case, these parameters are the gains of the PI-controllers shown in Figure 2.6.

2.4. Results

The control methodology presented in Section 2.3 is evaluated in the wind tunnel setup presented in Section 3.4. As discussed in Section 2.2.1, four different wind conditions have been studied for three different wind speeds. First, the results for constant wind conditions is presented, followed by the experiments with changing wind conditions.

2.4.1. Constant operating conditions

The results of the SPRC-IPC implementation on the scaled wind turbine in constant operating conditions are presented. All figures shown are for an inflow wind speed of 5 m/s.

SPRC is compared with Conventional IPC (CIPC, see [Bossanyi \(2003\)](#)) to evaluate the performance of the control algorithm. This is done by executing 120 s experiments for both control strategies, as well as a baseline experiment with no IPC. For clarity, the time domain figures show the loads over smaller time intervals, whereas the power spectra and load reductions are determined using the data of the entire 120 s interval. With a sampling interval of 200 Hz, this results in data sets of 24000 load measurements.

The loads on the blades for the three previously introduced strategies, for the static 0° grid mode, are shown in Figure 2.7a. This figure shows that both methods significantly decrease the periodic loads. With CIPC, the variance of the blade loads is reduced with 61.7%, while with SPRC the reduction is even larger: 86.8%.

Figure 2.8 shows the individual pitch action of the blades when SPRC is applied.

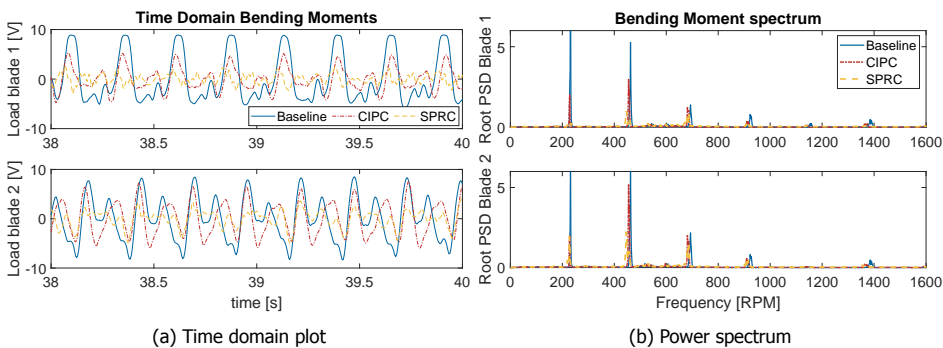


Figure 2.7: Time domain (left) and frequency domain (right) plot of the loads on blades 1 (top) and 2 (bottom) of the turbine for three different situations: the baseline case where no IPC is implemented, CIPC and SPRC. The inflow wind speed is 5 m/s with a static 0° grid configuration (centerline TI: 2.5%), resulting in a rotor speed of 230 rpm.

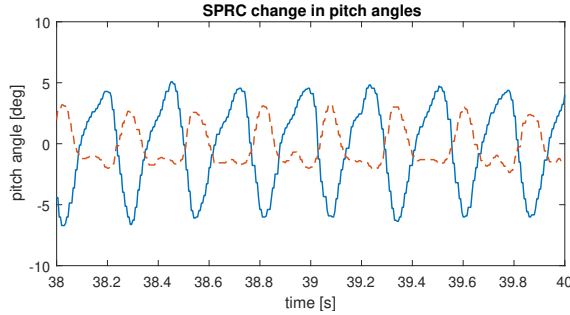


Figure 2.8: The individual pitch angles for blade 1 (blue) and blade 2 (red) as applied on the turbine by the SPRC algorithm. The inflow wind speed is 5 m/s with a static 0° grid configuration (centerline TI: 2.5%), resulting in an rotor speed of 230 rpm.

Clearly, the signals are not symmetrical. This is caused by the rotor imbalance and other system imperfections, which SPRC accounts for by generating pitch angles for each blade individually. These signals are constructed using exclusively sinusoids of 1P and 2P frequency.

The frequency domain plot of the signals shown in Figure 2.7a are depicted in Figure 2.7b. As expected, this figure shows large peaks at the frequencies 1P and 2P. At higher harmonics (3P, 4P, etc.) these peaks become significantly smaller, validating the choice to only apply control on the 1P and 2P frequencies. Figure 2.7b also shows that SPRC achieves a substantial reduction of the 1P and 2P loads compared to both the baseline case and Conventional IPC.

It is clear that at constant, low turbulent conditions, SPRC achieves a larger load reduction than conventional IPC. These results are in line with the experiments with no turbulence done by Navalkar *et al.* (2015). In the following, it is shown that positive results can also be achieved at higher turbulent wind conditions generated by the active grid.

The excitation protocol that generates the highest turbulence is the lidar mode (see Table 2.1). As a result, significantly higher blade loads are expected for this mode compared to the results shown above. This can also be observed in Figure 2.9a. The peak loads in this figure are more irregular than in Figure 2.7a due to the loads induced by turbulence. Nonetheless, both control strategies still clearly produce load reductions, although it is less clear to see which of the two performs better. Evaluating the variance of the blade loads shows a reduction of 57.0% for CIPC and 65.1% for SPRC.

The power spectrum of these measurements with the active grid in lidar mode are shown in Figure 2.9b. Notice that the rotor speed slightly decreased compared to Figure 2.7b, from 230 rpm to 210 rpm. This can be explained by the active grid: the inflow velocity is 5 m/s *before* the active grid. As the grid is enabled, it reduces the wind velocity perpendicular to the turbine, resulting in a decrease of the rotor speed.

Figure 2.9b also exhibits a much broader peak around the 1P and 2P frequen-

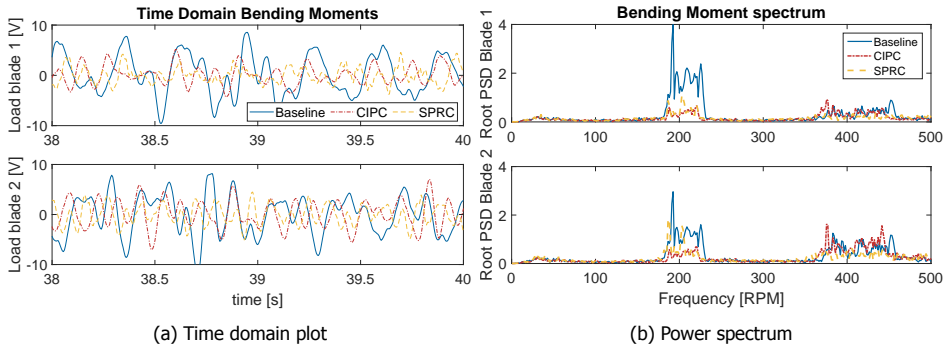


Figure 2.9: Time domain (left) and frequency domain (right) plot of the loads on both blades of the turbine for three different situations: the baseline case of no IPC, CIPC and SPRC. The inflow wind speed is 5 m/s with a lidar grid configuration (centerline TI: 8.8%), resulting in a rotor speed of 210 rpm.

cies than the low-TI case. Due to the turbulence, the rotor speed fluctuates more. Consequently, the power spectrum shows a 1P peaks over a broad range of frequencies in which the rotor speed moves. Despite the changing rotor speed, Figure 2.9b clearly shows a reduction of the 1P loads attained by both controllers, and SPRC also achieves a 2P load reduction.

Similar results are obtained for the experiments at different wind speeds and with other grid modes active. All these results are summarized in Table 2.2. This table also shows the performance of SPRC when it only targets the 1P loads.

Notice that out of the 12 experiments, SPRC outperforms CIPC in 10. Only in one case (Static 45° with 4 m/s), SPRC is unable to reduce the variance of the loads. On average, SPRC for 1P and 2P achieves a reduction of load variance of 59%, whereas conventional IPC leads to an average reduction of 49%. Furthermore, on average, the variance of the pitch signals is 21% lower for SPRC compared to CIPC, indicating that the performance improvement does not come at the cost of a higher actuator duty.

Based on these results, it can be said that SPRC is able to reduce blade loads in more realistic high turbulent wind conditions. Next, the performance of SPRC in changing operating conditions is discussed.

Table 2.2: Load reductions compared to baseline (no control) for all investigated inflow conditions. The numbers indicate the reduction of the variance of the load in % for all 4 grid modes. The different inflow velocities of the experiments (4, 4.5 and 5 m/s) are also given.

	Static 0° (TI: 2.5%)			Static 45° (TI: 3.7%)			Lidar (TI: 8.8%)			Gusts (TI: 4.2%)		
	4 m/s	4.5 m/s	5 m/s	4 m/s	4.5 m/s	5 m/s	4 m/s	4.5 m/s	5 m/s	4 m/s	4.5 m/s	5 m/s
CIPC [%]	38.7	56.8	61.7	55.9	74.4	37.1	17.6	50.6	57.0	38.0	52.8	47.7
SPRC												
1P [%]	57.3	53.1	61.7	1.1	62.6	47.2	17.4	44.4	23.4	-6.4	84.4	72.0
1P2P [%]	73.1	82.9	86.8	-20.2	44.2	93.0	27.8	52.4	65.1	59.4	81.3	57.7
Var(u)												
1P [%]	24.1	36.0	35.6	36.5	-15.0	-12.8	44.2	5.1	-12.8	-72.7	26.0	-3.8
1P2P [%]	-29.0	25.8	-2.4	70.4	61.4	-32.9	29.0	43.7	10.7	51.4	29.7	-4.6

2.4.2. Changing operating conditions

The authors of [Navalkar et al. \(2015\)](#) show that SPRC is able to adapt to changing operating conditions in a laminar wind flow. In this section, it is shown that similar results can be obtained in more turbulent wind conditions. Experiments are conducted where either the collective pitch angles or the wind speed is changed during operation. The performance of SPRC in these changing conditions is evaluated.

With adaptive SPRC, the system parameters are being identified continuously: as defined in (2.13), new values of the Markov parameters are determined at every time instant k . Due to this feature, the algorithm is able to quickly adapt to changing operating conditions. As new measurements show a change in behavior, the system parameters are changed accordingly.

The first adaptive experiment was conducted with a wind speed of 4.2 m/s using the Gusts grid protocol. Figure 2.10a shows the effect of changing the collective pitch during operation, resulting in a decrease of rotor speed from 240 to 210 rpm. The blade loads and pitch angles for both blades are shown for SPRC and the baseline case of no control. This figure shows that the loads are again reduced after a short increase in blade loads when the pitch is changed at approximately 40 seconds.

The amplitudes θ of the sinusoids that determine the pitch signal of blade 1 are shown in Figure 2.11. Here, it can be seen that the control input is quickly changed after the change of operating conditions. The oscillations in Figure 2.11 show that the algorithm converges to the optimal values in approximately 15 seconds, and subsequently it can be seen in Figure 2.10a that the loads are reduced at the end of the experiment.

Figure 2.10b shows the power spectral density of the loads. As the rotor speed is changed due to the altered collective pitch, two peaks are visible at each harmonic. This figure demonstrates that SPRC significantly reduces the 1P and 2P blade loads of the turbine even when operating conditions are altered.

In the second experiment, the effect of a change in wind speed on the effec-

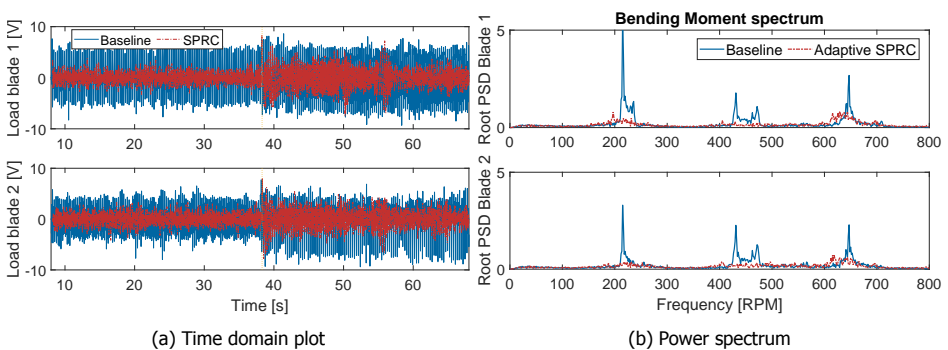


Figure 2.10: Adaptive SPRC versus no IPC for a change in collective pitch angle (from 2 to 10°). Shown on the left are the blade loads over the time of the experiments. The vertical line indicates the moment the collective pitch angles are changed. On the right, the power spectrum of the blade moments is shown.

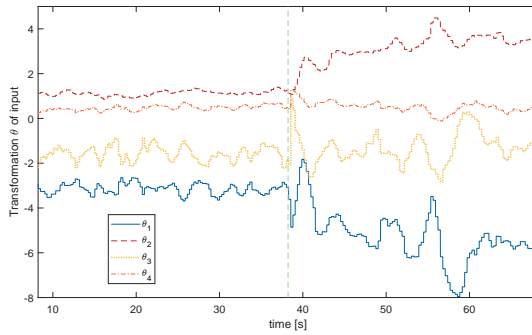


Figure 2.11: The values of θ for blade 1, see (2.29). The vertical line indicates the moment the collective pitch angles are changed.

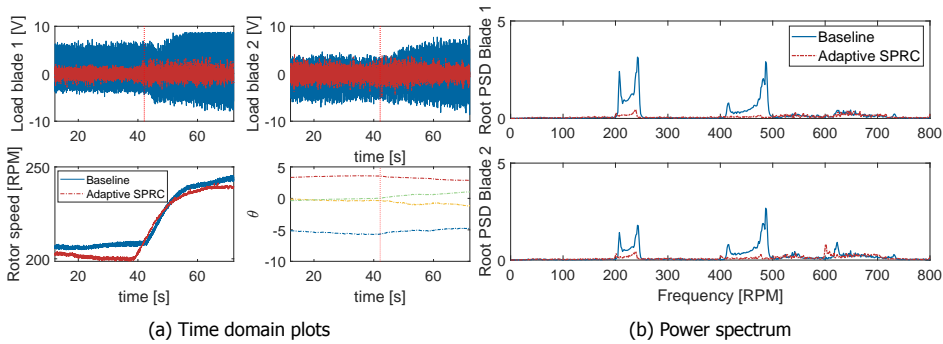


Figure 2.12: Adaptive SPRC (red) versus no control (blue) for a wind speed change from 4.5 m/s to 5 m/s after approximately 40 seconds. In these experiments, the static 45° grid protocol was used. The upper left figures show the loads of blade 1 and 2 respectively, the lower left figures the rotor speed and the values of input θ for blade 1. The right figures show the power spectrum of the blade moments.

tiveness of SPRC is shown. This experiment is conducted using the static 45° grid protocol. During the experiment, the wind speed is increased from 4.5 m/s to 5 m/s, while the collective pitch stays constant at 2°. This results in a significant increase in rotor speed: from approximately 200 rpm to 240 rpm.

The results of this experiment are shown in Figures 2.12a and 2.12b. Comparing with Figure 2.10a shows that a changing wind speed has a smaller effect on the performance of SPRC than changing the collective pitch. As can be seen in the bottom right figure, the control input only changes marginally after the wind speed is increased. The upper figures show that with SPRC, the loads barely increase when the wind speed increases, even though in the baseline case there is a substantial increase.

The two example cases in this section show that adaptive SPRC, where the system parameters are updated using online subspace identification, is able to quickly adjust the optimal RC when circumstances alter, resulting in a varying rotor speed, even in realistic turbulence conditions.

2.5. Conclusions

This chapter presents a series of unique wind tunnel experiments that have been conducted by implementing a large active grid on an open jet wind tunnel. It is shown that with this active grid, it is possible to produce wind conditions similar to real world conditions. Furthermore, the active grid creates reproducible wind conditions, which enables a fair evaluation of different control methodologies.

Using a two-bladed scaled wind turbine, the effectiveness of Subspace Predictive Repetitive Control (SPRC) for individual pitch control in high-turbulent wind conditions is evaluated. Dedicated changes were made to the SPRC algorithm to ensure performance in the case of a varying rotor speed. The results of the wind tunnel experiments show that it is possible to reduce the variance of the blade loads significantly using SPRC under realistic high-turbulent wind conditions. This is achieved by specifically targeting the 1P and 2P loads on the blades using basis functions.

A comparison with Conventional Individual Pitch Control (CIPC) shows that overall, SPRC outperforms CIPC in both low and high turbulent experiments. SPRC shows better performance in both blade load reduction and pitch actuator duty cycle. Averaged over all the different experiments, SPRC achieves a reduction of the blade load the variance of 59%, an improvement of 10% compared to CIPC. Furthermore, the variance of the pitch angles is on average 21% lower than with CIPC. It can therefore be concluded that the SPRC algorithm is successful at targeting only the relevant disturbances, and subsequently the load reduction is not obtained at the cost of a higher actuator duty cycle. This is supported by the power spectra of the blade loads, which shows a considerable reduction of the loads at the 1P and 2P frequencies.

Finally, the results presented here show that adaptive SPRC is able to handle changes in operating conditions, resulting in a varying rotor speed, even in high-turbulent wind conditions. Changes in pitch angles and in wind speed were applied, and in both cases, the algorithm quickly converges to a new optimum, maintaining performance.

In conclusion, the performance of data-driven repetitive individual pitch control under realistic wind conditions was demonstrated for the first time. Based on the results shown here, it can be concluded that SPRC is a very promising control methodology to achieve a load reduction of turbine blades.

3

Dynamic induction control

*ἢ δοκοῦσί τί σοι τυφλῶν διαφέρειν ὁδὸν ὀρθῶς πορευομένων
οἱ ἄνευ νοῦ ἀληθές τι δοξάζοντες;*

*Or do you think that those who hold a correct opinion without understanding
differ noticeably from blind men who go the right way?*

– Socrates, as quoted by Plato,
on the importance of solid argumentation.

As wind turbines in a wind farm interact with each other, a control problem arises that has been extensively studied in literature: how can we optimize the power production of a wind farm as a whole? A traditional approach to this problem is called induction control, in which the power capture of an upstream turbine is lowered for the benefit of downstream machines. In recent simulation studies, an alternative approach, where the induction factor is varied over time, has shown promising results. In this chapter, the potential of this Dynamic Induction Control (DIC) approach is further investigated. Only periodic variations, where the input is a sinusoid, are studied. A proof of concept for this periodic DIC approach is given by execution of scaled wind tunnel experiments, showing for the first time that this approach can yield power gains in real-world wind farms. Furthermore, the effects on the Damage Equivalent Loads (DEL) of the turbine are evaluated in a simulation environment. These indicate that the increase in DEL on the excited turbine is limited.

The contents of this chapter have been published as a peer-reviewed research paper in the Wind Energy Science journal:

J.A. Frederik, R. Weber, S. Cacciola, F. Campagnolo, A. Croce, C. Bottasso and J.W. van Wingerden, *Periodic dynamic induction control of wind farms: proving the potential in simulations and wind tunnel experiments*, Wind Energy Science **5**(1) 245 (2020).

3.1. Introduction

The interaction between wind turbines in a wind farm through their wake is a field of research as old as wind farms themselves. The wake of a turbine has a wind field with a lower velocity and a higher Turbulence Intensity (TI), resulting in a lower power production and higher relative loads for downstream turbines. To exploit this interaction between turbines, induction control (sometimes called "derating"), with induction defined as the in-wake speed deficit, has been a popular research topic in recent years. The concept of this control approach is schematically shown in Fig. 3.1. Despite initial promising results (Marden *et al.*, 2013; Gebraad *et al.*, 2013), recent studies indicate that the power gain that can be achieved with steady-state induction control is limited to non-existing (Campagnolo *et al.*, 2016b; Nilsson *et al.*, 2015; Annoni *et al.*, 2016).

An alternative approach, first mentioned in Westergaard (2013), is to actively manipulate wake recovery. Recent simulation studies (Goit and Meyers, 2015; Munters and Meyers, 2017) have shown that so-called Dynamic Induction Control (DIC) improves the power production in small to medium-sized wind farms. This approach, where the induction factor is varied over time, generates a turbulent wind flow that enables enhanced wake recovery. Consequently, downstream turbines compensate for the power loss of the upstream turbine, leading to a higher overall power production of the wind farm. In Munters and Meyers (2017), the optimal dynamic control inputs are found using a computationally expensive adjoint-based Model Predictive Control (MPC) approach. The thrust coefficient C_T' of each turbine is used as the control input. This input is only constrained by different wind turbine response times τ and maximum allowable thrust coefficient settings $C_T'^{\max}$, resulting

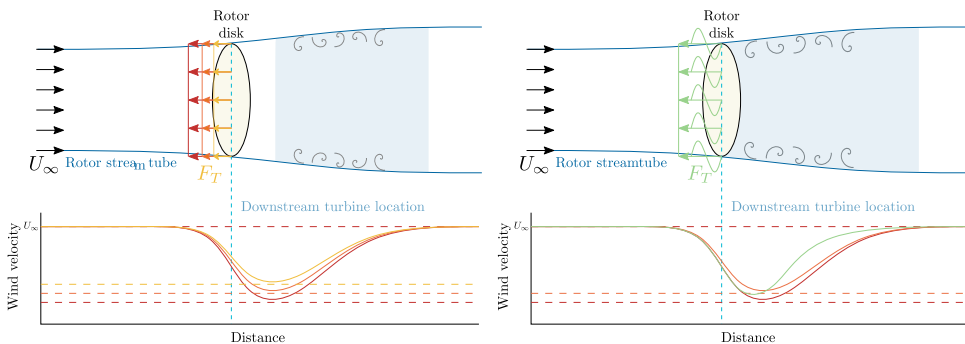


Figure 3.1: A schematic representation of a wind turbine in a flow field, showing the working principles of static (left) and dynamic induction control (right). On the top, the turbine is simplified as a rotor disk, and its streamtube - the area where the wind speed is affected by the turbine settings - is depicted. The force F_T exerted on the wind is shown for different induction settings a , where red depicts "greedy" settings that result in optimal single turbine power capture ($a = 1/3$). The orange ($a \approx 0.3$) and yellow ($a \approx 0.25$) lines depict arbitrary static derating settings that can be achieved by changing either the generator torque or the collective pitch angles of the turbine. The green lines represent periodic DIC. The bottom figures show the corresponding wind velocity profiles, with respect to inflow velocity U_∞ , as a function of the distance from the turbine. The area highlighted in blue is where a downstream turbine is typically located.

in non-smooth control signals.

In [Munters and Meyers \(2018a\)](#), a simpler approach is suggested: the induction variation is limited to a sinusoidal signal implemented on an actuator disk. This approach is here dubbed *periodic DIC*. A grid search with different amplitudes and frequencies is performed to find the periodic dynamic signal that results in the maximum energy extraction in a high-fidelity simulation environment. The effect of this approach on the streamtube and downstream wind velocity is shown in [Fig. 3.1](#). It should be noted that the applied excitation is very low-frequency.

However, no experiments have yet been executed that validate this approach on actual, either scaled or full-sized, wind turbines. Furthermore, the effects of DIC on the loads of the turbines are yet to be evaluated. This chapter aims to bridge this knowledge gap by executing a thorough evaluation of DIC both in simulation environments and in wind tunnel experiments. The effects of DIC on the loads on turbine level are evaluated using the aeroelastic tool C_p -Lambda (Code for Performance, Loads, Aeroelasticity by Multi-Body Dynamic Analysis, see [Bottasso and Croce \(2018\)](#); [Bottasso et al. \(2006\)](#)). For the wind tunnel experiments, the Atmospheric Boundary Layer (ABL) wind tunnel of the Politecnico di Milano (Polimi) is used ([Bottasso et al., 2014](#)). Three G1 scaled turbine models, which have a rotor diameter of 1.1 m and are developed by the Technical University of Munich (TUM) ([Campagnolo et al., 2016a,b,c](#)), are used.

To verify the validity of the periodic dynamic induction approach for fast wake recovery in a wind farm, a number of wind tunnel experiments in both low and high Turbulence Intensity (TI) conditions are executed. All experiments are executed at a below-rated wind speed, i.e., in operating region II. The effect of varying the amplitude and frequency of the signals is studied, and the performance of this approach is compared with state-of-the-art wind farm power maximization control strategies. As comparison cases, static induction control and wake redirection control ([Fleming et al., 2014](#)), where upstream turbines are yawed with respect to the wind direction to redirect the wake away from downstream machines, are implemented in the wind tunnel. A positive result in these experiments would be an important step towards proving the validity of this approach in real wind farms.

The structure of this chapter is as follows: in [Section 3.2](#), the DIC strategy is explained. [Sections 3.3](#) and [3.4](#) elaborate on the simulation environment and the experimental setup, respectively. In [Section 3.5](#), the simulation results are presented, followed by the experimental results obtained in the wind tunnel in [Section 3.6](#). Finally, the conclusions are drawn in [Section 3.7](#).

3.2. Control Strategy

In this section, the strategy behind dynamic induction control is discussed shortly. As mentioned in the introduction, the approach presented in [Munters and Meyers \(2018a\)](#) is used as a basis for this chapter: the thrust force of the upstream wind turbine is excited to induce wake mixing, in order for downstream turbines to increase their power capture. It is shown that the amplitude and frequency of a sinusoid determine the overall power production. The optimum found in here is a Strouhal number of $St = 0.25$, with an amplitude of the disk-based thrust coefficient

$C'_T = 1.5$. The Strouhal number is defined as $St = fD/U_\infty$ for a given frequency f , rotor diameter D and inflow velocity U_∞ , while $C'_T = 4a/(1-a)$, with a the axial induction factor (Goit and Meyers, 2015). This disk-based thrust coefficient relates to the thrust coefficient C_T as $C_T = C'_T(1-a)^2$. For the G1 models (rotor diameter $D = 1.1$ m) and an inflow velocity of 5.65 ms^{-1} , this Strouhal number would result in an excitation frequency of approximately 1.3 Hz.

However, there are some fundamental differences between Munters and Meyers (2018a). First of all, due to the size of the wind tunnel (see Section 3.4), a 3-turbine wind farm is the deepest possible array configuration. The amplitude and frequency ranges were slightly reduced due to limits on the available time in the wind tunnel. Furthermore, the number of experiments executed in this chapter is slightly lower. The amplitudes and frequencies for the wind tunnel experiments are chosen such that sufficient data points can be investigated around the optimum found in Munters and Meyers (2018a). For the aero-elastic simulations, three different frequency points are evaluated to demonstrate the effect on the turbine loads. Finally, a method should be found to vary the thrust coefficient of a real (scaled) wind turbine. The thrust coefficient can be manipulated by varying either the collective pitch angle or the generator torque of the turbine. Of these two, the former approach is the most straightforward and easy to implement. Therefore, the collective pitch angle β of the upstream model was excited periodically. This results in a slightly different thrust signal, as shown in Fig. 3.2, but simulations show that the difference in output for these input signals is limited. All these differences are summarized in Table 3.1

For the tests performed within the research described in this chapter, the standard power controller was augmented in order to enable the rotor thrust coefficients following a specific sine wave function. However, there is not a unique way of achieving this goal, since a specific thrust coefficient $C_T(\lambda, \beta)$ can be obtained by

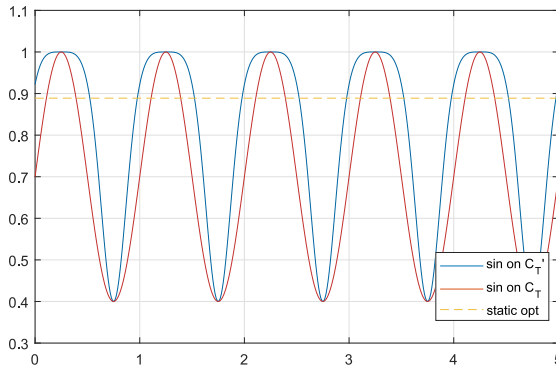


Figure 3.2: Values of C_T for different types of input signals, created using a look-up table of the G1 turbine model. The thrust coefficient is shown for three different sinusoidal excitations: on C_T , on C'_T and on the collective pitch angle β , tuned such that the amplitude of C'_T is 1.5. The dashed line shows the steady-state optimal C_T .

Table 3.1: Differences between the approach in [Munters and Meyers \(2018a\)](#) and both the simulations and wind tunnel experiments presented in this chapter. The number of experiments executed here is slightly lower. As a result, choices are made with regards to the excitation amplitudes and frequencies that have been investigated.

	Munters et al	Simulations	Experiments
Layout	4 turbines in a row	Single turbine	3 turbines in a row
Environment	LES code	Aero-elastic code	Wind tunnel experiments
Control input	Sinusoid on C_T'	Sinusoid on β	Sinusoid on β
Amplitude of pitch excitation	N/A	2	1.7, 2.8, 5
Amplitude of C_T' excitation	0.5, 1, 1.5, 2	1	1, 1.5, 2
Number of frequency data points	12	3	8
Frequency range in St [-]	[0.05, 0.6]	[0.3, 0.5]	[0.09, 0.41]

operating at different combinations of tip-speed-ratio λ and blade pitch β . In turn, the tip speed ratio can be varied either by changing the reference followed by the generator torque or changing the blade pitch. In this chapter, a strategy that only changes the blade collective pitch is adopted. The implementation of this strategy simply requires changing the collective fine pitch at which the model blades are set when the machine operates in partial load conditions (region II). The fine pitch was tuned experimentally, by means of a trial and error procedure conducted with a stand-alone model, to achieving the desired mean \bar{C}_T and amplitude A as reported in Table 3.2. The effects of these control actions in terms of impacts on the power output of the 3-turbine wind farm are discussed in Section 3.6.

Finally, the performance of periodic DIC as a wind farm power maximization strategy is evaluated. To achieve this, a comparison is made with wind farm power maximization approaches that have already been investigated more extensively in literature:

- *Greedy control*: all turbines operate at their individual optimum, disregarding wake interaction between turbines. This means that all turbine have an induction factor of $a = 1/3$ (or a thrust coefficient of $C_T = 8/9$ or $C_T' = 2$) and a yaw angle of 0 degrees with respect to the wind direction.
- *Static induction control* (also called derating control): the induction settings of upstream turbines are manipulated such that the wind farm power capture can be maximized. In this chapter, the induction factor is controlled by means of the collective pitch angles of the (upstream) turbines, although using the

Table 3.2: Average \bar{C}_T and amplitude A_{C_T} of the three different thrust coefficient oscillations whose results are discussed in Section 3.6, as well as the mean pitch angle average $\bar{\beta}$ and amplitude A_β used to achieve these signals. Note that, as explained in Section 3.2, these collective pitch settings are not identical for different frequencies. Instead, they are tuned such that the mean and amplitude of C_T as given below are followed as accurately as possible.

Amplitude C_T'	\bar{C}_T [-]	A_{C_T} [-]	$\bar{\beta}$ [deg]	A_β [deg]
$A = 1$	0.8	0.17	0.7	1.7
$A = 1.5$	0.7	0.3	1.8	2.8
$A = 2$	0.5	0.5	4	5

generator torque is also an option. This strategy has been a popular research topic in recent years, and has shown both promising (Marden *et al.*, 2013; Gebraad *et al.*, 2013) and inconclusive (Campagnolo *et al.*, 2016b; Nilsson *et al.*, 2015; Annoni *et al.*, 2016) results.

- *Yaw control* (also called wake redirection control): upstream turbines are yawed with respect to the wind direction such that the wake is steered away from downstream machines. For this approach, the control inputs are the yaw angles of the (upstream) turbines with respect to the wind. Yaw control has been demonstrated to effectively increase the wind farm power capture in wind tunnel experiments (Campagnolo *et al.*, 2016a) and full-scale experiments (Fleming *et al.*, 2017; Howland *et al.*, 2019).

The control inputs that lead to the highest power capture are found using the static FLOW Redirection and Induction in Steady-state (FLORIS) model (Annoni *et al.*, 2018; Doekemeijer and Storm, 2018). This parametric model is calibrated with wind tunnel measurements, as described in Schreiber *et al.* (2017). The control settings are then implemented on the same wind farm set-up in the wind tunnel such that a fair comparison can be made. In Section 3.6, the results of these experiments are evaluated.

3.3. Simulation environment

In order to evaluate the effect of DIC on turbine level, the aeroelastic tool C_p - Λ (Code for Performance, Loads, Aeroelasticity by Multi-Body Dynamics Analysis, see Bottasso and Croce (2018); Bottasso *et al.* (2006)) has been used. This software is an aeroelastic code based on finite element multibody formulation, which implements a geometrically exact non-linear beam formulation (Bauchau, 2011) to model flexible elements such as blade, tower, shaft and drive train. The generator-drive train model can include speed-dependent mechanical losses. The rotor aerodynamics are modelled via Blade Element Momentum (BEM) theory or a dynamic inflow model, and may consider corrections related to hub- and tip-losses, tower shadow, unsteadiness and dynamic stall, whereas lifting lines can be attached to both tower and nacelle to model the related aerodynamic loads.

For the fatigue analysis, the model of a 5 MW reference wind turbine developed by the National Renewable Energy Laboratory (NREL) was considered (Jonkman *et al.*, 2009). This reference NREL 5 MW wind turbine, with a 126 m rotor diameter and a rated wind speed of 11.4 ms^{-1} , is a well-known model, widely analyzed in literature and able to represent modern and already working wind turbines. Each blade is discretized with 30 cubic finite elements, the tower with 20 cubic elements. Additionally, pitch and torque actuators are modeled respectively as second and first order systems and the model is completed by a standard Proportional-Integral-Derivative (PID) controller (Jonkman *et al.*, 2009). Finally, 10-minute wind time histories of turbulence class "A", according to Design Load Case (DLC) 1.1 of IEC 61400-1 (2004), generated by the software TurbSim (Jonkman and Buhl Jr., 2006), were given as input to the aeroelastic solver.

3.4. Experimental Setup

The experimental results presented in this chapter were gathered by performing dedicated tests within the wind tunnel of the Politecnico di Milano (Polimi), which is a closed-return configuration facility arranged in a vertical layout and equipped with two test rooms. A detailed description of the facility can be found in [Bottasso *et al.* \(2014\)](#). The tests were performed within the boundary layer test section, which has been conceived for civil, environmental and wind energy applications. This section has a large cross-sectional area of 13.84×3.84 m, which allows for low blockage effects even with several relatively large turbine models installed within the test section.

Roughness elements located on the floor and turbulence generators placed at the chamber inlet are commonly used to mimic the atmospheric boundary layer to scale in terms of vertical shear and turbulence spectrum. During the experiments described later on, two boundary layer configurations were used: one generating low turbulent (low-TI) and one generating highly turbulent (high-TI) flow conditions. These conditions roughly correspond to off- and onshore operation respectively. The flow characteristics are shown in Fig. 3.3 together with the extension of the model's rotor disk along the vertical axis. The coefficients of the vertical-shear exponential law, shown in the same picture, that best fit the experimental data are 0.144 and 0.214 for the low-TI and high-TI cases, respectively.

3.4.1. Wind turbine models

Three G1 scaled wind turbine models, developed at the Technical University of Munich (TUM), were used to perform the experiments reported in this chapter. This model type was widely employed and described in detail in previous research ([Campanolo *et al.*, 2016a,b,c](#)) and is shown within the boundary layer test section of

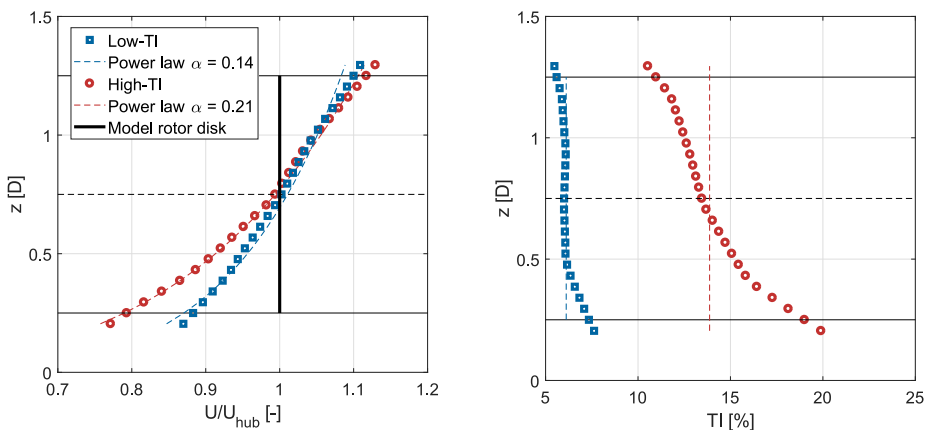


Figure 3.3: Vertical wind speed profile (left) and turbulence intensity (right) as a function of height above the tunnel floor, for low (low-TI) and high (High-TI) turbulence experiments.



3

Figure 3.4: A $G1$ scaled wind turbine model within the wind tunnel of the Politecnico di Milano. The yellow and red arrows show the pitch and yaw control possibilities respectively. The yellow spires and bricks in front of the model create the high-TI flow conditions.

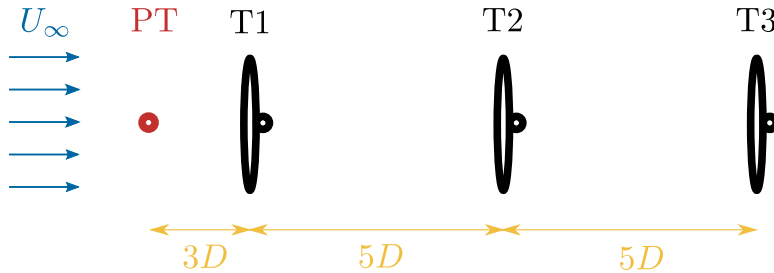


Figure 3.5: A schematic top view of the wind farm setup in the wind tunnel. The pitot tube (PT), which measures the inflow velocity, is located 2 rotor diameters D in front of Turbine 1 (T1). The spacing between the turbines is $5D$ and the wind flows from left to right.

the Polimi wind tunnel in Fig. 3.4. The setup of the turbines in the tunnel is shown in Figure 3.5.

With a rotor diameter of $D = 1.1$ m and a rated rotor speed of 850 rpm, the model was designed to have a realistic energy conversion process and wake behavior: it exhibits a power coefficient $C_p \approx 0.41$ and a thrust coefficient $C_T \approx 0.81$ for a tip speed ratio $\lambda \approx 8.2$ and a blade pitch $\beta \approx 0.4^\circ$.

The turbine is actively controlled with individual pitch, torque and yaw actuators and features comprehensive on-board sensorization. Three individual pitch actuators and connected positioning controllers allow for an overall accuracy of the pitch system of 0.1 degrees for each blade and the ability to oscillate the blade pitch with an amplitude of 5 degrees at 15 Hz around any desired pitch angle. Strain gauges are installed on the shaft to measure bending and aerodynamic torsional loads, as well as at the tower foot to measure fore-aft and side-side bending moments. A pitot tube, placed three rotor diameters upstream of the first turbine model, provides measurements of the undisturbed wind speed at hub height. Finally, air pressure, temperature and humidity transducers allow for measurements of the air density within the test section. The measurements of these sensors are

used to determine the performance of the turbine models. The thrust coefficient is obtained using measurements of the pitot tube wind speed measurement and fore-aft bending moment, while correcting for the effects of the tower and nacelle drag.

3.4.2. Control system

For each wind turbine model, control algorithms are implemented on a real-time modular Bachmann M1 system. Demanded values (e.g., pitch angle or yaw angle references) are then sent to the actuators, where the low level control is performed. Torque signals, shaft bending moments and rotor azimuth position are recorded with a sampling rate of 2.5 kHz, while all other measurements are acquired with a sampling rate of 250 Hz. A standard power controller is implemented on each M1 system based on [Bossanyi \(2000\)](#), with two distinct control regions. Below rated wind speed, blade pitch angles are kept constant, while the generator torque reference follows a function of the rotor speed with the goal of maximizing the energy extraction. Above rated wind speed, the generator torque is kept constant and a Proportional-Integral (PI) controller adjusts the collective pitch of the blades in order to keep the generated power at the desired level. All experiments presented in this work are performed below rated wind speed.

3.5. Simulation Results

To evaluate the effects of DIC on the loads of the excited turbine, a full set of aeroelastic turbulent simulations (DLC 1.1) has been executed. These analyses have been conducted on the NREL 5 MW wind turbine with the main goal of quantifying the effect of this DIC on the fatigue loads. Force and moment sensors have been placed on the main components of the wind turbine, such as: tower base and tower top, blade root, hub and drive train. The results presented in the next sections focus on the main sensors, such as the blade root flap- and edge-wise bending moments, tower base fore-aft bending and hub torsional moments, as well as some controller data (blade pitch and rotor speed), that highlight the effects of the controllers.

DIC was assumed to be activated for wind speeds between 3 and 25 ms^{-1} , to cover the totality of regions I-1/2, II, II-1/2 and III. Notice that 25 ms^{-1} seems a rather high speed, considering the fact that so far, the effectiveness of DIC has only been evaluated in region II. In region III, the lower rotor inductions (i.e a lower in-wake speed deficit) may guarantee, together with the high inflow velocity, the full power region for the downwind rotor(s). Nevertheless, in the 10-minute simulation, the high turbulence intensity (class "A") causes a relatively long period where the mean wind speed is below the rated one and hence DIC may have an important effect on the wake. From this point of view, extending the authority of DIC up to 25 ms^{-1} is to be regarded as a conservative choice. For clarity, the rated wind speed of 11.4 ms^{-1} is shown in the figures showing the DELs at different mean wind speeds.

Strouhal numbers of $St = [0.3, 0.4, 0.5]$ and a pitch amplitude $\beta_{\text{DIC}} = 2^\circ$ were

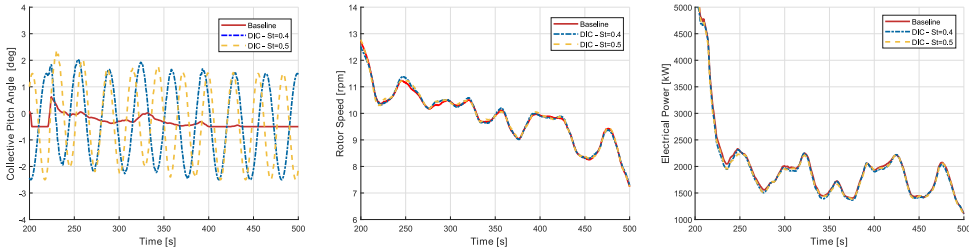


Figure 3.6: Comparison of pitch activity (left), rotor speed (middle) and power (right) between baseline (solid red) and DIC controlled with $St = 0.4$ (dash-dotted blue) and $St = 0.5$ (dashed yellow) turbine for NTM class "A" at 9 ms^{-1} .

used in the aeroelastic simulations of the 5 MW turbine. Considering the diameter of this wind turbine model (126 m), the frequency of DIC f_{DIC} is between $6.94 \cdot 10^{-3} \text{ Hz}$ at 3 ms^{-1} (and $St = 0.4$) and $5.95 \cdot 10^{-2} \text{ Hz}$ at 15 ms^{-1} (and $St = 0.5$), which correspond to a period equal to between 105 and 16.8 s respectively.

Due to the relatively low excitation frequency, the baseline turbine control is able to trim the machine without a significant additional effort or detrimental performance. Moreover, a coalescence between the DIC input frequency and turbine vibratory modes is not to be expected, at least for on-shore or off-shore turbines installed on rigid foundations.

Figure 3.6 shows an example of the time response of the machine with and without DIC. These simulations have been performed with a Normal Turbulence Model (NTM) of class-A wind (IEC 61400-1, 2004) with a mean hub wind speed of 9 ms^{-1} , generated with TurbSim (Jonkman and Buhl Jr., 2006). In these conditions, the wind turbine baseline control switches between region II, II-1/2 and III. The figure shows the baseline condition, i.e., the one without the DIC controller, and two simulations with Strouhal number $St = 0.4$ and $St = 0.5$. The plot on the left refers to the pitch activity, the plot in the middle to the rotor speed and the plot on the right to the power. The collective pitch angle time histories show the DIC activity superimposed to the trim-pitch. As can be seen, the rotor speed and power production with DIC active behave very similar to that of the baseline case (solid lines), showing that the addition of the periodic pitch motion is not detrimental in terms of trimmer performance.

Figure 3.7 shows the power spectral density (PSD) of the rotor speed (left) and blade root flapwise bending moment with a NTM at 15 ms^{-1} , again for the baseline case (solid-red) and for DIC with Strouhal numbers $St = 0.4$ and $St = 0.5$. Both figures show a new frequency corresponding to the DIC excitation. This peak is far from the other aeroelastic frequencies of the wind turbine (the first being the tower fore-aft at $f = 0.31 \text{ Hz}$), but may have an important role on the fatigue loads.

From the 10-minute simulations computed according to DLC 1.1 of IEC 61400-1 (2004), the stochastic time histories of the wind turbine loads are converted into simplified DELs through a rainflow analysis and depicted in Fig. 3.8 and 3.9 as a function of the mean wind speed. These figures show that DELs computed for the baseline case are almost always lower compared to when DIC is active, as would

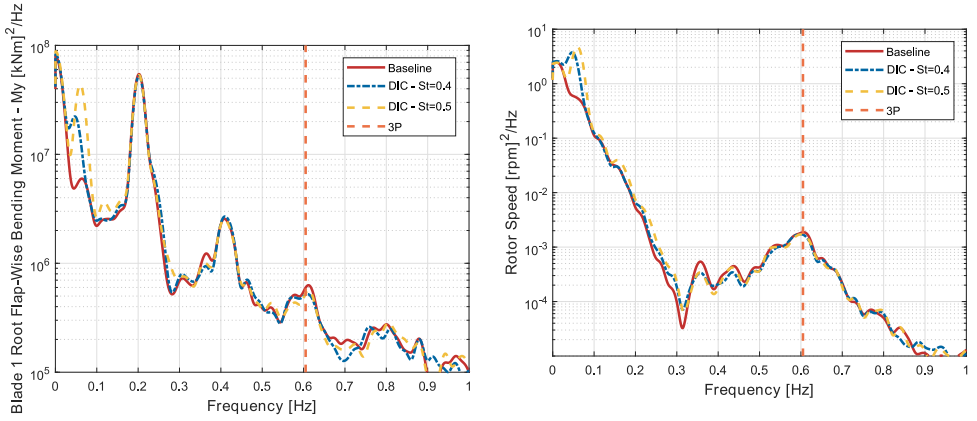


Figure 3.7: PSD comparison of the rotor speed (left) and blade root flap-wise bending moment (right) between baseline (solid red) and DIC controlled with $St = 0.4$ (dash-dotted blue) and $St = 0.5$ (dashed yellow) turbine for NTM class "A" at 15 ms^{-1} .

be expected based on Fig. 3.7. For each mean wind speed, the DIC frequencies correspond to Strouhal numbers 0.4 and 0.5. In these figures, DIC was always active, even for high wind speed values close to the cut-out. As a result, the baseline curves are always lower than the controlled curves. For clarity, the rated wind speed of 11.4 ms^{-1} is also shown in the figures. As can be seen, the tower base fore-aft bending moment and the blade root flapwise are affected the most by this controller. As expected, the blade edge-wise bending moment is only slightly affected, since the DEL in edge-wise direction is mainly driven by gravity.

In order to have a more comprehensive indication about the impact of DIC on fatigue loads, one can consider the Weibull-weighted DELs, i.e., the DELs weighted throughout the probability distribution of the wind as expressed by the Weibull distribution $p_w(V)$

$$p_w(V) = k \frac{V^{(k-1)}}{C^k} e^{-\left(\frac{V}{C}\right)^k}, \quad (3.1)$$

where k is the shape parameter and $C = 2V_{av}/\sqrt{\pi}$ the scale factor and V_{av} the average wind speed.

The Weibull-weighted DEL, DEL_w , is hence computed as

$$DEL_w = \int_{V_{CI}}^{V_{CO}} p_w(V) DEL dV, \quad (3.2)$$

where V_{CI} and V_{CO} are respectively the cut-in and cut-out wind speed.

Considering the class "A", where the Weibull distribution has $k = 2$ and $V_{av} = 10 \text{ ms}^{-1}$, it is possible to compute the Weibull-weighted DELs for the previously considered loads. To this aim, as discussed before, DIC would normally be deactivated for wind speeds higher than 15 ms^{-1} . Therefore, in the second part of region III (from 17 ms^{-1} to 25 ms^{-1}), the DELs would normally be equal to the baseline

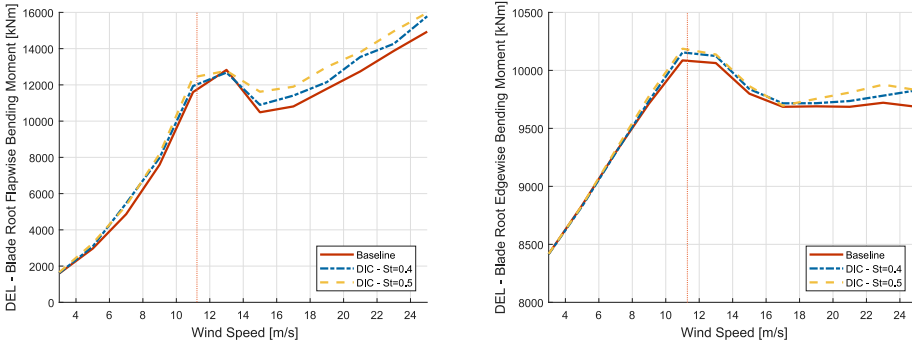


Figure 3.8: Comparison between blade root flap-wise (left) and edge-wise (right) DEL of the baseline (solid red) and DIC with $St = 0.4$ (dash-dotted blue) and $St = 0.5$ (dashed yellow) as functions of mean wind speed. The dashed yellow line indicates the rated wind velocity. Typically, DIC is only implemented at below-rated inflow velocities.

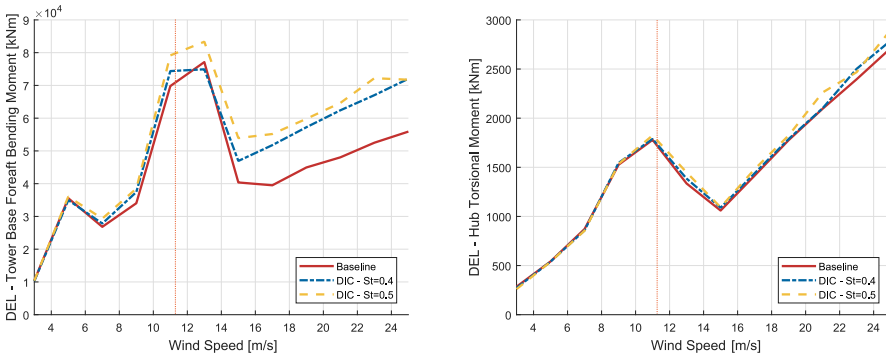


Figure 3.9: Comparison between tower base fore-aft bending moment (left) and hub torsional moment (right) DEL of the baseline (solid red) and DIC with $St = 0.4$ (dash-dotted blue) and $St = 0.5$ (dashed yellow) as functions of mean wind speed. The dashed yellow line indicates the rated wind velocity. Typically, DIC is only implemented at below-rated inflow velocities.

Table 3.3: Percentage increases of the Weibull-weighted DELs and AEP (from 3 ms^{-1} to 25 ms^{-1}) of the excited turbine compared to the baseline for different Strouhal numbers. DIC is deactivated for wind speeds higher than 15 ms^{-1} .

	Blade Edgewise	Blade Flapwise	Tower Fore-aft	Hub Torsion	AEP
$St = 0.3$	+0.21%	+2.66%	+ 7.06%	+0.94%	-0.46%
$St = 0.4$	+0.40%	+1.80%	+ 7.26%	+1.67%	-0.54%
$St = 0.5$	+0.41%	+4.92%	+11.78%	+1.80%	-0.59%

values. The Weibull-weighted DELs, computed as discussed in full operating region (from 3 ms^{-1} to 25 ms^{-1}) together with the corresponding Annual Energy Production (AEP), are summarized in Table 3.3. As can be seen, the tower base load is affected the most (7 to 11%), while loads on the blade flapwise root loads increase with about 2%. A negligible impact is found in the blade edge-wise (+0.4%) and in the hub (1 to 2%).

It is important to stress that, so far, the analyses have not considered the probability of activation of the DIC-based wind farm control, which depends on the specific farm layout and wind rose. From this point of view, the computed DEL increments seen before, as well as the AEP decrease, are to be considered as the worst possible case, as if DIC would always be implemented regardless of wind direction and subsequent wake interaction. It is therefore possible to assess that the impact of DIC on turbine fatigue loads for the analyzed NREL 5 MW reference machine is small compared to the possible gains.

3

3.6. Experimental Results

In this section, the results of the experiments executed in the wind tunnel at Polimi, as described in Section 3.4, are presented. The effects of periodic DIC on the power production of a 3-turbine wind farm are presented for two cases, similar to onshore and offshore wind conditions. The performance of DIC is compared with the state-of-the-art wind farm control strategies: greedy control, "static" induction control and wake redirection control.

3.6.1. Power production

First, the results with low turbulent wind (TI of approximately 5%) are evaluated. For this case, 3 different sets of experiments have been conducted, as defined in Table 3.2. These sets each represent one specific amplitude of excitation of the upstream machine: an amplitude of $A = 1, 1.5$ and 2 of C'_T respectively. All other machines operate at their greedy optimum.

Figure 3.10 shows the mean power of the turbines and the total wind farm. To account for the small variations in flow conditions, the power is divided by the available power in the wind. As such, these values can be seen as power coefficients. Increasing the amplitude of the sinus decreases the power coefficient of turbine 1, while it increases the power coefficient of the downstream machines. However, for higher A , the loss at turbine 1 is too significant to compensate for by the downstream turbines. The unexpectedly high power loss at turbine 1 could partly be caused by a rotor imbalance that is worsened by higher amplitudes of excitation, leading to significant vibrations of the excited machine. As a result, the case with the lowest amplitude proves to be the most effective.

The highest increase in power extraction is found with $A = 1$ and $St = 0.32$, resulting in a 2.4% gain. It should be noted that this gain is mostly obtained at turbine 2, while the power at turbine 3 is only marginally higher than in the baseline case. This corresponds to the conclusions drawn in Munters and Meyers (2018a), where a positive effect is observed for turbine 2, but not for machines further

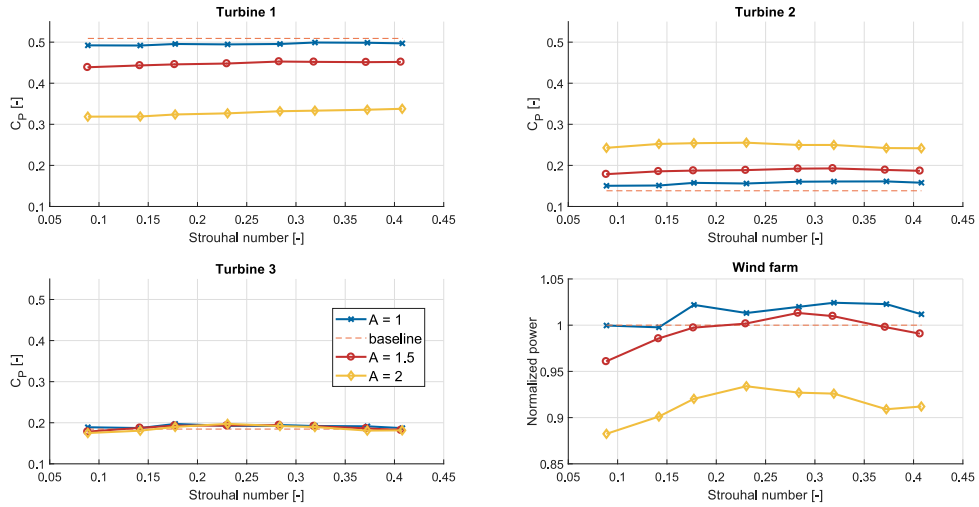


Figure 3.10: \bar{C}_p of the wind farm in low TI conditions for different amplitudes A of C'_T , as defined in Table 3.2. The bottom right figure shows the total power conversion compared to the baseline case.

downstream. Table 3.4 gives an overview of the effect of different amplitudes and frequencies on the power production of the 3-turbine model wind farm.

For the sake of reproducibility, Fig. 3.11 shows the measurements of thrust coefficients C_T and C'_T , as well as the pitch signal and rotor speed during 10 s of experiments in the optimal control settings ($St = 0.32$, $A = 1$). It should be noted that the thrust coefficient is obtained by using the definition

$$C_T = \frac{F_T}{0.5\rho A_r U_\infty^2}, \tag{3.3}$$

where F_T is the thrust exerted on the rotor by the wind, ρ the air density, A_r the rotor area and U_∞ the inflow wind velocity. F_T is determined using the fore-aft bending moment, compensating for tower and nacelle drag, and the pitot measurements in front of turbine 1 (see Fig. 3.5) are used as data for U_∞ . This results in a C_T -signal disturbed by high frequency noise. For this purpose, a low-pass filter with a passband frequency of 12.5 Hz was designed. This filter removes the high frequency noise signals, while keeping the excitations caused by DIC (at $f \leq 2.3$ Hz)

Table 3.4: An overview of the total power increase with respect to the baseline case by applying dynamic induction control with different amplitudes (A , rows) and frequencies (columns) for the low TI case. In bold are the experiments that lead to the highest power capture for each amplitude, showing an optimum around $St = 0.28$.

Frequency [Hz]	0.5	0.8	1	1.3	1.6	1.8	2.1	2.3
Strouhal [-]	0.09	0.14	0.18	0.23	0.28	0.32	0.37	0.41
$A = 1.0$	-0.04%	-0.24%	+2.20%	+1.30%	+1.6%	+2.4%	+2.3%	+1.2%
$A = 1.5$	-3.92%	-1.44%	-0.27%	+0.20%	+1.3%	+1.0%	-0.20%	-0.92%
$A = 2.0$	-11.76%	-9.89%	-7.97%	-6.61%	-7.30%	-7.41%	-9.09%	-8.80%

intact. Furthermore, a sinusoid is fitted on the measurement data using the `MATLAB` function `lsqcurvefit`. This function determines the amplitude, offset and phase of the sinusoid that best fit the data. The original data, filtered data and fitted sinusoid are all shown in Fig. 3.11. Finally, the pitch excitation and rotor speed are depicted, the latter clearly showing oscillations caused by DIC. However, these oscillations are relatively small compared to variations caused by changing wind conditions, as the baseline rotor speed shows.

Finally, the reliability of these results are examined. To do this, the results are divided into four segments of 60 seconds. These shorter segments of measurements, still containing 15000 measurement points and between 30 (0.5 Hz) and 138 (2.3 Hz) sine cycles, are then used to determine the variance of the measurements.

Figure 3.12 shows box plots of these data sets for $A = 1$, normalized by the steady state optimal C_p of turbine 1. This figure shows that the variance becomes larger at each downstream row due to the increased turbulence. As a result, the variance is significant in the total power production: up to $\pm 2\%$ of the power. However, this figure also shows that the variance is lower than the power gained by using dynamic induction control: the lowest values of the box plot around the optimal frequency of 1.8 Hz are still higher than the baseline value. This analysis therefore indicates that the power increase is significant, as it is not a coincidental result of measurement errors.

Next, the results of the experiments with high turbulence intensity conditions (TI of approximately 10%) are shown. The results for all the amplitudes and frequencies that were studied are shown in Fig. 3.13. The main conclusion that can be drawn from this figure, is that the effect of exciting the first turbine on the power production of this turbine is lower in these conditions. Due to the turbulence, the baseline power production of this turbine is already slightly lower than in low TI

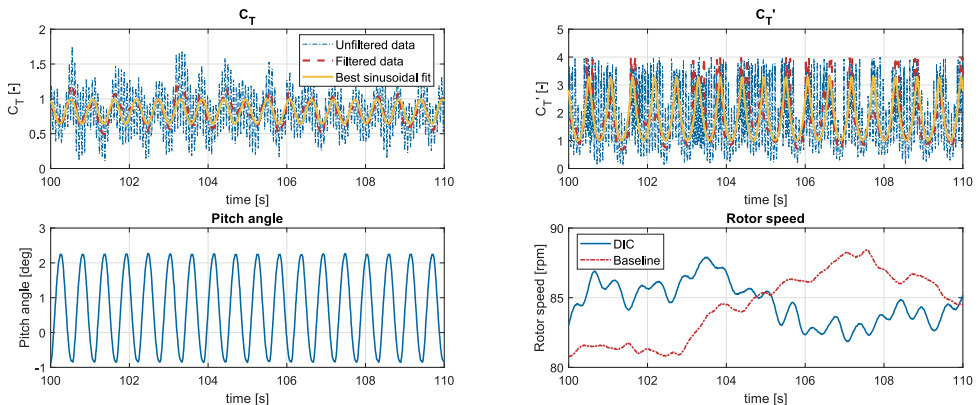


Figure 3.11: Clockwise, the measured C_T , C_T' , rotor speed and pitch angles of turbine 1 are shown during 10 s of the optimal $St = 0.32$, $A = 1$ DIC experiments in low TI. In the first two figures, the unfiltered data, low-pass filtered data and a best sinusoidal fit are shown. In the fourth figure, the rotor speed during 10 s of the baseline experiment is shown for comparison.

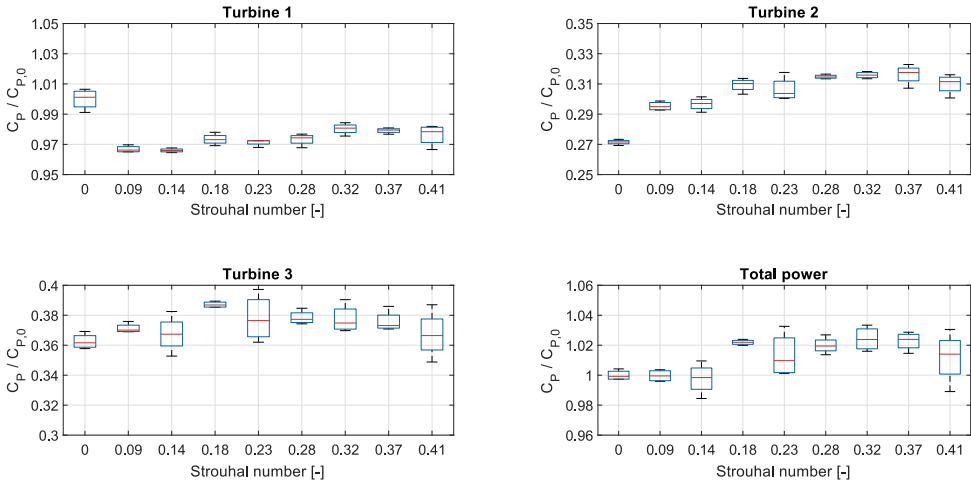


Figure 3.12: A boxplot showing the variance of the C_p measurements for the low turbulent, $C_T' = 1$ experiments, for all turbines individually as well as for the entire wind farm. The $f = 0$ measurement represents the baseline case of no dynamic control.

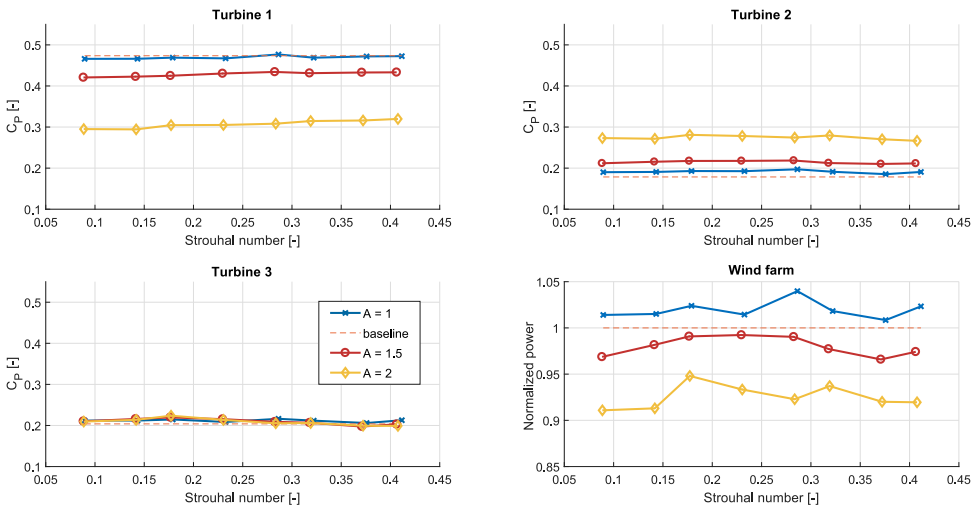


Figure 3.13: \bar{C}_p of the wind farm for different amplitudes A of C_T' , as defined in Table 3.2, in the high TI case. The bottom right figure shows the total power conversion compared to the baseline case.

conditions. As a result, the power loss at turbine 1 is negligible for the $A = 1$ case. As the power gain at the downstream turbines is similar, the total power gain for this case is 4%. This gain is found with $A = 1$ and $St = 0.28$, as can be seen in Table 3.5 where the results are summarized.

When the amplitude of the excitation is increased, the power loss at turbine 1 is comparable with the results in low TI conditions. However, since the power gain

Table 3.5: An overview of the total power increase by applying dynamic induction control with different amplitudes (A , rows) and frequencies (columns) for the high TI case.

Frequency [Hz]	0.5	0.8	1	1.3	1.6	1.8	2.1	2.3
Strouhal [-]	0.09	0.14	0.18	0.23	0.28	0.32	0.37	0.41
$A = 1.0$	+1.4%	+1.5%	+2.4%	+1.4%	+4.0%	+1.8%	+0.8%	+2.3%
$A = 1.5$	-3.1%	-1.8%	-0.9%	-0.8%	-1.0%	-2.3%	-3.4%	-3.6%
$A = 2.0$	-8.9%	-8.7%	-5.2%	-6.7%	-7.7%	-6.3%	-8.0%	-8.1%

3

at turbine 2 is slightly lower, the total power is also lower than in the baseline case. Subsequently, it seems that the amplitude of the excitation is more important than the frequency in these conditions.

3.6.2. Controller comparison

To emphasize the value of the results shown in the previous subsection, a comparison of the effectiveness of the periodic DIC approach with state-of-the-art wind farm control approaches is executed in the case of full wake interaction. The optimal inputs are found using the steady-state FLOW Redirection and Induction in Steady-state (FLORIS) model (Annoni *et al.*, 2018; Doekemeijer and Storm, 2018), which is calibrated using measurements from the wind tunnel (Schreiber *et al.*, 2017). As explained in Section 3.2, three different control strategies are implemented in the wind tunnel: greedy control, static induction control and yaw control.

The results of these experiments are shown in Fig. 3.14. Similar to results in literature (Campagnolo *et al.*, 2016b), static induction control is found to be unable to increase the power production of this wind farm. Yaw control on the other hand results in a benefit of 3.1%. As reported earlier, DIC was able to increase the power production with 2.4% in these conditions. It can therefore be concluded that the potential profit of periodic DIC is significantly higher than with static induction, while it is comparable to that of yaw control when full wake interaction is present.

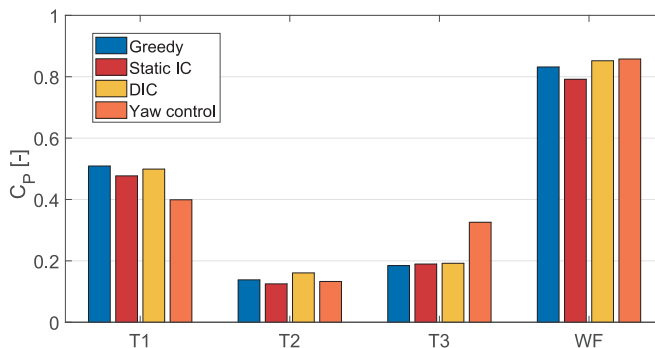


Figure 3.14: The power capture of three state-of-the-art control approaches compared with periodic DIC in low TI conditions. The power capture of the three individual turbines (T1-3), as well the total Wind Farm (WF) is shown.

3.7. Conclusions

The effect of periodic Dynamic Induction Control (DIC) on both individual wind turbines and on small wind farms is investigated in this chapter. To this purpose, both aero-elastic simulation tools and scaled wind tunnel experiments are used. The unique wind tunnel experiments with DIC show, for the first time, that this control approach not only works in a simulation environment, but also in real world experiments. The results strengthen the results found in simulations executed by [Munters and Meyers \(2018a\)](#), showing a potential increase in power production of up to 4%, with most of the gain coming from the first downstream turbine. Some minor differences were observed as well. First of all, the optimal Strouhal number is found to be slightly higher in the wind tunnel experiments, around $St = 0.3$. Secondly, a smaller optimal amplitude of excitation was found. This could partly be caused by a slight rotor imbalance, which resulted in significant power losses at the excited turbine. Although higher gains were observed at turbine 2, the power loss of turbine 1 could not be compensated for at higher amplitudes of excitation.

A comparison between DIC and static induction control as well as wake redirection control shows that this approach works significantly better than the former and approximately as good as the latter. This greatly strengthens the premise that DIC is an effective method to increase the power production of a wind farm as a whole. Furthermore, by means of the aeroelastic tool C_p - Λ , it was shown that the effect of DIC on the Damage Equivalent Loads (DEL) of the excited wind turbine is relatively small. For the given wind turbine example, the weighted blade root edgewise DEL was in the order of 0.3 to 0.4% higher than in the baseline greedy control case.

In all, it can be concluded that the dynamic induction control approach shows great promise, as now both simulations and scaled experiments show that it is possible to achieve a power gain. However, some minor differences are found between simulation studies in literature and the experiments presented here, which still need to be addressed. Future research can therefore be directed into clarifying these differences, as well as executing additional experiments, for example with different inflow velocities inside and outside the region II regime.

As the amplitude and frequency of the excitation are shown to be important control parameters, it would be a very interesting challenge to develop an algorithm that is able to optimize these parameters. Furthermore, additional analysis on the increased loads on the (downstream) turbines can be done to investigate the effect of these loads on the lifetime of turbines, as well as the tradeoff between power and load effects. Another possible approach would be to investigate the effects of applying periodic DIC on intermediate wind turbines on the performance of the wind farm. Finally, application on full-scale wind turbines could be the last step in proving the validity of this approach.

4

The helix approach

*Veniet tempus quo posterī nostri
tam aperta nos nescisse mirentur.*

*There comes a time when our descendants will be astonished
that we did not know things that are so straightforward to them.*

– Lucius Annaeus Seneca the Younger,
on how scientific discoveries can seem obvious once revealed.

Wind farm control using dynamic concepts is a research topic that is receiving an increasing amount of interest. The main concept of this approach is that dynamic variations of the wind turbine control settings lead to higher wake turbulence, and subsequently faster wake recovery due to increased mixing. As a result, downstream turbines experience higher wind speeds, thus increasing their energy capture. The current state of the art in dynamic wind farm control is to vary the magnitude of the thrust force of an upstream turbine. Although very effective, this approach also leads to increased power and thrust variations, negatively impacting energy quality and fatigue loading. In this paper, a novel approach for the dynamic control of wind turbines in a wind farm is proposed: using individual pitch control, the fixed-frame tilt and yaw moments on the turbine are varied, thus dynamically manipulating the wake. This strategy is named the helix approach since the resulting wake has a helical shape. Large eddy simulations of a two-turbine wind farm show that the helix approach leads to enhanced wake mixing with minimal power and thrust variations.

The contents of this chapter have been published as a peer-reviewed research paper in the Wind Energy journal:

J.A. Frederik, B.M. Doekemeijer, S.P. Mulders and J.W. van Wingerden, *The helix approach: Using dynamic individual pitch control to enhance wake mixing in wind farms*, Wind Energy. **23**(8) 1739 (2020).

4.1. Introduction

The interaction between wind turbines in a wind farm through their wakes is a phenomenon that has been studied for decades (Lissaman, 1979; Jensen, 1983; Katic *et al.*, 1987), and is still a relevant topic today (Bastankhah and Porté-Agel, 2016; Annoni *et al.*, 2018). For the purpose of power maximization and load minimization, this interaction can be manipulated using techniques from the control engineering community. A comprehensive survey on wind farm modelling and control can be found in Boersma *et al.* (2017). In wind farm control, two different approaches can be distinguished: induction control (sometimes called de-rating control) and wake redirection control (sometimes called wake steering). The former approach uses the induction factor, i.e., the in-wake velocity deficit, of the turbines as control input, whereas the latter approach exploits the yaw angle of turbines. Both approaches follow the same strategy: the upstream machines in a wind turbine array lose power due to locally suboptimal induction or yaw settings, and downstream machines experience higher wind speeds which increases their power generation.

The examples of induction control and wake redirection control are plentiful. Induction control has shown promising results in different simulation environments using model-free optimization (Marden *et al.*, 2013; Ciri *et al.*, 2017) or Model Predictive Control (MPC) (Vali *et al.*, 2016). However, recent studies with high-fidelity simulation models (Annoni *et al.*, 2016), scaled wind tunnel experiments (Campagnolo *et al.*, 2016b) and full-scale experiments (van der Hoek *et al.*, 2019) indicate that the potential wind farm power gain of induction control is minor to non-existent. Therefore, the focus in the literature for power maximization in wind farms is shifted towards wake redirection. Wake deflection through yaw is first modelled in Jiménez *et al.* (2010), and is also investigated on full-scale turbines using lidar measurements (Raach *et al.*, 2016). Both scaled wind tunnel experiments (Campagnolo *et al.*, 2016a) and full-scale tests (Fleming *et al.*, 2017; Howland *et al.*, 2019) indicate that this strategy can effectively increase the power generation of a wind farm. All these references have in common that they focus on steady-state optimal control of a wind farm. Therefore, time-varying control inputs that purposely influence the inherently dynamic nature of the wind are disregarded.

To the best of the authors' knowledge, the first mention of dynamic control being used to increase the performance of wind farms is in an industrial patent (Westergaard, 2013). This patent describes different control methods involving either dynamic induction, dynamic yawing or wake deformation through cyclic pitch signals. What these control methods have in common, is that they aim to increase wake mixing by changing the control inputs over time. Wake mixing is the phenomenon where the wake interacts with the adjacent, higher velocity, free-stream flow. As a result, the wake recovers some of the energy extracted by the upstream turbine, such that a downstream turbine experiences a higher wind velocity. However, only the general idea is described; no experiments or simulations are performed, and the effectiveness of these methods is not evaluated.

Recently, dynamic wind farm control has gained interest in the scientific field. Dynamic Induction Control (DIC) specifically is a research topic that has seen a

number of publications studying its potential in simulations (Munters and Meyers, 2016, 2017, 2018a) and in scaled wind tunnel experiments (see Chapter 3). To enable practical implementation, the most recent papers focus on a smaller subset of dynamic signals, namely sinusoidal signals (Munters and Meyers, 2018a). In Munters and Meyers (2018a), a grid search is performed using Large Eddy Simulations (LES) to determine the amplitude and frequency of the sinusoidal excitation that maximize the farm-wide power generation. In Chapter 3, wind tunnel experiments are performed to validate this approach, showing positive results. A different dynamic control approach is investigated using high-fidelity simulations in Kimura *et al.* (2019). Here, the yaw angle of a turbine is varied sinusoidally, such that increased wake meandering is induced.

4

The above-mentioned approaches do have an important drawback: because of the varying induction factor or yaw angle signals of the upstream turbine, the thrust force on the rotor varies significantly. As a result, this turbine experiences substantial power and load fluctuations, which is disadvantageous from a power quality perspective. In this chapter, a novel approach to dynamic wake mixing is introduced, which is expected to lead to lower power and thrust variations. This approach makes use of Individual Pitch Control (IPC), a procedure in which the blade pitch angles of a wind turbine are controlled independently of each other.

IPC is a well-known strategy in the wind turbine control community. It is usually applied to alleviate periodic loads on turbines with minimal power loss, as first proposed in Bossanyi (2003, 2005). Further research into load reducing IPC algorithms is still a relevant research direction, for example into using an azimuth offset (Mulders *et al.*, 2019) or implementing more advanced control strategies (see, e.g., Chapter 2). Research where IPC is used to increase the power generation of a wind farm is limited. Experiments have been conducted where IPC is used for wake steering (Fleming *et al.*, 2014) or power maximization in case of partial wake overlap (Fleming *et al.*, 2015). However, the results were inconclusive and no further research has been published since.

In this chapter, wake steering through individual pitch control is combined with the concept of dynamic wind farm control to forge a novel approach. This approach, called Dynamic IPC (DIPC), uses the Multi-Blade Coordinate (MBC) transformations to vary the tilt and yaw moments on the rotor. Thus, the wake is manipulated, slowly varying its direction over time. This is hypothesized to result in enhanced wake mixing, such that downstream turbines in a wind turbine array can increase their power generation with minimal rotor thrust fluctuations. A patent by the authors describing this concept is pending (van Wingerden *et al.*, 2019).

The main contributions of this chapter are threefold. First of all, the novel DIPC approach is described. Secondly, a specific DIPC strategy called the *helix approach* is defined, which dynamically moves the wake both horizontally and vertically. Finally, the effectiveness of this helix approach is evaluated through high-fidelity simulations. These simulations are executed using the LES code called Simulator for On/Offshore Wind Farm Applications (SOWFA, see Churchfield and Lee (2012)). The effects of DIPC both on the wake and on a downstream turbine is investigated. A thorough comparison is made with existing control strategies to evaluate the

performance of DIPC.

This chapter is organized as follows: in Section 4.2, the simulation environment is defined. Section 4.3 describes the working principles of DIPC in general and the helix approach specifically. The potential of this approach as a wind farm control approach is then demonstrated in Section 4.4 through high-fidelity simulations. Finally, conclusions are drawn and future work is discussed in Section 4.5.

4.2. Simulation Environment

The proposed control strategy is evaluated in the Simulator fOr Wind Farm Applications (SOWFA, see Churchfield and Lee (2012)), which is a high-fidelity simulation environment developed by the U.S. National Renewable Energy Laboratory (NREL). SOWFA is a large-eddy solver for the fluid dynamics in the turbulent atmosphere. The interaction with one or multiple wind turbines, accounting for the Coriolis force and Buoyancy effects, is included in SOWFA (Churchfield *et al.*, 2012). Turbines are modelled as actuator disks or actuator lines as demonstrated in Sørensen and Shen (2002). The SOWFA source code was adapted to allow for specifications of a different pitch setpoint for each individual blade, enabling the implementation of Individual Pitch Control (IPC).

In this work, two different simulation cases are defined. First of all, wind with a uniform inflow profile is used to demonstrate the working principles of Dynamic IPC (DIPC). It is recognized that these conditions do not represent realistic working conditions in an actual wind farm. However, due to the absence of turbulence, these simulations are perfectly suited to visualize the effects of DIPC on the wake of a turbine, as presented in Section 4.3.

The second simulation case employs more realistic wind conditions to evaluate the potential of Dynamic IPC. These simulations are of a neutral Atmospheric Boundary Layer (ABL) in which the inflow was generated through a so-called precursor simulation. Several properties of both simulation setups are listed in Table 4.1.

Two different wind farm cases are investigated in these conditions. Firstly, simulations with a single turbine, in which the effects on the turbine and wake are investigated, have been executed. Then, a second turbine is added, to assess the gain in energy capture that can be achieved with DIPC. The second turbine is situated 5 rotor diameters ($5D$) behind the upstream turbine, the same axial distance as investigated in Chapter 3. All these results are presented in Section 4.4.

Table 4.1: Details on the numerical simulation scheme in SOWFA for uniform and turbulent flow simulations.

	Case I: uniform flow	Case II: turbulent flow
Turbine	DTU 10MW (Bak <i>et al.</i> , 2013)	DTU 10MW (Bak <i>et al.</i> , 2013)
Rotor diameter	178.3 m	178.3 m
Domain size	2.5 km × 1 km × 0.6 km	3 km × 3 km × 1 km
Cell size (outer region)	50 m × 50 m × 50 m	10 m × 10 m × 10 m
Cell size (near rotor)	3.125 m × 3.125 m × 3.125 m	1.25 m × 1.25 m × 1.25 m
Inflow wind speed	9.0 m/s	9.0 m/s
Inflow turbulence intensity	0.0 %	5.0 %

4.3. Control Strategy

In this section, the Dynamic Individual Pitch Control (DIPC) strategy is further elaborated, as well as the already existing control strategies with which it is compared. In Section 4.3.1, static induction strategies are explained, which includes *greedy* control, where each turbine operates using its individual steady-state optimal settings. These strategies are currently the industry standard, and commonly applied in actual wind farms. They therefore serve as a useful baseline case for cutting edge control concepts such as periodic Dynamic Induction Control (DIC) and the novel DIPC approach. Periodic DIC, as described in Chapter 3, is shortly covered in Section 4.3.2, and Section 4.3.3 presents a thorough explanation of the DIPC approach as proposed in this chapter.

4

4.3.1. Static Induction Control

Static Induction Control (SIC) is a generic term for all induction control strategies that use time-invariant control set-points that depend on the inflow conditions. The most simple static induction wind farm control strategy is to operate all turbines at their individual (static) optimum for power generation. This approach is called *greedy control*, as all turbines greedily extract as much power from the wind as possible. As this approach is the simplest and most commonly applied, greedy control is considered the baseline case in this chapter.

An alternative approach is to (statically) lower the induction factor, i.e., the in-wake velocity deficit, of upstream turbines such that downstream turbines can increase their power capture. This has for long been the most popular concept in wind farm control research, but recent studies show that the achievable gains with respect to greedy control are minor to non-existent (Annoni *et al.*, 2016; Campagnolo *et al.*, 2016b; Nilsson *et al.*, 2015). Nonetheless, SIC for power maximization remains of interest to the industry. Hence, it is used as a comparison case in this article to show the potential of DIPC.

4.3.2. Periodic Dynamic Induction Control

A recent research area of interest, as an alternative to SIC, is Dynamic Induction Control (DIC). With this control method, the induction factor of an upstream turbine is varied over time to enhance wake mixing, such that downstream turbines experience higher wind velocities and can subsequently increase their power generation. Finding the optimal time-varying induction settings is a very complex control problem (Munters and Meyers, 2017). A more practical approach is proposed in Munters and Meyers (2018a), where sinusoidal input signals on the thrust force C_T' are suggested. This method is called *periodic DIC* and is also used in this chapter. It is shown to increase the power generation of small wind farms both in simulations (Munters and Meyers, 2018a) and in wind tunnel experiments (see Chapter 3).

In Chapter 3, for reasons of practical implementation, a periodic excitation is realized by superimposing a low-frequent sinusoidal signal on the static collective pitch angles of the turbine. This approach is also used in this chapter. As the control signal is now confined to a sinusoid, the control parameters are reduced to the

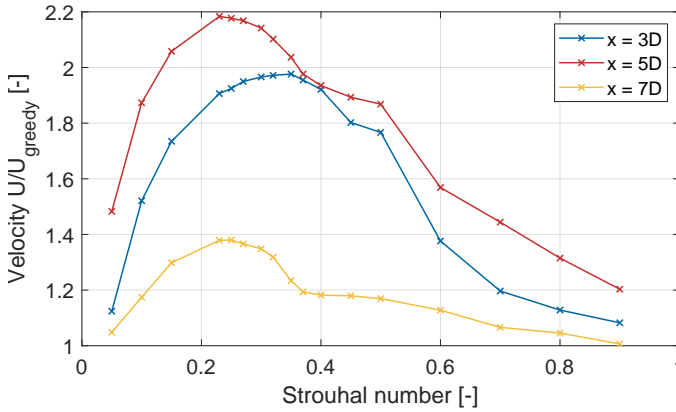


Figure 4.1: The average wake velocity at $3D$, $5D$ and $7D$ behind an DIC-excited turbine with an pitch amplitude of 4 degrees, for different Strouhal numbers St . The results are normalized with respect to the baseline case.

amplitude and the frequency of excitation. The frequency is usually characterized in terms of the dimensionless Strouhal number St :

$$St = \frac{f_e D}{U_\infty}, \quad (4.1)$$

where f_e is the frequency [Hz], D the rotor diameter [m] and U_∞ the inflow velocity [m/s]. As the Strouhal number is dimensionless, it accounts for different turbine sizes or inflow velocities. In the above-mentioned references, an optimal Strouhal number of $St \approx 0.25$ is found. In this chapter, the 10MW reference turbine developed by the Technical University of Denmark (DTU) is used (Bak *et al.*, 2013) (see Table 4.1). The dimensions of this turbine determine an excitation frequency of $f_e = 0.0126$ Hz for an inflow velocity of 9 m/s. To verify this optimal frequency, an extensive evaluation is performed in SOWFA. A single DTU 10MW wind turbine is placed in laminar flow conditions (see Table 4.1), and the velocity is measured at integer multiples of the rotor diameters D behind the turbine. The results are presented in Figure 4.1 and show that for a distance $\geq 5D$, the optimum is indeed around $St = 0.25$. As a physical explanation for the optimal frequency is not yet investigated, this excitation frequency was used in the simulations presented here. To take into account the effect of different excitation amplitudes, two different DIC cases are considered: a low amplitude case with a collective pitch amplitude of 2.5° and a high amplitude case of 4° , respectively.

4.3.3. Dynamic Individual Pitch Control

In this section, the novel Dynamic Individual Pitch Control (DIPC) approach is described. The goal of this approach is to enhance wake mixing analogous to DIC, but without the large fluctuations in thrust and power. To achieve this, the individual pitch angles are altered in such a way that the wake behind the excited turbine is manipulated dynamically.

Fundamentally, DIPC works as follows. The individual blade pitch angles of the turbine can be used to generate a directional moment on the rotor. Consequently, the direction of the force vector exerted on the airflow can be manipulated. With DIPC, the direction of this force vector is slowly varied, thereby continuously changing the direction of the wake. This is expected to increase wake mixing without significant variations in the magnitude of the rotor thrust force.

A directional thrust force can be accomplished by implementing the Multi-Blade Coordinate (MBC) transformation (Bir, 2008). This transformation decouples – or stated differently: *projects* – the blade loads in a non-rotating reference frame. As a result, the measured out-of-plane blade root bending moments $M(t) \in \mathbb{R}^3$ are projected onto a non-rotating reference frame. For a three-bladed turbine, the MBC transformation is given as:

$$\begin{bmatrix} M_0(t) \\ M_{\text{tilt}}(t) \\ M_{\text{yaw}}(t) \end{bmatrix} = T(\psi) \underbrace{\begin{bmatrix} M_1(t) \\ M_2(t) \\ M_3(t) \end{bmatrix}}_{M(t)}, \quad (4.2)$$

with

$$T(\psi) = \frac{2}{3} \begin{bmatrix} 0.5 & 0.5 & 0.5 \\ \cos(\psi_1) & \cos(\psi_2) & \cos(\psi_3) \\ \sin(\psi_1) & \sin(\psi_2) & \sin(\psi_3) \end{bmatrix},$$

where ψ_b is the azimuth angle for blade b , with $\psi = 0^\circ$ indicating the vertical up-right position. The collective mode M_0 represents the cumulative out-of-plane rotor moment, and M_{tilt} and M_{yaw} represent the fixed-frame and azimuth-independent tilt- and yaw-moments, respectively.

In a similar fashion, the inverse MBC transformation can be used to obtain implementable pitch angles based on the fixed-frame collective, tilt and yaw pitch signals, θ_0 , θ_{tilt} and θ_{yaw} , respectively:

$$\underbrace{\begin{bmatrix} \theta_1(t) \\ \theta_2(t) \\ \theta_3(t) \end{bmatrix}}_{\theta(t)} = T^{-1}(\psi) \begin{bmatrix} \theta_0(t) \\ \theta_{\text{tilt}}(t) \\ \theta_{\text{yaw}}(t) \end{bmatrix}, \quad (4.3)$$

with

$$T^{-1}(\psi) = \begin{bmatrix} 1 & \cos(\psi_1) & \sin(\psi_1) \\ 1 & \cos(\psi_2) & \sin(\psi_2) \\ 1 & \cos(\psi_3) & \sin(\psi_3) \end{bmatrix}.$$

The concept of DIPC is to achieve a dynamically varying tilt and/or yaw moment, such that the wake of the turbine is manipulated in vertical and/or horizontal direction, respectively, over time. To give a proof of concept, a simple feedforward strategy is implemented, where a sinusoidal excitation is superimposed on θ_{tilt} and

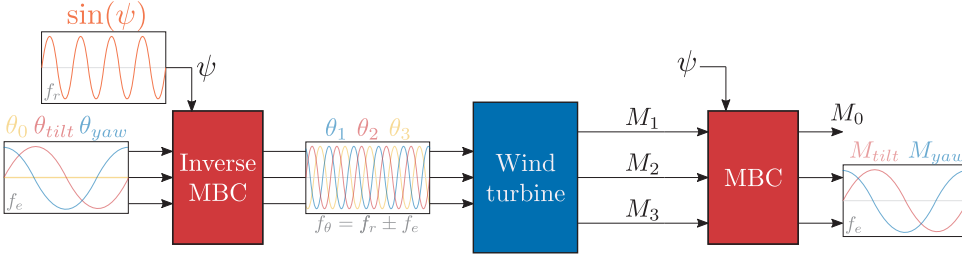


Figure 4.2: A schematic representation of how the MBC transformation is used to achieve periodic yaw and tilt moments on the turbine. Note that the pitch frequency f_θ is slightly different than the rotation frequency f_r due to excitation frequency f_e .

θ_{yaw} , as shown in Figure 4.2. The excitation frequency of θ_{tilt} and θ_{yaw} is chosen to be identical to the DIC case, i.e., $St = 0.25$. Note once more that this is a low-frequency excitation, typically in the range of 10 times slower than the rotational frequency f_r . It is shown later that the resulting tilt and yaw moments are indeed sinusoidal with frequency f_e .

When the tilt and yaw pitch angles inserted into the inverse MBC transformation are constant over time, the resulting pitch angles $\theta(t)$ behaves sinusoidally with frequency f_r . However, when $\theta_0 = 0$ and the tilt and yaw pitch angles are sinusoidal (with frequency f_e), as depicted in Figures 4.2, this leads to a slightly altered frequency of $\theta(t)$. Using (4.3), it can be deduced that:

$$\begin{aligned} \theta_b(t) &= \begin{bmatrix} 1 & \cos(\psi_b) & \sin(\psi_b) \end{bmatrix} \begin{bmatrix} \theta_0(t) \\ \theta_{tilt}(t) \\ \theta_{yaw}(t) \end{bmatrix} \\ &= \theta_0 + \cos(\omega_r t + \psi_{0,b})\theta_{tilt}(t) + \sin(\omega_r t + \psi_{0,b})\theta_{yaw}(t) \\ &= \cos(\omega_r t + \psi_{0,b}) \sin(\omega_e t) + \sin(\omega_r t + \psi_{0,b}) \cos(\omega_e t) \\ &= \sin[(\omega_r + \omega_e)t + \psi_{0,b}], \end{aligned}$$

where ω_r is the rotational velocity [rad/s], and $\omega_e = 2\pi f_e$ [rad/s]. Assuming that ω_r is constant over time, $\psi_b(t) = \omega_r t + \psi_{0,b}$ with $\psi_{0,b}$ the azimuth angle of blade b at $t = 0$. Since the excitation frequency is very low (i.e., $\omega_e \ll \omega_r$) the frequency of the resulting sinusoid, f_θ , differs only slightly from the rotational frequency f_r .

In Figure 4.2, a shift of 90 degrees between the yaw moment and the tilt moment is depicted. As a result, the tilt moment is maximal when the yaw moment is zero, and vice versa. Using the uniform simulation setup in SOWFA, the resulting wake location over time can be visualized. Figure 4.3 shows this wake at eight instances during one excitation period $T_e = D/(St \cdot U_\infty) \approx 80$ s. It can be observed here that this DIPC strategy results in a wake that makes a (counterclockwise) circular motion. This motion can be considered forced wake meandering, and is expected to lead to increased wake mixing.

Figure 4.3 displays the wake for a phase delay of 90 degrees between the tilt and yaw pitch angle, leading to a counterclockwise motion of this wake. This motion

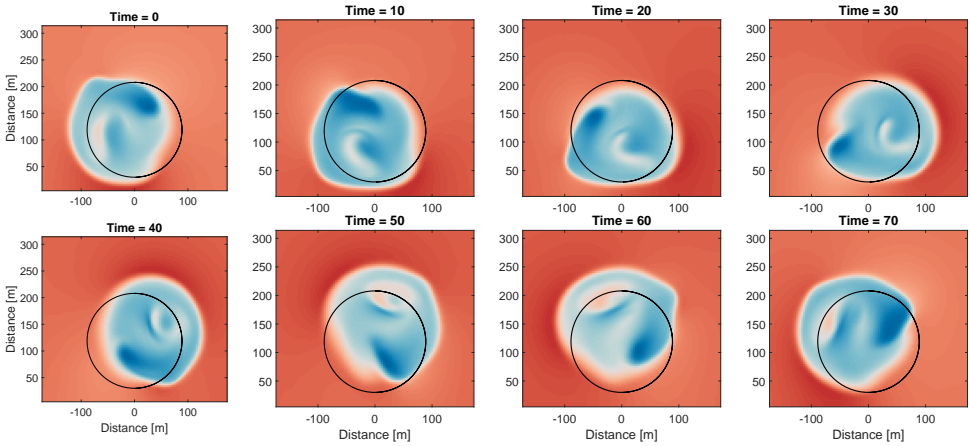


Figure 4.3: A wake as measured at 3D behind the turbine at different time instances when the signals for θ_{ilt} and θ_{yaw} as displayed in Figure 4.2 are applied. Obtained using uniform inflow simulations in SOWFA.

can be explained by the frequency f_θ of the blade pitch, which is slightly higher than the rotation frequency f_r . Therefore, one period of pitching requires slightly less time than one rotation. As wind turbine blades conventionally rotate in clockwise direction, this results in a wake that rotates in counterclockwise direction. Note that a clockwise-rotating wake can subsequently be created by taking a pitch frequency that is slightly *lower* than the rotation frequency f_r . In that case, a phase delay of 270 degrees between the tilt and yaw moment would need to be applied, resulting in:

$$\begin{aligned}\theta_b(t) &= \cos(\omega_b t) \sin(\omega_e t + \psi_{0,b}) - \sin(\omega_b t) \cos(\omega_e t + \psi_{0,b}) \\ &= -\sin[(\omega_b - \omega_e + \psi_{0,b})t].\end{aligned}$$

The propagation of the wake through space is illustrated in Figure 4.4. As this DIPC input results in a wake that has a helical shape, this specific approach is called the *helix strategy*, respectively in counterclockwise (CCW) or clockwise (CW) direction.

Earlier in this section, the claim was made that a sinusoidal tilt and yaw moment can be achieved by simply applying a sinusoidal tilt and yaw angle. To confirm that this is indeed the case, Figure 4.5 shows the tilt and yaw moment for the CCW helix strategy. These moments were obtained using the out-of-plane root bending moments on the individual blades as obtained from SOWFA, subsequently projected onto the non-rotating frame using the MBC transformation (4.2). Afterwards, a low-pass filter was applied to account for high frequency noise on the signal.

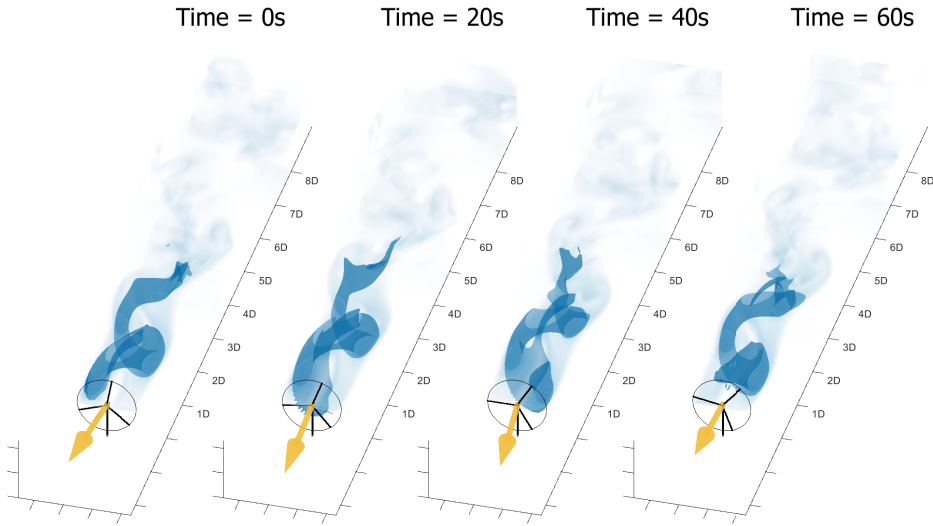


Figure 4.4: Wake propagation for different time instances when the helix strategy is applied. The counterclockwise rotation of the wake can be seen and the near wake clearly exhibits the helix shape that the approach is named after. The yellow arrow represents the vector of the thrust applied on the flow.

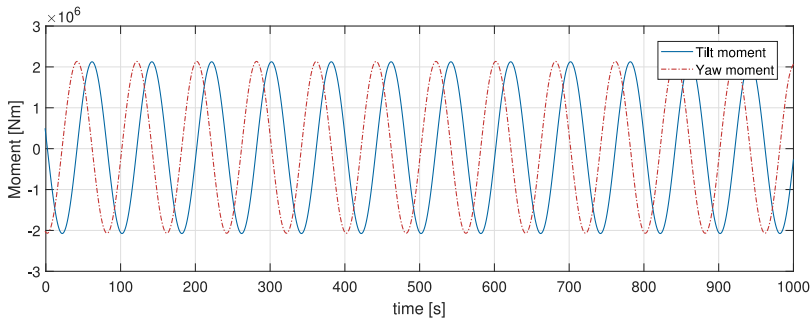


Figure 4.5: The tilt and yaw moments from a turbine operating with the CCW helix approach. Obtained using uniform inflow conditions in SOWFA.

4.4. Results

In this section, the results obtained from the SOWFA simulations with turbulent inflow, as described in Section 4.2, are presented. The helix approach is compared to the baseline greedy control case, as well as with Static Induction Control (SIC) and Dynamic Induction Control (DIC). First, simulations with a single turbine are evaluated. These simulations allow for the investigation of the helix approach on the excited turbine and on the wake behind this turbine. Afterwards, a second turbine is placed in the wake, 5D behind the first turbine, to study the

effect of DIPC on the power generation of this small 2-turbine wind farm.

4.4.1. Single turbine

For the single turbine case, a total of 9 different simulations have been carried out. A comparison between cases is made based on both the performance of the turbine and the energy available in the wake. The simulation cases are specified below:

1. *Baseline case*: static greedy control. All other cases are normalized with respect to this case;
2. *Static Induction Control (SIC), 1°*: SIC where the collective pitch angles are derated with 1°;
3. *SIC, 2°*: Same as case 8, but with the pitch angles derated 2°;
4. *Dynamic Induction Control (DIC), 2.5°*: DIC where the collective pitch angles are excited sinusoidally with an amplitude of 2.5°;
5. *Counterclockwise (CCW) helix, 2.5°*: the helix approach with a phase offset between tilt and yaw moments of 90 degrees (as shown in Figure 4.2). This results in a wake that rotates in counterclockwise direction. The amplitude of the tilt and yaw angles is chosen such that the variation of the implemented pitch angles has an amplitude of 2.5°;
6. *Clockwise (CW) helix, 2.5°*: the helix approach with a phase offset between tilt and yaw moments of 270°. This results in a wake rotating in clockwise direction;
7. *DIC, 4°*: Same as case 2, but with an amplitude of 4°;
8. *CCW helix, 4°*: Same as case 3, but with an amplitude of 4°;
9. *CW helix, 4°*: Same as case 4, but with an amplitude of 4°.

First of all, the effect of the helix approach on the wake is investigated. For this purpose, the mean wind velocity behind the excited turbine is visualized with respect to the baseline case. The resulting figures show how the applied control algorithms change the wake properties. Figure 4.6 shows this mean velocity disparity with respect to the baseline case for case 7 (DIC, 4°). Different cross-sections of the flow field are depicted here to show the effect of DIC on the average wake velocity. Figure 4.7 depicts the same cross-sections for the case 8 (CCW helix, 4°) and Figure 4.8 for case 9 (CW helix, 4°). Remember that, as mentioned in Section 4.3.3, the optimal amplitude and frequency for the helix approach are as of yet unknown. The results presented here should therefore be considered a proof of concept for this approach, not an upper limit of its potential.

Based on these figures, a number of conclusions are drawn. First of all, it is clear that all three strategies successfully increase the average wind velocity in the wake. DIC and CCW helix seem to be equally effective at $3D$, while the helix approach

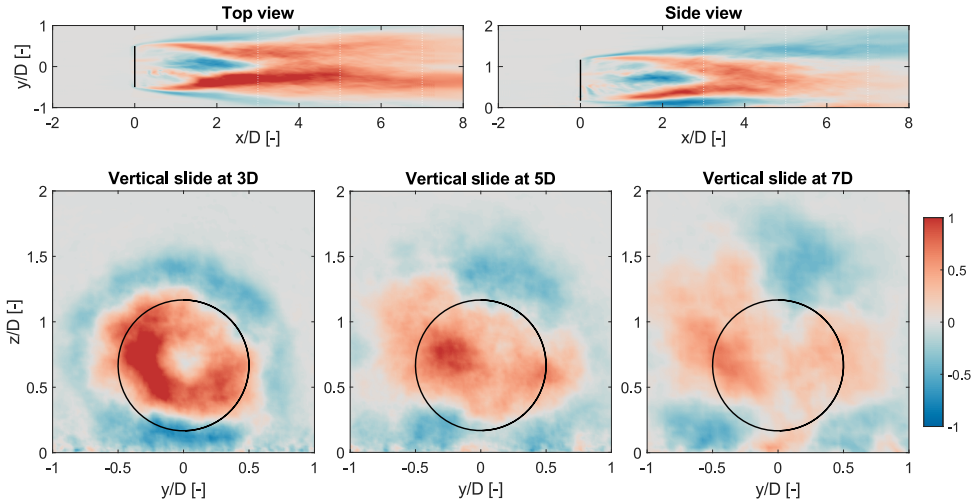


Figure 4.6: The mean wind speed in a wake with respect to the baseline case when DIC is applied (case 7). The turbine location is indicated in black. The top figures give a top and side view of the flow, and the bottom figures show vertical slices at different distances behind the excited turbine. The red areas indicate that DIC increases the wind velocity in the wake significantly, while blue areas indicate where the wind speed is decreased.

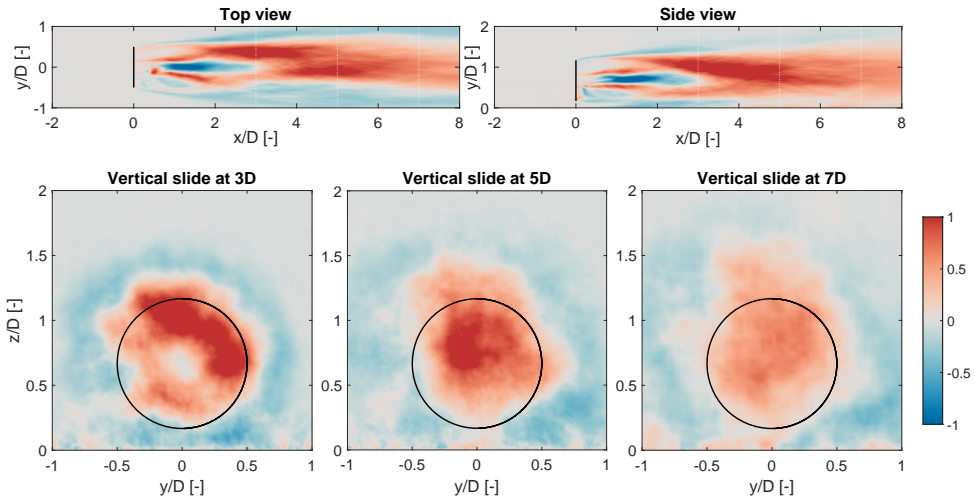


Figure 4.7: The mean wind speed in a wake with respect to the baseline case when CCW helix is applied (case 8), similar to Figure 4.6.

performs increasingly well further downstream. In general, the CW helix appears to be less effective than the CCW helix. Figure 4.8 reveals that the lower performance of the CW approach is caused by the lower velocity in the center of the wake, which is considerably more distinct than in Figure 4.7.

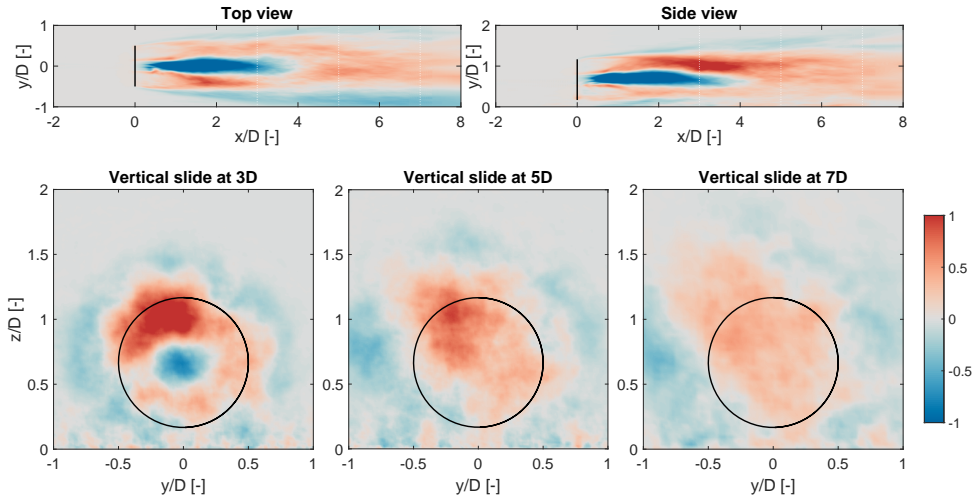


Figure 4.8: The mean wind speed in a wake with respect to the baseline case when CW helix is applied (case 9), similar to Figures 4.6 and 4.7.

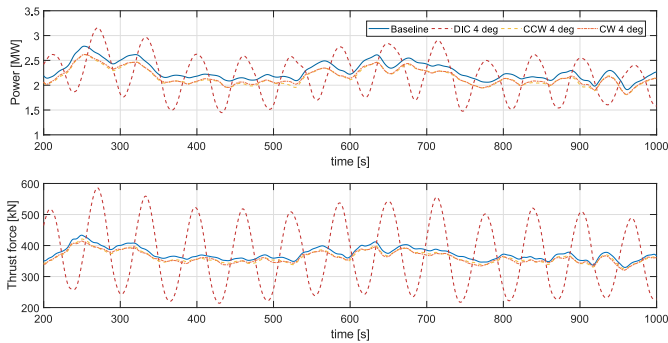


Figure 4.9: The power (top) and thrust (bottom) signals of the wind turbine for the baseline, DIC, CCW helix and CW helix case.

The average kinetic energy increase in the wake at 5D behind the turbine is 23.8 % for DIC, 36.7 % for CCW helix and 19.3 % for CW helix. This indicates that the power increase that can be expected of a second, waked turbine when the CCW helix is applied is higher than in the DIC case.

The mean wake velocities are nonetheless not the most significant difference between DIC and the helix approach. The main advantage of the helix approach becomes clear when the power and thrust signals of the excited turbine are examined, as shown in Figure 4.9. These plots shows that, as expected, DIC results in large variations of both the power generation and the thrust force. Both helix approach simulations show no such variations: the power and thrust are in both cases very similar to the baseline case, although slightly lower. This is also con-

firmed when the variance of these signals is calculated. Compared to the baseline case, the variance of the power and the thrust increases with 80 % and 583 %, respectively, when DIC is applied. With the helix approach, on the other hand, the variance of these signals is more or less the same as in the baseline case.

This significant improvement with regards to the thrust and power variations does not come completely free of charge. Since individual pitch control is used for the helix method, the pitch rate, and subsequently the actuator duty cycle, is higher than with DIC. As visualized in Figure 4.2, the frequency of the pitch signal is determined by the rotational frequency $f_r \approx 0.12$ Hz, slightly altered by the excitation frequency. The pitch signals in DIC, on the other hand, have a much lower frequency of $f_e \approx 0.0126$ Hz, resulting in a very low average pitch rate variation of $0.08^\circ/\text{min}$. As a consequence of the higher pitch frequency, the pitch rate variance of the helix approach with a 4 degree amplitude is $12.5^\circ/\text{min}$ and $8.1^\circ/\text{min}$ for the CCW and CW direction, respectively. Note that although this is significantly higher than with DIC, such a pitch rate should not be considered unreasonably high. In fact, the pitch rate is comparable to that used in load alleviating IPC strategies such as [Bossanyi \(2003, 2005\)](#).

All the results mentioned above, both in terms of turbine performance and wake recovery, are summarized in Table 4.2. This table includes the results obtained for the cases with SIC and with a smaller pitch amplitude of 2.5° . As expected, the lower amplitude has less effect on both the excited turbine and the wake recovery. Apart from that, no significant discrepancies are found between the 2.5° and 4° cases. The SIC results show that, in general, the power lost at the upstream turbine is comparable, while the energy gained in the wake is lower than with the CCW helix approach. Even more so than DIC, SIC seems to be less effective at larger downstream distances. It can therefore be concluded that the helix approach is more effective in increasing the potential energy capture of a wind farm than SIC.

Table 4.2: Turbulent inflow, single turbine results. All but the pitch variation are relative results with respect to the baseline case.

	Static 1°	Static 2°	DIC 2.5°	CCW helix 2.5°	CW helix 2.5°	DIC 4°	CCW helix 4°	CW helix 4°
Power	-1.0%	-3.1%	-1.1%	-1.1%	-1.0%	-2.8%	-2.8%	-2.6%
Variation of power	-2.2%	-5.8%	+79.5%	-3.5%	-1.5%	+194.1%	-7.9%	-5.2%
Variation of thrust	-11.2%	-22.1%	+583.2%	-1.5%	+1.2%	+1423%	-3.7%	+0.3%
Energy at 3D	+14.1%	+31.7%	+20.3%	+20.5%	+7.2%	+42.6%	+47.4%	+21.9%
Energy at 5D	+3.7%	+8.3%	+13.3%	+16.6%	+6.5%	+23.8%	+36.7%	+19.3%
Energy at 7D	+2.0%	+3.7%	+7.3%	+12.4%	+5.5%	+13.4%	+25.6%	+14.7%
Pitch variation [°/min]	0	0	0.08	4.94	3.22	0.20	12.52	8.13

4.4.2. Two-turbine wind farm

In this section, the performance of a two-turbine wind farm is discussed. The same cases of the single turbine simulations are used, but a second turbine is now placed $5D$ behind the first turbine. In all cases, the second turbine operates at its static optimum, i.e., the different control strategies are only implemented on the upstream machine.

The results that are presented here, focus again on the cases with a pitch amplitude of 4 degrees. The power and thrust signals of both turbines in these simulations are shown in Figure 4.10. From this figure, it follows that the power gains obtained at turbine 2 are similar with both dynamic control strategies. However, the plot also shows that DIC not only increases the variations in power and thrust of the excited turbine, but also of the downstream turbine. This effect is significantly less pronounced for the helix strategies.

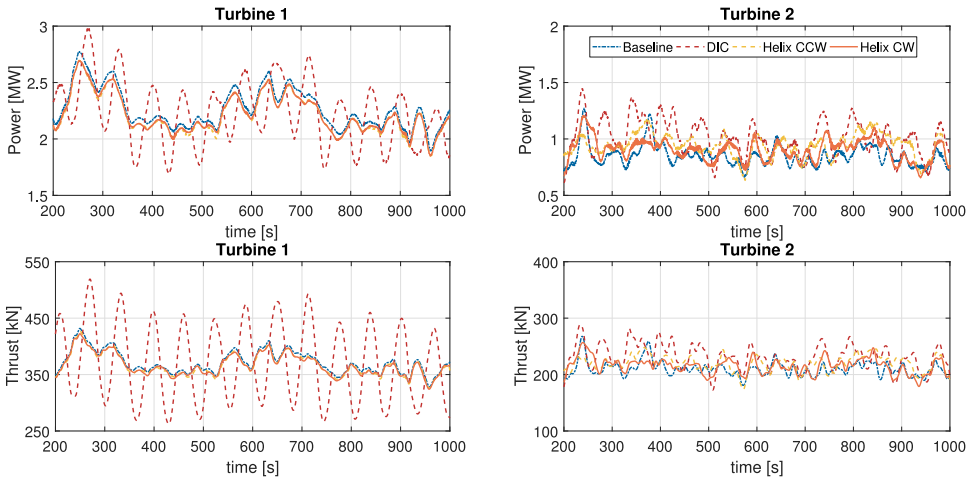


Figure 4.10: The power (top) and thrust (bottom) signals of turbines 1 (left) and 2 (right) for cases 1, 5, 6 and 7. The variations in power and thrust associated with DIC are not present with the helix approach. As a result, the power and thrust variations at the downstream turbine are also significantly lower.

Table 4.3: Turbulent inflow, two-turbine results. All results are relative with respect to the baseline case.

	Static 1°	Static 2°	DIC 2.5°	CCW helix 2.5°	CW helix 2.5°	DIC 4°	CCW helix 4°	CW helix 4°
Power T1	-1.0%	-3.1%	-1.1%	-1.1%	-1.0%	-2.8%	-2.8%	-2.6%
Power T2	+1.6%	+5.3%	+14.6%	+17.2%	+6.3%	+27.3%	+39.5%	+18.0%
Total power generation	-0.3%	-1.0%	+2.8%	+3.4%	+0.8%	+4.6%	+7.5%	+2.5%
Variance of power T1	-2.2%	-5.8%	+79.6%	-3.4%	-1.4%	+194.0%	-7.9%	-5.1%
Variance of power T2	-11.0%	-17.6%	+280.8%	+143.0%	+82.2%	+583.6%	+239.4%	+187.2%
Variance of thrust T1	-11.3%	-22.1%	+580.7%	-1.5%	+1.1%	+1416.7%	-3.9%	+0.4%
Variance of thrust T2	-13.0%	-25.9%	+165.1%	+71.6%	+45.5%	+340.9%	+123.1%	+99.9%

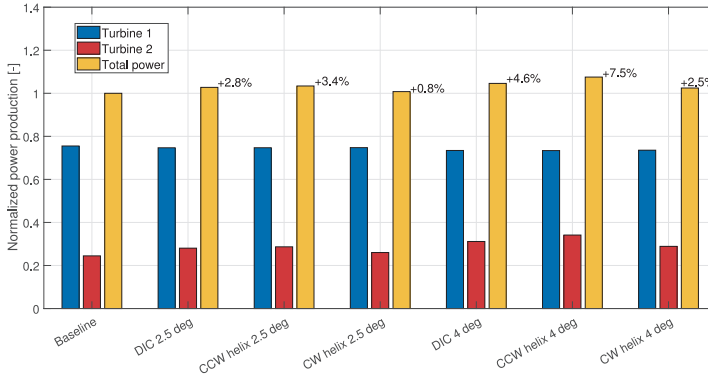


Figure 4.11: Power generation of the two-turbine wind farm for different control strategies, showing the limited power loss at turbine 1 with all methods. The power gain at turbine 2 results in a farm-wide increase in power generation.

All findings with respect to power and thrust are summarized in Table 4.3. Notice that the energy increase at $5D$ as predicted in Table 4.2 corresponds very well with the actual power increase of a turbine at $5D$. As a result, the CCW helix approach with a 4° pitch amplitude increases the power generation of this 2-turbine wind farm with 7.5%. This is considerably higher than the 4.6% gain obtained with DIC. The overall energy capture of all strategies is shown in Figure 4.11.

Apart from the power generation, it is also interesting to investigate the variations of power and thrust. With both helix approaches, the power and thrust variations of the excited turbine are, in general, slightly reduced. Due to the increased wake velocity and turbulence, the downstream turbines experience a significantly higher power and thrust variations than in the baseline case. However, compared to DIC, these variations are much lower. As a result, the fatigue loads that might lead to structural damage of the wind turbine are expected to be substantially lower than with DIC.

A final note should be made with respect to the performance of the helix approach: as the research presented in this chapter serves mainly as a proof of concept, the optimal settings for the helix approach are as of yet unknown. In this study, it was assumed that the optimal excitation frequency is identical to the optimal DIC frequency. As such, the 7.5% power gain found here can be considered conservative, as a different dynamic input signal might lead to better performance.

4.5. Conclusions

This chapter proposes a novel wind farm pitch control strategy. The strategy involves using Individual Pitch Control (IPC) to dynamically vary the direction of the thrust force exerted on the flow by a wind turbine, leading to a helical wake that increases mixing. As a result, downstream turbines experience higher wind speeds and subsequently have a higher power generation. Due to the helical

shape of the wake, this approach is named the *helix approach*. A proof of concept is given for this novel dynamic wind farm control strategy.

The strategy is tested using high-fidelity LES simulations, proving that the helix approach is effective at increasing wake recovery: the energy in the wake can be increased by up to 47%. Furthermore, it is observed that a helix rotating in counterclockwise direction results in better wake recovery than a helix rotating in clockwise direction. Simulations with a second turbine in the wake of the controlled turbine, located 5 rotor diameters downstream, show that the energy capture can be increased with up to 7.5% for this two-turbine wind farm. As the optimal control settings for the helix approach have not yet been evaluated, this gain should be seen as an indication of its potential, not as an upper limit.

The helix approach is compared with different existing control strategies. The current simulations show that it is a more effective method to increase the energy capture of a wind farm than both static derating and dynamic induction control. Compared to the latter, the helix approach results in power and thrust variations that are over a factor 2 lower. Furthermore, unlike yaw-based wake redirection, the operational strategy used in the helix approach does not deviate from the operating range for which the turbine was designed. This should allow for a much quicker adaptation of the technology by the industry, perhaps delivering the first wind farm control methodology that can reliably increase the power generation in existing wind farms without the need for slow certification protocols and fundamental turbine redesign.

This chapter should be considered as a proof of concept. As the helix approach, or dynamic IPC in general, is a completely novel concept, this chapter only shows that it *can* be an effective wind farm control strategy. To determine its full potential, further exploration is necessary. Future research possibilities include, but are limited to, studying the difference between the clockwise and counterclockwise helix, finding the optimal blade excitation signals, investigating the damage equivalent load effects on both the excited and downstream turbine, applying closed-loop control on the yaw and tilt moments, increasing the farm size to study the effect on turbines further downstream, executing scaled wind tunnel experiments and full scale tests on an actual wind turbine or wind farm.

5

Conclusion and recommendations

De waarheid is nooit precies zoals je denkt dat hij zal zijn.

The truth is never exactly as you think it will be.

– Johan Cruijff,
on the deceitfulness of scientific truth.

The closing chapter of this dissertation wraps up the research presented and produces the overarching conclusions. Two existing pitch control strategies that have the potential to improve the levelized cost of wind energy are validated by means of successful wind tunnel campaigns. A third novel technology was developed and evaluated in high-fidelity simulations. The novelty of these technologies implies that the maturity level is still relatively low. Subsequently, an elaborate list of recommendations for future research is included to further mature these technologies.

Conclusions

The research objective formulated in Chapter 1 of this dissertation was to *develop and validate novel pitch control technologies that further decrease the levelized cost of wind energy*. This dissertation contributed to developing two existing control technologies that achieve this in different ways, and proposes a third, novel approach. Each of these methods could improve the performance of large scale wind farms in the future. As the results presented in this dissertation are positive, these technologies open up a wide range of new research opportunities that could further decrease the levelized cost of wind energy. By answering the research sub-questions posed in Chapter 1, the contribution of this dissertation with respect to the literature is highlighted.

I: How do different individual pitch control technologies that aim to mitigate blade loads compare in wind tunnel experiments that generate realistic, reproducible wind conditions?

Two different Individual Pitch Control (IPC) strategies are evaluated in Chapter 2: data-driven Subspace Predictive Repetitive Control (SPRC) and Conventional IPC (CIPC). SPRC is a technology that uses subspace identification to obtain a linear model of the turbine and applies repetitive control to mitigate loads. The results show that, in realistic wind conditions, SPRC performs slightly better than CIPC, with average load reductions of 59 % and 49 %, respectively. Apart from improved load alleviation, SPRC is also found to achieve this with an average 21 % lower pitch actuation. This indicates that SPRC not only alleviates blade loads, but also reduces wear on the blade pitch bearings – which is considered the major downside to IPC.

It is essential for load alleviation technologies that they are able to adapt to changes in wind conditions, as this commonly occurs in the field. The results presented in Chapter 2 show that SPRC is able to adapt to changing operating conditions. The subspace identification process refines the turbine model and the repetitive control action is adjusted accordingly to retain load mitigating performance. It can therefore be concluded that SPRC can be considered as a viable alternative to conventional IPC.

II: How does periodic dynamic induction control perform with respect to wind farm power generation in scaled wind tunnel experiments?

Chapter 3 presents the results of the first set of wind tunnel experiments in which dynamic wake mixing was used to increase the energy capture of a wind farm. The outcome was telling: where [Campagnolo et al. \(2016a\)](#) showed in similar experiments that the benefit of static induction control is minimal, periodic Dynamic Induction Control (DIC) was able to increase wind farm power capture by 4 %. In the case that was investigated, with full wake interaction between turbines, DIC displayed similar effectiveness as wake redirection by yawing.

This outcome confirms the results of simulation experiments ([Munters and Meyers, 2018a](#)), showing that DIC is a viable technology to enhance wake mixing for

wind farm power maximization purposes. This approach is more effective than static induction, and the gain in power yield in case of full wake interaction is comparable to wake redirection control. It can be considered as an alternative to wake redirection control, which is already being implemented in wind farms ([Siemens Gamesa Renewable Energy, 2019](#)).

III: How much do the turbine damage equivalent loads rise when dynamic control technologies are applied, and are these increased loads compensated for by the higher power generation?

To answer this sub-question, aeroelastic simulations with and without DIC have been executed, which are presented in Section 3.5. To determine the effect of DIC on the lifetime of the components of the controlled turbine, the Damage Equivalent Load (DEL) on the blades, tower and hub is computed.

When DIC is applied with a frequency that corresponds to the optimum found in Section 3.6, the hub and blade DELs increase slightly. However, these negative effects are smaller than or similar to the positive effect on power generation. The DEL experienced by the tower on the other hand, increases at a substantially higher rate. These results therefore do not give a uniform answer to whether or not the benefit of additional power generation outweighs the increased loads. To draw a final conclusion on whether the balance of power and load increase with DIC is positive, additional research, for example on the downstream turbines, is necessary.

IV: Can an alternative dynamic control technology be developed that maximizes power generation while minimizing additional turbine loads?

In Chapter 4, a novel, patent-pending ([van Wingerden *et al.*, 2019](#)) dynamic control technology is introduced: the helix approach. This technique uses individual pitch control instead of collective pitch to enhance wake mixing, and is validated using high-fidelity simulations. The outcome of these simulations indicate that helix approach results in more wake mixing and subsequently a higher wind farm power generation. The energy capture of an aligned 2-turbine wind farm can be increased with up to 7.5%, compared to 4.6% for DIC. It can therefore be concluded that the helix approach is a viable, possibly more potent control technology to maximize wind farm power generation.

The helix approach does not make use of variations in the thrust force, and is therefore expected to result in lower tower loads than DIC. This is demonstrated in Section 4.4, where the variations in tower thrust are shown to decrease when the helix approach is implemented, whereas DIC leads to a substantial increase. Therefore, the helix approach could prove to be not only a more desirable control technology from a power maximization perspective, but also from a loads perspective. Nevertheless, additional research on this new technology is necessary to further strengthen these conclusions. Regardless, it is undeniable that the helix approach adds a control degree of freedom which can be exploited to find optimal solutions to the wind farm control problem.

Recommendations

New research also brings to light new research questions. This is especially true for the research presented in this dissertation, as novel technologies are proposed and investigated. As the maturity level of these technologies is still relatively low, many questions still remain to be investigated. This section lists the most important open questions related to this dissertation, sorted by subject.

Subspace Predictive Repetitive Control

- The next crucial step towards implementation of SPRC-based IPC in commercial wind turbines is a set of field experiments. A comparison could be made with field tests that have already been executed with conventional IPC (see, e.g., [Bossanyi et al., 2013](#); [van Solingen et al., 2016](#)).
- Recent simulation experiments have shown that SPRC, unlike conventional IPC, maintains load mitigating performance in case of blade actuator faults ([Liu et al., 2020](#)). This is an interesting result that could be an important argument to favor SPRC above conventional IPC. To validate these results, wind tunnel experiments or field tests with a dysfunctional or disabled blade need to be conducted.
- In this dissertation, SPRC was tested on a horizontal-axis wind turbine, which is the most common type of commercial turbine. However, the principles could also be implemented on vertical-axis turbines, where the MBC transformation used in conventional IPC is not applicable.

Enhanced wake mixing

This section mentions recommendations that apply to dynamic pitch strategies for enhanced wake mixing, of which DIC and the helix approach are examples. The following two sections list recommendations that apply specifically for DIC and the helix approach, respectively.

- In this dissertation, two different dynamic wake mixing strategies have been evaluated. Both methods are effective in terms of increasing power generation, but these technologies might only be scratching the surface. Other dynamic control strategies might emerge that prove to be even more effective. Research into alternative dynamic control strategies could therefore be a very interesting future research topic. This includes, but is not limited to:
 - Using different control degrees of freedom of a turbine. This dissertation investigates only pitch action, both collective and individual. Research is also being conducted in dynamic yawing ([Munters and Meyers, 2018b](#); [Kimura et al., 2019](#)), but perhaps the generator torque or, in the future, the turbine tilt angle could also be used effectively.
 - This dissertation focuses on sinusoidal signals, but different time-varying control signals might prove to be more effective.

- Applying dynamic control strategies on waked wind turbines. [Munters and Meyers \(2018a\)](#) show that, at least in a simulation environment, a sinusoidal signal on the second turbine in a row is not effective in increasing wind farm power. Nevertheless, this result only proves that it does not work in this specific case. This does not guarantee that dynamic control strategies can never work on downstream turbines.
- Combining dynamic wake mixing with other control strategies. For example, DIC could be combined with IPC to alleviate loads, or with yaw control to further increase the control authority on the wake of a turbine.
- The results of this dissertation show that dynamic wake mixing works as a power maximization technique. However, it does not fully answer the question *why* it works. The physics behind dynamic wake mixing are not completely understood yet. Answering the following questions could perhaps shed some light on this phenomenon:
 - The results of both simulations and wind tunnel tests show that certain excitation frequencies work better than others. It is not fully understood yet why this is the case. Perhaps, dynamic modeling of the flow, for example with Dynamic Mode Decomposition (DMD) (see, e.g., [Schmid, 2010](#); [Kutz et al., 2016](#)), could explain this result.
 - In [Munters and Meyers \(2018a\)](#), it is hypothesized that the optimal excitation frequency relates to the Strouhal number, which scales the frequency for rotor diameter and wind speed. Although plausible, this hypothesis has not been thoroughly tested as of yet. If the optimum scales with the Strouhal number, it should be the same for different turbine sizes, turbine spacing and wind speeds. Experiments in which one or all of these parameters are changed could prove or disprove the Strouhal-hypothesis.
 - Wind tunnel experiments with Particle Image Velocimetry (PIV) measurements (see, e.g., [Tescione et al., 2014](#)) could explain what is happening in the wake of a turbine operating with dynamic control. Analysis of PIV-data could therefore help clarify the physics behind the effectiveness of dynamic wake mixing.
- This dissertation shows that dynamic wake mixing can work under constant operating conditions. In actual wind farms, the operating conditions are subject to change, which usually requires the control approach to adapt. Therefore, for application in commercial wind farms, a closed-loop control algorithm would need to be developed that determines the optimal dynamic control strategy based on the current operating conditions.
- Chapters 3 and 4 have demonstrated that in case of full wake interaction, dynamic control can compete with the state-of-the-art static control technologies. The case of partial wake overlap has not yet been investigated, and could reveal the true potential of dynamic wake mixing.

Dynamic Induction Control

- The results presented in this dissertation show that, in contrast with results found in simulations (Munters and Meyers, 2018a), increasing the amplitude of excitation had a negative effect on the wind farm power generation. In the wind tunnel, the power drop of the upstream turbine at higher amplitudes was substantially higher than in simulation experiments. It is hypothesized that this is partly caused by rotor instability of the utilized G1 turbine models. However, further research is necessary to validate this hypothesis.
- The load analysis presented in Chapter 3 looks only at the excited turbine. It can be expected that downstream turbines also experience increased loads, as turbulence is induced with DIC. Future research could therefore be directed towards the overall load experienced by a wind farm that applies DIC. This could give the full picture of how the benefit of increased power generation balances with the drawback of higher farm-wide loads.
- Field tests of DIC would mean the final crucial step towards implementation in commercial wind farms. These tests should analyse both the overall power capture and the load impact of DIC on the wind farm.

5

Helix approach

- Chapter 4 gives a proof of concept of the helix approach. To validate these results, the following additional experiments could be executed:
 - Experiments with different wind speeds and turbulence intensities can be conducted to confirm that the helix approach works under different operating conditions.
 - In this dissertation, only a simple 2-turbine wind farm has been investigated. Experiments with different wind farm layouts could give a better indication of the full potential of this technology.
 - By conducting wind tunnel experiments and field tests, the next crucial steps towards proving the effectiveness of this strategy and applying it to commercial wind farms could be taken. Plans for wind tunnel experiments with the helix are currently being planned at the TU Delft. Meanwhile, the helix approach is also part of the plans for the *Hollandse Kust Noord* wind farm. These plans aim to execute field experiments with the helix by the year 2023.
- A complete load analysis on a turbine that applies the helix approach, as well as on potential downstream turbines, is paramount in assessing whether this technology is able to improve the levelized cost of wind energy.
- In Section 4.4, it was demonstrated that a helix rotating in counterclockwise direction is more effective in terms of wake mixing than a clockwise helix. This result is not fully understood yet, and could be an interesting topic for future investigations.

- In the simulations performed in Chapter 4, it was assumed that the optimal frequency of the yaw and tilt excitation is the same as for DIC. Experiments where this frequency is varied are necessary to confirm this hypothesis.

Bibliography

- J. Annoni, P. M. Gebraad, A. K. Scholbrock, P. A. Fleming, and J. W. van Wingerden, *Analysis of axial-induction-based wind plant control using an engineering and a high-order wind plant model*, *Wind Energy* **19**, 1135 (2016).
- J. Annoni, A. Scholbrock, M. Churchfield, and P. Fleming, *Evaluating tilt for wind plants*, *2017 American Control Conference (ACC)*, 717 (2017).
- J. Annoni, P. Fleming, A. Scholbrock, J. Roadman, S. Dana, C. Adcock, F. Porté-Agel, S. Raach, F. Haizmann, and D. Schlipf, *Analysis of control-oriented wake modeling tools using lidar field results*, *Wind Energy Science* **3**, 819 (2018).
- T. Ashuri, M. B. Zaaijer, J. R. Martins, G. J. Van Bussel, and G. A. Van Kuik, *Multi-disciplinary design optimization of offshore wind turbines for minimum levelized cost of energy*, *Renewable energy* **68**, 893 (2014).
- D. Attenborough, *The people's seat address*, (2018), speech by Sir David Attenborough at the 24th Conference of the Parties to the United Nations Framework Convention on Climate Change, Katowice, Poland. Accessed: 06-10-2020.
- C. Bak, F. Zhale, R. Bitsche, T. Kim, A. Yde, L. C. Henriksen, M. H. Hansen, J. P. A. A. Blasques, and A. Gaunaa, M abd Natarajan, *The DTU 10-MW Reference Wind Turbine*, Tech. Rep. (Technical University of Denmark (DTU), Department of Wind Energy., 2013).
- T. K. Barlas and G. A. van Kuik, *Review of state of the art in smart rotor control research for wind turbines*, *Progress in Aerospace Sciences* **46**, 1 (2010).
- M. Bastankhah and F. Porté-Agel, *Experimental and theoretical study of wind turbine wakes in yawed conditions*, *Journal of Fluid Mechanics* **806**, 506 (2016).
- O. A. Bauchau, *Flexible Multibody Dynamics*, Solid Mechanics and its Applications, Vol. 176 (Springer Netherlands, Dordrecht, 2011).
- J. D. Berman and K. Ebisu, *Changes in us air pollution during the covid-19 pandemic*, *Science of the Total Environment* **739**, 139864 (2020).
- A. Betz, *Das maximum der theoretisch möglichen ausnutzung des windes durch windmotoren*, *Zeitschrift fur das gesamte Turbinenwesten* **20** (1920).
- G. Bir, *Multi-blade coordinate transformation and its application to wind turbine analysis*, in *46th AIAA aerospace sciences meeting and exhibit* (2008) p. 1300.

- S. Boersma, B. Doekemeijer, P. M. Gebraad, P. A. Fleming, J. Annoni, A. K. Scholbrock, J. A. Frederik, and J. W. van Wingerden, *A tutorial on control-oriented modeling and control of wind farms*, *2017 American Control Conference (ACC)*, **1** (2017).
- E. A. Bossanyi, P. A. Fleming, and A. D. Wright, *Validation of individual pitch control by field tests on two-and three-bladed wind turbines*, *IEEE Transactions on Control Systems Technology* **21**, 1067 (2013).
- E. A. Bossanyi, *The design of closed loop controllers for wind turbines*, *Wind Energy* **3**, 149 (2000).
- E. A. Bossanyi, *Individual blade pitch control for load reduction*, *Wind Energy* **6**, 119 (2003).
- E. A. Bossanyi, *Further load reductions with individual pitch control*, *Wind Energy* **8**, 481 (2005).
- C. L. Bottasso and A. Croce, *Cp-Lambda user manual*, Tech. Rep. (Dipartimento di Scienze e Tecnologie Aerospaziali, Politecnico di Milano, Milano, Italy, 2009–2018).
- C. L. Bottasso, A. Croce, B. Savini, W. Sirchi, and L. Trainelli, *Aero-servo-elastic modeling and control of wind turbines using finite element multibody procedures*, *Multibody Systems Dynamics* **16**, 291 (2006).
- C. L. Bottasso, F. Campagnolo, and V. Petrović, *Wind tunnel testing of scaled wind turbine models: Beyond aerodynamics*, *Journal of Wind Engineering and Industrial Aerodynamics* **127**, 11 (2014).
- F. Campagnolo, V. Petrović, J. Schreiber, E. M. Nanos, A. Croce, and C. L. Bottasso, *Wind tunnel testing of a closed-loop wake deflection controller for wind farm power maximization*, *Journal of Physics: Conference Series* **753**, 7 (2016a).
- F. Campagnolo, V. Petrović, C. L. Bottasso, and A. Croce, *Wind tunnel testing of wake control strategies*, in *2016 American Control Conference (ACC)* (2016) pp. 513–518.
- F. Campagnolo, V. Petrović, E. Nanos, C. Tan, C. Bottasso, H. K. I. Paek, and K. Kim, *Wind tunnel testing of power maximization control strategies applied to a multi-turbine floating wind power platform*, *Proceedings of the International Offshore and Polar Engineering Conference* (2016c).
- Centraal Bureau van de Statistiek, *Statline*, (2019), accessed: 15-09-2020.
- K. Chen, M. Wang, C. Huang, P. L. Kinney, and P. T. Anastas, *Air pollution reduction and mortality benefit during the covid-19 outbreak in china*, *The Lancet Planetary Health* **4**, e210 (2020).

- A. Chiuso, *The role of vector autoregressive modeling in predictor-based subspace identification*, *Automatica* **43**, 1034 (2007).
- M. Churchfield and S. Lee, *NWTC design codes – SOWFA*, Tech. Rep. (National Renewable Energy Laboratory (NREL), 2012).
- M. J. Churchfield, S. Lee, J. Michalakes, and P. J. Moriarty, *A numerical study of the effects of atmospheric and wake turbulence on wind turbine dynamics*, *Journal of Turbulence* **13**, N14 (2012).
- U. Ciri, M. A. Rotea, and S. Leonardi, *Model-free control of wind farms: A comparative study between individual and coordinated extremum seeking*, *Renewable energy* **113**, 1033 (2017).
- DNV-GL, *Energy Transition Outlook*, Tech. Rep. (2020).
- B. M. Doekemeijer and R. Storm, *Floris_m*, (2018).
- B. M. Doekemeijer, S. Kern, S. Maturu, S. Kanev, B. Salbert, J. Schreiber, F. Campagnolo, C. L. Bottasso, S. Schuler, F. Wilts, *et al.*, *Field experiment for open-loop yaw-based wake steering at a commercial onshore wind farm in Italy*, *Wind Energy Science Discussions* (2020), 10.5194/wes-2020-80.
- B. Doekemeijer, *Closing the loop in model-based wind farm control* (2020).
- J. Dong and M. Verhaegen, *On the equivalence of closed-loop subspace predictive control with l_{qg}*, in *2008 47th IEEE Conference on Decision and Control* (IEEE, 2008) pp. 4085–4090.
- Eurostat, *Share of renewable energy in the EU up to 18.0%*, (2020), accessed: 15-09-2020.
- P. A. Fleming, P. M. Gebraad, S. Lee, J. W. van Wingerden, K. Johnson, M. Churchfield, J. Michalakes, P. Spalart, and P. Moriarty, *Evaluating techniques for redirecting turbine wakes using SOWFA*, *Renewable Energy* **70**, 211 (2014).
- P. Fleming, P. M. Gebraad, S. Lee, J. W. van Wingerden, K. Johnson, M. Churchfield, J. Michalakes, P. Spalart, and P. Moriarty, *Simulation comparison of wake mitigation control strategies for a two-turbine case*, *Wind Energy* **18**, 2135 (2015).
- P. Fleming, J. Annoni, J. J. Shah, L. Wang, S. Ananthan, Z. Zhang, K. Hutchings, P. Wang, W. Chen, and L. Chen, *Field test of wake steering at an offshore wind farm*, *Wind Energy Science* **2**, 229 (2017).
- P. Fleming, J. King, K. Dykes, E. Simley, J. Roadman, A. Scholbrock, P. Murphy, J. K. Lundquist, P. Moriarty, K. Fleming, *et al.*, *Initial results from a field campaign of wake steering applied at a commercial wind farm—part 1*, *Wind Energy Science* **4** (2019), 10.5194/wes-4-273-2019.

- P. Fleming, J. King, E. Simley, J. Roadman, A. Scholbrock, P. Murphy, J. K. Lundquist, P. Moriarty, K. Fleming, J. v. Dam, *et al.*, *Continued results from a field campaign of wake steering applied at a commercial wind farm—part 2*, *Wind Energy Science* **5**, 945 (2020).
- P. Gebraad, F. van Dam, and J. van Wingerden, *A model-free distributed approach for wind plant control*, *2013 American Control Conference (ACC)* , 628 (2013).
- J. P. Goit and J. Meyers, *Optimal control of energy extraction in wind-farm boundary layers*, *Journal of Fluid Mechanics* **768**, 5 (2015).
- F. Gustafsson, *Adaptive filtering and change detection*, Vol. 1 (Citeseer, 2000).
- R. Hallouzi, M. Verhaegen, R. Babuška, and S. Kanev, *Model weight and state estimation for multiple model systems applied to fault detection and identification*, *IFAC Proceedings Volumes* **39**, 648 (2006).
- H. Heißelmann, J. Peinke, and M. Hölling, *Experimental airfoil characterization under tailored turbulent conditions*, *Journal of Physics: Conference Series* **753**, 072020 (2016).
- I. Houtzager, J. W. van Wingerden, and M. Verhaegen, *Rejection of periodic wind disturbances on a smart rotor test section using lifted repetitive control*, *IEEE Transactions on Control Systems Technology* **21**, 347 (2012).
- M. F. Howland, S. K. Lele, and J. O. Dabiri, *Wind farm power optimization through wake steering*, *Proceedings of the National Academy of Sciences* **116**, 14495 (2019).
- IEC 61400-1, *Wind Turbines — Part 1: Design requirements*, Tech. Rep. (Garrad Hassan and Partners Ltd, 2004).
- N. O. Jensen, *A note on wind generator interaction* (1983).
- Á. Jiménez, A. Crespo, and E. Migoya, *Application of a les technique to characterize the wake deflection of a wind turbine in yaw*, *Wind energy* **13**, 559 (2010).
- K. E. Johnson and N. Thomas, *Wind farm control: Addressing the aerodynamic interaction among wind turbines*, in *2009 American Control Conference* (IEEE, 2009) pp. 2104–2109.
- B. J. Jonkman and M. L. Buhl Jr., *TurbSim user's guide*, Tech. Rep. (National Renewable Energy Laboratory (NREL), 2006).
- J. M. Jonkman, S. Butterfield, W. Musial, and G. Scott, *Definition of a 5-MW reference wind turbine for offshore system development*, Tech. Rep. (National Renewable Energy Laboratory (NREL), 2009).
- I. Katic, J. Højstrup, and N. O. Jensen, *A simple model for cluster efficiency*, in *European wind energy association conference and exhibition* (1987).

- K. Kimura, Y. Tanabe, Y. Matsuo, and M. Iida, *Forced wake meandering for rapid recovery of velocity deficits in a wind turbine wake*, in *AIAA Scitech 2019 Forum* (2019) p. 2083.
- P. Knebel, A. Kittel, and J. Peinke, *Atmospheric wind field conditions generated by active grids*, *Experiments in fluids* **51**, 471 (2011).
- A. Kolmogorov, *The local structure of turbulence in an incompressible viscous fluid for very high reynolds number*, in *Dokl. Akad. Nauk. SSSR*, Vol. 30 (1941) p. 301.
- L. Kröger, J. A. Frederik, J. W. van Wingerden, J. Peinke, and M. Hölling, *Generation of user defined turbulent inflow conditions by an active grid for validation experiments*, *Journal of Physics: Conference Series* **1037** (2018), 10.1088/1742-6596/1037/5/052002.
- J. N. Kutz, S. L. Brunton, B. W. Brunton, and J. L. Proctor, *Dynamic mode decomposition: data-driven modeling of complex systems* (SIAM, 2016).
- C. Le Quéré, R. B. Jackson, M. W. Jones, A. J. Smith, S. Abernethy, R. M. Andrew, A. J. De-Gol, D. R. Willis, Y. Shan, J. G. Canadell, *et al.*, *Temporary reduction in daily global co2 emissions during the covid-19 forced confinement*, *Nature Climate Change* , 1 (2020).
- P. Lissaman, *Energy effectiveness of arbitrary arrays of wind turbines*, *Journal of Energy* **3**, 323 (1979).
- Y. Liu, J. Frederik, A. Fontanella, R. M. Ferrari, and J. W. van Wingerden, *Adaptive fault accommodation of pitch actuator stuck type of fault in floating offshore wind turbines: a subspace predictive repetitive control approach*, *2020 American Control Conference (ACC)* , 4077 (2020).
- H. Makita, *Realization of a large-scale turbulence field in a small wind tunnel*, *Fluid Dynamics Research* **8**, 53 (1991).
- J. R. Marden, S. D. Ruben, and L. Y. Pao, *A model-free approach to wind farm control using game theoretic methods*, *IEEE Transactions on Control Systems Technology* **21**, 1207 (2013).
- Mathworks, *Simulink Real-Time*, (2015).
- S. P. Mulders, A. K. Pamososuryo, G. E. Disario, and J. W. van Wingerden, *Analysis and optimal individual pitch control decoupling by inclusion of an azimuth offset in the multiblade coordinate transformation*, *Wind Energy* **22**, 341 (2019).
- W. Munters and J. Meyers, *Effect of wind turbine response time on optimal dynamic induction control of wind farms*, *Journal of Physics: Conference Series* **753**, 052007 (2016).
- W. Munters and J. Meyers, *An optimal control framework for dynamic induction control of wind farms and their interaction with the atmospheric boundary layer*, *Philosophical Transactions of the Royal Society A* **375**, 20160100 (2017).

- W. Munters and J. Meyers, *Towards practical dynamic induction control of wind farms: analysis of optimally controlled wind-farm boundary layers and sinusoidal induction control of first-row turbines*, *Wind Energy Science* **3**, 409 (2018a).
- W. Munters and J. Meyers, *Dynamic strategies for yaw and induction control of wind farms based on large-eddy simulation and optimization*, *Energies* **11**, 177 (2018b).
- L. Mydlarski, *A turbulent quarter century of active grids: from makita (1991) to the present*, *Fluid Dynamics Research* **49**, 061401 (2017).
- S. T. Navalkar, J. W. van Wingerden, E. van Solingen, T. Oomen, E. Pasterkamp, and G. Van Kuik, *Subspace predictive repetitive control to mitigate periodic loads on large scale wind turbines*, *Mechatronics* **24**, 916 (2014).
- S. T. Navalkar, E. van Solingen, and J. W. van Wingerden, *Wind tunnel testing of subspace predictive repetitive control for variable pitch wind turbines*, *IEEE Transactions on Control Systems Technology* **23**, 2101 (2015).
- S. T. Navalkar, L. O. Bernhammer, J. Sodja, E. v. Solingen, G. A. van Kuik, and J. W. van Wingerden, *Wind tunnel tests with combined pitch and free-floating flap control: data-driven iterative feedforward controller tuning*, *Wind Energy Science* **1**, 205 (2016).
- K. Nilsson, S. Ivanell, K. S. Hansen, R. Mikkelsen, J. N. Sørensen, S.-P. Breton, and D. Henningson, *Large-eddy simulations of the lillgrund wind farm*, *Wind Energy* **18**, 449 (2015).
- N. Panwar, S. Kaushik, and S. Kothari, *Role of renewable energy sources in environmental protection: A review*, *Renewable and sustainable energy reviews* **15**, 1513 (2011).
- S. Raach, D. Schlipf, and P. W. Cheng, *Lidar-based wake tracking for closed-loop wind farm control*, *Journal of Physics: Conference Series* **753**, 052009 (2016).
- Rijksoverheid, *Klimaatakkoord*, Tech. Rep. (2019).
- Rijksoverheid, *Windenergie op zee*, (2020), accessed: 07-10-2020.
- M. A. Rotea, *Dynamic programming framework for wind power maximization*, *IFAC Proceedings Volumes* **47**, 3639 (2014).
- P. J. Schmid, *Dynamic mode decomposition of numerical and experimental data*, *Journal of fluid mechanics* **656**, 5 (2010).
- J. Schreiber, E. Nanos, F. Campagnolo, and C. L. Bottasso, *Verification and calibration of a reduced order wind farm model by wind tunnel experiments*, in *Journal of Physics: Conference Series*, Vol. 854 (IOP Publishing, 2017) p. 012041.

- K. Selvam, S. Kanev, J. W. van Wingerden, T. van Engelen, and M. Verhaegen, *Feedback-feedforward individual pitch control for wind turbine load reduction*, *International Journal of Robust and Nonlinear Control* **19**, 72 (2009).
- Siemens Gamesa Renewable Energy, *Wake adapt*, (2019), accessed: 14-10-2020.
- J. N. Sørensen and W. Z. Shen, *Numerical Modeling of Wind Turbine Wakes*, *Journal of Fluids Engineering* **124**, 393 (2002).
- V. Spudic, M. Jelavic, M. Baotic, and N. Peric, *Hierarchical wind farm control for power/load optimization*, *The science of making torque from wind (TORQUE2010)* (2010).
- H. J. Sutherland, *On the fatigue analysis of wind turbines*, Tech. Rep. (1999).
- G. Tescione, D. Ragni, C. He, C. S. Ferreira, and G. Van Bussel, *Near wake flow analysis of a vertical axis wind turbine by stereoscopic particle image velocimetry*, *Renewable Energy* **70**, 47 (2014).
- M. Vali, J. W. van Wingerden, S. Boersma, V. Petrović, and M. Kühn, *A predictive control framework for optimal energy extraction of wind farms*, *Journal of Physics: Conference Series* **753**, 052013 (2016).
- D. van der Hoek, S. Kanev, J. Allin, D. Bieniek, and N. Mittelmeier, *Effects of axial induction control on wind farm energy production-a field test*, *Renewable Energy* **140**, 994 (2019).
- G. van der Veen, J. W. van Wingerden, and M. Verhaegen, *Global identification of wind turbines using a hammerstein identification method*, *IEEE transactions on control systems technology* **21**, 1471 (2012).
- G. Van der Veen, J. W. van Wingerden, M. Bergamasco, M. Lovera, and M. Verhaegen, *Closed-loop subspace identification methods: an overview*, *IET Control Theory & Applications* **7**, 1339 (2013).
- G. Van Kuik, J. Peinke, R. Nijssen, D. Lekou, J. Mann, J. N. Sørensen, C. Ferreira, J. van Wingerden, D. Schlipf, P. Gebrad, *et al.*, *Long-term research challenges in wind energy—a research agenda by the european academy of wind energy*, *Wind energy science* **1**, 1 (2016).
- E. van Solingen and J. W. van Wingerden, *Linear individual pitch control design for two-bladed wind turbines*, *Wind Energy* **18**, 677 (2015).
- E. Van Solingen, S. Navalkar, and J. W. Van Wingerden, *Experimental wind tunnel testing of linear individual pitch control for two-bladed wind turbines*, *Journal of Physics: Conference Series* **524**, 012056 (2014).
- E. van Solingen, P. A. Fleming, A. Scholbrock, and J. W. van Wingerden, *Field testing of linear individual pitch control on the two-bladed controls advanced research turbine*, *Wind Energy* **19**, 421 (2016).

- J. W. van Wingerden, B. M. Doekemeijer, and J. A. Frederik, *Enhanced wind turbine wake mixing*, (2019), Octrooicentrum Nederland.
- M. Verhaegen and V. Verdult, *Filtering and system identification: a least squares approach* (Cambridge university press, 2007).
- C. H. Westergaard, *A method for improving large array wind park power performance through active wake manipulation reducing shadow effects*, (2013), United States Patent and Trademark Office (USPTO).
- Wind Denmark, *Branchestatistik for vindmøllebranchen 2019*, Tech. Rep. (Wind Denmark, 2020).

Acknowledgements

*Whatever you do in this life, it's not legendary
unless your friend are there to see it.*

– Barney Stinson,
on the true value of friendship.

As part of my PhD, I followed a large number of Graduate School courses. From the fellow PhD candidates that I met there, I learned that they usually have one of roughly two completely different motives to start a PhD: 1) as a well thought through, vital step in a (usually already clearly defined) career path, or 2) because why not? Everybody who know me, also knows to which of these two groups I belong. I never planned on starting a PhD. I might have even proclaimed on one or two occasions that I would *never* do a PhD. So how did I end up doing a PhD?

I think it has to do with a combination of three things: my lack of a career plan at the time, my wish to stay in Delft for a couple more years, and the fact that Jan-Willem offered me the position. Still, I wasn't sure whether I really wanted to commit to 4 more years of doing research on a topic that I worked on for over a year during my master thesis. I had liked studying, but I wasn't sure I really wanted to prolong it any further. However, Jan-Willem was very convincing. He invited me to join a diner in De Waag with other PhD candidates, during which a significant amount of *speciaalbiertjes* was consumed. Afterwards, I didn't really see any reason anymore *not* to accept the position.

Hence, Jan-Willem is the first person I need to acknowledge here. If anybody else would have offered me the position, I probably would have said no. From my master thesis project, I already knew what kind of supervisor you are, and also in my PhD it was always pleasant to work with/for you (in practice, I was usually working for you, but it never really felt like that). I highly admire your incredible intelligence and drive, but what I will remember most are the social talks. During our weekly meeting, the first minutes would always be reserved for talking sports – my football or your kids' waterpolo results, the upcoming skiing holidays, or simply the latest performance of PSV and AZ. Doing a PhD wasn't always easy for me, but your involvement and positive attitude kept me motivated to see it through. It will undoubtedly be hard for my future bosses to live up to the standard that you have set.

Secondly, I owe thanks to my fellow PhD's, the *Klasbakken*: Sjoerd, Sebastiaan, Bart and Daan. I thoroughly enjoyed your company, especially at the different conferences that we were able to attend together. Sjoerd, it was always interesting to talk to you, and I learned a lot from the discussions we had. Sebastiaan, I've had

many laughs with you, often concerning things that were wrong with the academic world. Unclear templates, badly designed websites, you always knew how to point out the flaws in the system in the most hilarious possible way. Bart, sharing an office with you was both inspiring and sometimes a bit intimidating. Your work ethic and productivity is off the charts, and your aggressively fast typing skills make it seem like you can write books in the time that mortal people write sentences. Yet you were always willing to help others (me included), for which I am eternally grateful. Daan, I loved our discussions about sports – especially about the mistakes we had both made in our Tour de France pools. I think we learned a lot together during the wind tunnel experiments in the OJF, and I do hope our paths will cross again in the future. Also the newer members of the Data-Driven Control group, that I got to know in a later stage of my PhD, cannot go unmentioned here. Yichao, you are such a friendly guy and I really enjoyed our discussions, especially about the differences between the Netherlands and China. Unai, I really wish you would have been able to come to Delft more often, as you were always a lot of fun to be around. Maarten, Atin, Sara, Yasin, Delphine, Livia, Ming, Alessandro, Zhenyu, Folkert, Jean, Daniël, Zhixin, David, Claudia, Marcus, and any other colleague I might have forgotten: thank you all for being part of my PhD, and the best of luck in your future careers.

DCSC is more than just PhD candidates, and the numerous people of the department have helped make my PhD process go as smoothly as I could have possibly hoped for. First of all, I would like to thank prof. Michel Verhaegen and dr. Riccardo Ferrari for their role as (co-)promotor and the useful feedback they have provided me along the way. Kees, Will and Alejandro: thanks for all the technical support. Kees and Will deserve a special thanks for helping me with the transportation and set-up of our turbine during the first wind tunnel experiments I did in Oldenburg. Carlas, Moses and Laurens: I really enjoyed working together with you for Stochastic Signal Analysis, and I learned new things from each of you. Marieke, Heleen, Kiran, Francy and Erica: thank you for taking care of all the practical matters involved in the department, and for organizing the numerous DCSC social events. Without you, the department would probably be a lot less exciting.

This dissertation would not have been possible without the people I collaborated with during my PhD. First of all, the people of the University of Oldenburg, where I did my first set of wind tunnel experiments: Mehdi, Michael, Vlaho, Lars, and many others. Lars, we had only spoken a couple of times on Skype before we had to spend 2 weeks together in the small control room of the Oldenburg wind tunnel. Like any test session, it didn't always go smoothly, but we never let that ruin the atmosphere. We had a blast at Stadtfest Oldenburg, as well as during subsequent nights when we met up at conferences. Thanks for all the laughs!

The next set of experiments were to take place at Polimi in Milan, together with the team of TUM, as part of the CL-Windcon project. Filippo, Alessandro, Paolo, Robin: thanks for making me feel at home every time I came to Milan. Robin, I really enjoyed working together with you – especially the daily lunches at Piadineria da Luca. I am glad to see you found a job that brings you joy and wish you all the best in your future career. The CL-Windcon project has played a large role in my PhD project, and I am grateful to have been a part of it. I would therefore like to

thank everyone who was involved in this project.

The PhD has played a major role in my life over the last 4 years, but I never made it a secret that my personal life was at least as important to me. It goes without saying that Ariston'80 has played an irreplaceable role in this part of my life. As a *sjaarsch*, in 2009, I considered switching sports after playing football my entire life. In the end, I decided to join Ariston'80 anyways, and I have not regretted it for a second. Over the years, I have seen the club grow exponentially, both in numbers and in activities. I have seen multiple generations of board members and teammates come and go. Yet the club still feels like home to me, and I am honoured to have a place in its (non-existing) history books. The amount of friends I made at the club who have made a significant impact on my life is too long to list here without risking to forget people. I would therefore like to thank everyone who has made Ariston'80 feel like home to me over the last 12 years.

During my time at Ariston'80, I also discovered the joy of cycling. First in Limburg with the men of *Kaas United*, sprinting to the top of every hill we encountered. This later evolved into longer "holidays" in the Alps, where we would tackle the toughest and most legendary *cols* of the Tour de France and the Giro d'Italia – at our own pace. In the summer of 2017, I was able to combine cycling in Bormio with wind tunnel experiments in Milan. Peter, Wim, Michel, Casper, Guido, Luc, Peer, Nick, Harm, Johan: thanks for sometimes making me feel like Tom Dumoulin, and other times like Kenny van Hummel. I hope to soon battle you again on cycling holidays to come.

Another place that has left a lasting mark on my life is Königsleiten. In the winter season of '08-'09, before I started at the TU Delft, I worked at Schischule Obermoser, and learned to take care of myself there. Along the way, I made some great and remarkable friends – some of which so different from me that we would probably never have become friends if we would have met anywhere else. Kimberly, Brenda, Jos, Stefan, Erwin, Michi, Dani, Kathi, Marloes, Liana, Lisa, Robyn, Maurits, Dennis, Floris, Philip, Rike, Felix, and anybody else that I might have forgotten to mention: thanks for everything and I hope to see you again next winter!

Melvin, you were always the center of attention, and somehow always managed to get everybody into party mode. You are sourly missed but will never be forgotten.

There are a couple of *Helden* from Königsleiten that need to be mentioned separately: *Beuk* (Wessel), *Oude Tim* (Tim) and *GapJump* (Wietse). What once started as ordinary friendships, much like other friendships I had with Obermoser-colleagues, has grown into the most close and time-resistant group of friend I have ever had. Beuk, we are so much alike, and yet you are so different from me. I both admire and envy your ability to socialize with anyone and everyone. Our competitiveness turns every single activity into a competition. Others might find that exhausting, but we thrive in these conditions and somehow manage to never turn it into a conflict. You better be prepared, because that medal belongs to me! Tim, we have a bit of a love-hate relationship at times. We don't always agree on things, but I appreciate your brutal honesty and value your friendship. Your unique sense of humor always makes me laugh, and especially *PosiTim* is a presence without whom our group is not complete. Wietse. Oh, Wietse. When we

met, we immediately became friends. At the time, I thought you were a nice guy, but not particularly exciting or adventurous. Beuk initially even described you as *boring*. Boy were we wrong. Not only are you an extremely loyal friend, but you also turn out to be our group's wild card. Every time we think we know you, you do something completely unexpected. Never change – keep surprising us. Recently, *Nieuwe Tim* (Thijs) joined our little group. Tim, you accomplished something that I did not imagine possible: you somehow managed to find a place for yourself in the unique dynamic of our group. After just a few days of skiing together, it already felt like I knew you for years. We quickly shared incredible laughs as well as personal stories.

Without a doubt, we work best as a group. We challenge each other and we never let anybody stay in his comfort zone for too long, yet we rarely have a serious argument. But most of all, we have an insane amount of fun together. In our own heads, the party always revolves around us. No matter how long it has been, it never feels awkward when we meet up again. Our skiing trip and participation in the EXTC tennis tournament are two of the highlights of my year. Perhaps we will grow too old for EXTC at some point not too far into the future. But I sincerely hope we will continue to go skiing together until we are no longer able to go downhill – and perhaps even longer.

Finally, I would not have become the person I am today without my family: my parents, Hans and Dorotheé, my brothers, Kevin and Martin, and more recently also my sister-in-law Melissa and my wonderful nephews Tijler and Quinn. Thanks to my family, my youth was as carefree as I could have wished for, but at the same time they helped me become an independent young adult.

Kev, I know it was sometimes hard for you to grow up as the “little brother of”, especially at school. At the same time, it wasn't always easy for me to have a little brother who is (at least) as athletic, competitive, clever and witty as I am. We drove each other to madness sometimes, but also to greater heights. As we grew up, combativeness and envy evolved into respect – although, naturally, we still don't like losing to each other.

Mart, although we did not really grow up together, you have always felt just as much a brother to me as Kevin. I love our nerdy discussions about Nintendo games, and having to teach you the basics of Pokémon when you started playing Go. You and Melissa serve as a role model of what I hope my life will look like in 12 years – although I could do without the X5.

Pap, you are probably my biggest fan and largest critic in one. I will never forget the time I came home with a report filled with 7's and 8's, and you asked me why I didn't get any 9's. I was thoroughly insulted at first, but a few months later these 7's and 8's had turned into 8's and 9's. You didn't say it because you weren't proud of the results that I got, but because you knew I could do better. In your own unorthodox way, you always push me to do the very best I can. I have the utmost respect for the way you continue working way past the retirement age, and still find the time to pursue a PhD. I know it's a struggle sometimes, but don't give up: I know you will finish it if you put your mind to it.

Mam, from a relatively young age, you told me and Kevin that we should move

out of the house as soon as possible. It was only years later that I discovered that when we actually did, it broke your heart. However, you felt like this was the best way to teach us to take care of ourselves. I will be eternally grateful for this act of selflessness. The last couple of years haven't always been easy for you, but you never seem to let it get to you. I sincerely hope I have the same strength you have in times of adversity.

They say you do not choose your family. Perhaps that's for the best, because I cannot imagine having chosen a better family. Even if I don't always say it or even show it, I love you and I am extremely grateful to have you in my life.

Friday March 29th, 2013 is a date I won't easily forget. A day earlier, I had flown back from Austria after spending 3 months there, to be able to attend my *Huischfeest* at Huize de Camping that same night. Barely recovered, Marlies – who also just returned from travels abroad – invited me to a small gathering of people from Ariston'80. It later turned out to be a memorable night. Not because anything special happened that night – absolutely nothing happened that night – but because Marlies met her now-husband Guido, and I met Saimi. Despite my ridiculous goggle-tan and the fact that we barely spoke to each other that night, you later admitted that I immediately caught your attention. Naturally, this feeling was mutual. Saimi, you are the sweetest, most patient and caring person I have ever met. I know I am not always the easiest person to live with, but you always know how to cope with me. When I am with you, I never feel like I have to pretend. Without writing a single word (apart from the cover), this dissertation belongs partly to you as well. You really are too good for this world, and I love you with all my heart.

Last but not least, to all the people who have managed to make it this far into my dissertation: thank you for sticking with me. I look forward to what the future might bring.

Joeri Alexis Frederik
Delft, Januari 2021

Curriculum Vitæ

Joeri Alexis Frederik

1990 Born in Utrecht, The Netherlands.

Education

- 2002–2008 Secondary School - Gymnasium (*cum laude*)
Christelijk Gymnasium, Utrecht
Profile *Nature & Technology* with classical languages
- 2009–2014 Bachelor's degree in Mechanical Engineering
Delft University of Technology, The Netherlands
- 2014–2017 Master's degree in Systems & Control (*cum laude*)
Delft University of Technology, The Netherlands
Thesis: Dynamic Wind Farm Control using the WFSim
flow model
Supervisor: dr. ir. J.W. van Wingerden
- 2017–2021 PhD degree in Systems & Control
Delft University of Technology, The Netherlands
Dissertation: Pitch control for wind turbine load mitigation
and enhanced wake mixing. A simulation and
experimental validation study
Promotors: prof. dr. ir. J.W. van Wingerden
prof. dr. ir. M.H.G. Verhaegen
Copromotor: dr. R. Ferrari

Patents

- 2019 J.W. van Wingerden, B.M. Doekemeijer and J.A. Frederik, "Enhanced wind turbine wake mixing." N2024238, Octrooicentrum Nederland, the Netherlands.

List of Publications

Journal publications

4. Y. Liu **J.A. Frederik**, R.M.G. Ferrari, P. Wu, S. Li and J.W. van Wingerden, *Fault-Tolerant Individual Pitch Control of Floating Offshore Wind Turbines via Subspace Predictive Repetitive Control*, [Wind Energy](#) (2021).
3. **J.A. Frederik**, B.M. Doekemeijer, S.P. Mulders and J.W. van Wingerden, *The helix approach: Using dynamic individual pitch control to enhance wake mixing in wind farms*, [Wind Energy](#). **23**(8) 1739 (2020).
2. **J.A. Frederik**, R. Weber, S. Cacciola, F. Campagnolo, A. Croce, C. Bottasso and J.W. van Wingerden, *Periodic dynamic induction control of wind farms: proving the potential in simulations and wind tunnel experiments*, [Wind Energy Science](#) **5**(1) 245 (2020).
1. **J.A. Frederik**, L. Kröger, G. Gülker and J.W. van Wingerden, *Data-driven repetitive control: Wind tunnel experiments under turbulent conditions*, [Control Engineering Practice](#) **80** 105 (2018).

Peer-reviewed conference papers

5. Y. Liu, **J.A. Frederik**, A. Fontanella, R.M.G. Ferrari and J.W. van Wingerden, *Adaptive fault accommodation of pitch actuator stuck type of fault in floating offshore wind turbines: A subspace predictive repetitive control approach*, [American Control Conference \(ACC\)](#), 4077 (2020).
4. **J.A. Frederik**, B.M. Doekemeijer, S.P. Mulders and J.W. van Wingerden, *On wind farm wake mixing strategies using dynamic individual pitch control*. [Journal of Physics: Conference Series](#) (2020).
3. L. Kröger, **J.A. Frederik**, J.W. van Wingerden and J. Peinke, *Generation of user defined turbulent inflow conditions by an active grid for validation experiments*, [Journal of Physics: Conference Series](#) **1037** 052002 (2018).
2. **J.A. Frederik**, L. Kröger, J. Peinke, M. Hölling and J.W. van Wingerden, *Validating subspace predictive repetitive control under turbulent wind conditions with wind tunnel experiment*, [Journal of Physics: Conference Series](#) **1037** 032008 (2018).
1. S. Boersma, B.M. Doekemeijer, P.M.O. Gebraad, P.A. Fleming, J. Annoni, A.K. Scholbrock, **J.A. Frederik** and J.W. van Wingerden, *A tutorial on control-oriented modeling and control of wind farms*, [American Control Conference \(ACC\)](#), 1 (2017).

